Numerical modeling of nonlinear Newwaves for impact assessment on offshore structures

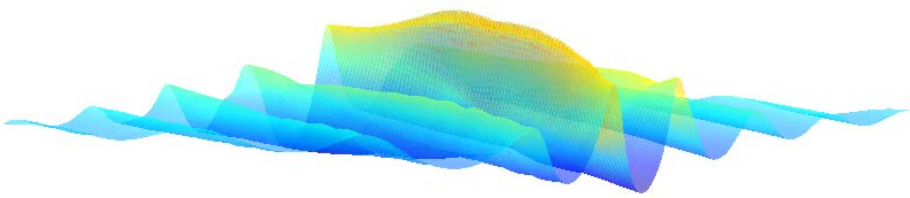

Wouter J. Burger

M.Sc. Thesis
Delft University of Technology
Faculty of Civil Engineering and Geosciences
Section Fluid Mechanics
January 2005

Thesis Committee
- Prof. dr. ir. G.S. Stelling (Delft University of Technology)
- Prof dr. ir. J.A. Pinkster (Delft University of Technology)
- Dr. ir. A.J.H.M. Reniers (Delft University of Technology)
- Dr. K. Ewans (Shell EP Projects)
- Ir. P.G.F. Sliggers (Shell EP Projects)
- Dr. G.Z. Forristall (Forristall Ocean Engineering)
- Dr. G.E. Loots (MARIN)

Unclassified **EP 2004-**

Numerical modeling of nonlinear Newwaves for impact assessment on offshore structures

by

W.J. Burger

Approved by: K. Ewans

Date of issue: January 2005

ECCN number: EAR 99

This report documents student work

SHELL INTERNATIONAL EXPLORATION AND PRODUCTION B.V., RIJSWIJK

Further copies can be obtained from the Global EP Library, Rijswijk

PREFACE

This report is a MSc thesis for Civil Engineering at Delft University of Technology. The work was carried out for, and facilitated by Shell EP Projects in Rijswijk.

I would like to thank all the members of the thesis committee for their advise and guidance, in particular my daily supervisors Kevin Ewans, Ad Reniers and Erwin Loots. I would like to thank Paul Taylor for providing me of Vijfvinkel's work, although the revitalization of the computer code took considerable effort.

Working with two numerical methods of different background was challenging. Challenging, when the achievements seemed not to be within reach. I would like to thank the thesis committee to let me continue to go after my original objectives, and Shell for supporting this.

I would like to thank my colleagues at Shell for my enjoyable time in Rijswijk. I would like to thank all my friends for the outstanding time in Delft. I would like to thank Daphne and my parents for their support.

Wouter Burger

Rijswijk, January 2005

SUMMARY

Offshore structures are designed to resist the impact of the extreme wave. Shell EP Projects desires a computer model that is able to simulate the impact of the design wave on gravity based offshore platforms, such as the Sakhalin PA-B platform. Comflow is a numerical model that simulates fluid flow, by solving the Navier-Stokes equations using the improved Volume-of-Fluid method. The wave inflow is prescribed at a side boundary of the Comflow domain.

Shell uses the Newwave theory to prescribe the wave group that contains the design wave. The shape of the wave train that contains the design wave is important for the impact on the structure as it influences wave run up and reflection; possibly causing the wave to slam against the bottom of an offshore platform deck. Shallow water and wave steepness influence the shape of the wave group; this can be simulated with nonlinear wave models. This thesis concerns the simulation of nonlinear Newwaves and the implementation in Comflow.

The goals of the thesis hence are to:

1. Find a wave model to simulate fully nonlinear Newwaves.
2. Couple the nonlinear wave model to Comflow.
3. Validate the wave impact on structures in Comflow with scale model tests.

Vijfvinkel [25] developed a quasi-spectral method to solve the wave potential equation; the one dimensional spatial domain is periodic and it requires solely an initial condition. The method is based on expansion of the Dirichlet-Neumann operator, which is substituted in the governing equations. The operator consists of the surface elevation and the velocity potential at the surface. These are the properties that are calculated in a time domain. A velocity profile can be reconstructed. The Vijfvinkel computer code was obtained and revitalised.

The Beji Battjes test [3] was simulated in Comflow. It confirmed the grid and time step requirements [19], and it showed that the nonlinear formation and release of higher harmonics are also simulated correctly following the requirements.

Three additional numerical tests were set up to indicate the validity of Newwave simulation. Each test highlights a separate aspects of nonlinear modeling of Newwaves.

- The second experiment consists of a tank in which a standing wave is sloshing. The simulation in Comflow is done for various relative water depths. It showed that, except for shallow water, wave propagation is simulated reasonably well, however, damping can play a significant role due to the upwind discretisation method and velocity extrapolation method at the surface.
- In the third experiment the wave steepness is increased up to near breaking conditions, in Comflow and in Vijfvinkel. It proved that Vijfvinkel has superiour performance in simulation of steep waves.

- In the fourth experiment Newwaves are simulated in Vijfvinkel. A method is used that transforms the linear initial condition to a quasi-nonlinear initial condition. Simulations with a starting time of more than 50 seconds prior to the linear focus time, have higher peaks before the wave group reaches the linear focus location. The wave group becomes a bound wave group; the shape of the wave group shows less variation, and it propagates with a common velocity.

Vijfvinkel is coupled to Comflow. The output of Vijfvinkel is transformed to comply with the Comflow domain, and the input procedure of Comflow is extended to be able to read external input files. This new input procedure allows the simulation of an arbitrary disturbance of the free surface. A simulation is performed in which Vijfvinkel prescribes the nonlinear Newwave to the inflow boundary in Comflow.

A necessity is the development on the numerical core of Comflow. This was identified and anticipated on in the Joint Industry Project, as a large number of grid cells is required to model propagating waves and damping plays a significant role. For the simulation of impact on offshore structures the implementation of local grid refinement will increase the accuracy and efficiency of the simulation of wave impact on structures. Only when these developments are achieved, validation with scale model tests is sensible, for Comflow to become a valuable design tool to assess wave impact on offshore structures.

KEYWORDS

Nonlinear Newwave, Comflow, Vijfvinkel

TABLE OF CONTENTS

LIST OF TABLES

LIST OF FIGURES

1. INTRODUCTION

The subject of the thesis concerns the numerical modeling of nonlinear Newwaves for impact assessment on offshore structures. Ocean surface waves can have powerful impact on offshore structures. One of the design criteria of offshore structures is the ability to resist a wave of an extreme height, with the wave height determined by statistical methods. The complex wave impact on the bottom of the deck of the Sakhalin II PA-B platform is one of the key design considerations. Currently for the design, laboratory scale model tests must be used to determine the structures ability to resist wave run up and wave slam under extreme conditions. This is time consuming and expensive. The development of computational methods opens perspectives.

A computer program that is able to simulate the complex wave impact on offshore structures is desired by Shell EP Projects. Comflow is the three dimensional Computational Fluid Dynamics program that will be used for this purpose, see Figure 1.1. The nonlinearities that are inherent in waves with extreme steepness in limited water depth are not modeled to full extent. Hence, a second program, that is well capable of simulating the propagation of fully nonlinear waves, must be coupled to Comflow.

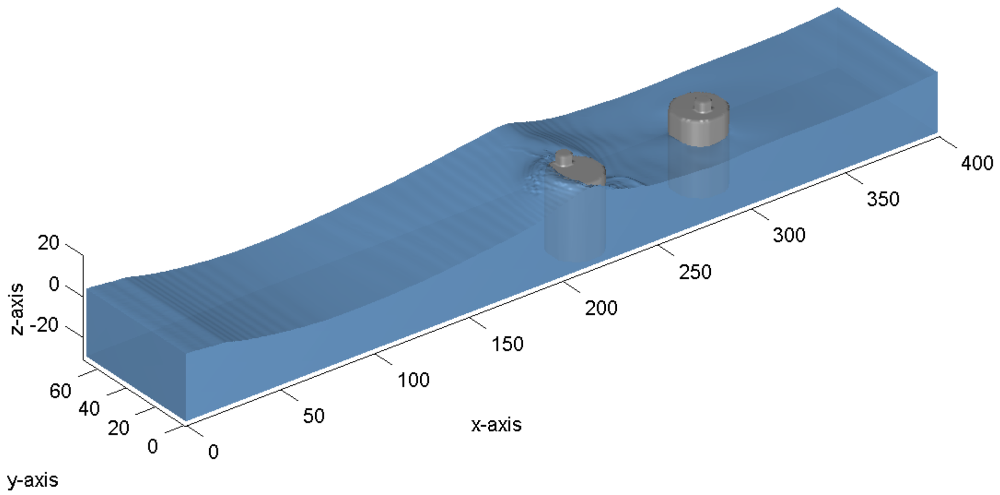

Figure 1.1: Comflow simulation of a wave impact on two legs of a platform.

Vijfvinkel is a potential solver, based on a spectral method, and is able to simulate fully nonlinear Newwaves. It is a one dimensional model, simulating the horizontal propagation of a surface disturbance in one direction, see Figure 1.2. However, the velocity profile can be reconstructed with the use of the calculated parameters.

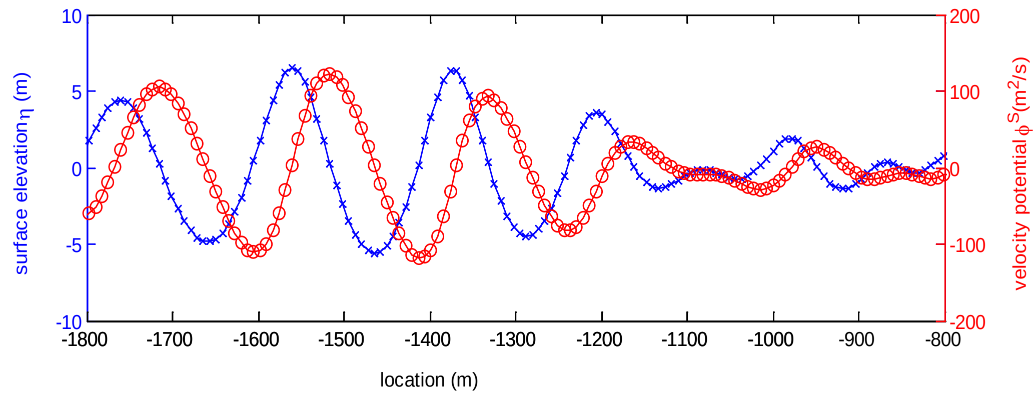

Figure 1.2: Vijfvinkel simulation showing surface elevation and velocity potential.

This thesis presents the coupling of potential solver Vijfvinkel to Navier Stokes solver Comflow. Newwave simulations in Vijfvinkel are performed, and the wave is recorded at a specified node (location) in the Vijfvinkel domain. This wave record is used to prescribe the inflow boundary in the Comflow domain.

First, several experiments are presented that indicate the range of applicability of both computer programs. Experiments are set up to indicate the performance of Comflow and Vijfvinkel with regard to the simulation of steep waves and waves in shallow water. Newwaves are steep waves and are applied to simulate the wave impact on structures that are in relatively shallow water. These experiments indicate if these computer programs are able to simulate the nonlinear conditions that are inherent to Newwaves.

1.1. Background

In this section the subject is introduced. First the background of nonlinear Newwaves is explained. Secondly the considered numerical models are introduced. The third subsection deals with the impact of waves on offshore structures.

Nonlinear Newwaves

An offshore structure is designed to resist the impact of the extreme wave. The shape of the wave train that contains this Ultimate Limit State (ULS) wave is of importance for accurate modeling of wave impact on offshore structures. How deep is the trough that comes prior to the high crest, and how powerful is this crest? Newwave theory approximates the shape of this design wave. A wave can be seen as a sine with a certain amplitude, frequency and phase. A sea state (random waves) can be decomposed in single waves, each characterized by an amplitude, frequency and phase. The distribution of these quantities is usually presented in spectra. The shape of spectra is standardized, depending on several parameters, e.g. the frequency of the most energetic waves. The standard spectrum shape that is used in this thesis is the JONSWAP spectrum. For a given location, a JONSWAP spectrum can be estimated that is representative of the expected sea state in which the extreme wave can take place. Secondly, with statistical methods the extreme wave height is determined. The spectrum and the extreme wave height are both used in the Newwave theory. The relation between the spectrum and the height of the extreme wave is made with a spectrum amplification factor. The Newwave is a wave group consisting of spectral components (waves) that come in phase at the same time and place. The waves amplify each other. In linear theory these waves are superimposed, in nonlinear theory these waves can not be seen independently.

Wave theories approximate reality by combining (substituting) a set of physical relations. The physical relations are often simplified (linearized) to reduce the mathematics, but this restricts the application. Linear wave theory is a good approximation for ocean waves with a small amplitude. However, this simplification shows large deviation for high waves and shallow water; the nonlinear terms are not negligible. Wave theories are often characterized by the order of truncation of the nonlinear terms; it indicates to what extent nonlinearity is accounted for. Second order Stokes theory for example includes the linear theory and a first order approximation of the nonlinear physical relations. The term *fully nonlinear* is used to denote an approximation to a high order, high enough that the truncation of the nonlinear relations implies negligible error. Strictly taken fully nonlinear is an incorrect name, as the order of truncation always is a finite number. Nonlinearity is expressed by the fact that waves interact, the crests get higher and more peaked, the troughs shallower and longer. If waves travel independently, with their natural speed, they are considered unbound. Nonlinear waves can travel bound to other waves; the propagation velocity of the bound waves differs from the natural propagation velocity.

Newwave theory originally is a linear wave theory, assuming the extreme waves to be perfectly sinusoidal. A correction was introduced, indicating the contribution of second order effects. The second order contribution increases the maximum wave height. To comply with the statistically determined extreme wave height, the spectral amplification factor is adapted. This is an iterative method and can also be applied to fully nonlinear Newwave.

Now the task lays ahead to model nonlinear Newwaves. This is done with the help of two computer programs, Comflow and Vijfvinkel. Comflow can accurately model the wave impact on offshore structures, while Vijfvinkel is well capable of accurately simulating the propagation of nonlinear waves. The benefit lies in the combination of strengths of both models.

Numerical modeling

Comflow solves the Navier-Stokes equations. The Navier-Stokes equations are a set of partial differential equations that describe fluid flow. To solve the equations an initial fluid configuration (initial condition) and specifications at all boundaries (boundary conditions) are required.

Comflow was developed in 1995 to simulate the complex flow of fluid around detailed bodies. A three dimensional model was set up that approximates the Navier Stokes equations with the Volume of Fluid method. Comflow uses a boundary fit, Cartesian grid, i.e. the domain is split in rectangular cells that fit exactly in the domain. For each of these cells the Navier Stokes equations are solved.

The power of this method is that it can accurately simulate the flow of fluids under influence of detailed obstacles (e.g. the deck of a ship) or in a specific domain (e.g. a fuel tank).

This model has been used for several purposes. A study was performed to simulate a 1998 spacecraft that missed the asteroid it was aimed at because fuel was sloshing in its partially filled fuel tank. Flow of blood has also been modeled in Comflow. Offshore engineering interests lay in the simulation of ocean surface waves to determine the resulting loads of waves overtopping vessels and structures. Comflow was used to simulate the load of a high wave overtopping static and moving impermeable (rigid) objects [7]. First the initial conditions were adapted; a wave was modeled as an initially, constantly sloping body of water. Meskers [19] implemented a new boundary condition to simulate regular waves. The boundary condition that was introduced consists of a surface elevation and velocity profile prescribed by linear wave theory. This was extended to second order Stokes and fifth order Stokes wave theory. Heemskerk [10] implemented a linear and second order Newwave. The boundary where the waves enter the domain is denoted as the inflow boundary, the outflow boundary is situated at the opposite side, here the boundary absorbs the disturbance. Usually a Sommerfeld outflow boundary is used [11].

The goal of this thesis is to implement fully nonlinear Newwaves. A second wave resolving code that can model nonlinear Newwaves effectively will prescribe the nonlinear Newwave as inflow boundary in Comflow.

Vijfvinkel is the denotation of a computer code that E. Vijfvinkel developed in 1996 [25] which is able to simulate one dimensional wave propagation. The method it uses is able to simulate fully nonlinear waves. It solves wave potential equation at the fluid surface. It calculates the surface elevation and the velocity potential at the free surface, with which the water velocities underneath the surface can be derived. Vijfvinkel is a program that takes little time to run, as it is uses Fast Fourier Transformation (FFT). A restriction is that depth variations and objects can not be modeled. It is based on an equally spaced (one dimensional) grid. The spatial domain is periodic; the domain can be repeated to infinity. It therefore does not use side boundaries; the wave that leaves at one side of the domain enters again on the other side. Only the initial surface elevation and velocity potential at the surface are required.

How do we model nonlinear Newwaves? In Vijfvinkel, the linear Newwave will be imposed as initial condition, and being a nonlinear code the wave will transform into a fully nonlinear wave as it propagates through the domain. At the location where the Comflow domain starts, the surface elevation and velocity potential at the surface are recorded. These parameters are used to construct a velocity profile. The record of the surface elevation and the velocity profiles are used as input for Comflow. The nonlinear simulation of the Newwave and the artificial damping in Comflow affect the wave height. To get the statistically determined wave height the input conditions need to be adapted, by changing the spectral amplification factor. This is an iterative process.

The Vijfvinkel code was written in 1996 at Shell as part of a postdoctoral degree in computational mechanics at Rijksuniversiteit Groningen (RuG) and was supervised by dr. P.H. Taylor of Shell Research Rijswijk. The author obtained it from dr. P.H. Taylor, now lecturer at the University of Oxford, but the code had not been used since it was written. The program had to undergo time consuming repair to be able to run it again.

Both Comflow and Vijfvinkel are written in Fortran 77. The interpretation of data of both programs is done with Matlab 6.1.

Impact on offshore structures

Now the wave theory and the computer models are introduced, we focus on the impact of these waves on offshore structures. Offshore structures can in principle be any type of rigid body in an offshore location. The Sakhalin PA-B platform is used as example since EP Project requires knowledge on wave impact on the deck of this platform. Waves of extreme height may hit the deck of the platform, from the side or from underneath. The load of this wave slam is one of the key design considerations. The PA-B platform is a Gravity Based Structure consisting of a rectangular, concrete base on which four legs are built to support the structure above the water line. The impact of waves can be decisive for the strength of the structure. Usually scale model tests are used to assess the impact, see Figure 1.3, but computer models as Comflow can become a valuable substitute.

Figure 1.3: Scale model of PA-B platform.

First we need to recognize the aspects of wave structure interaction. Static offshore structures influence the incoming wave pattern by reflection and diffraction of waves. Diffraction shows how waves move around a structure. When rigid bodies are moving they radiate waves, this process is denoted with radiation. Two methods can be used to model wave structure interaction:

- Navier-Stokes solvers, e.g. Comflow.
- Potential solvers. e.g. DELFRAC. This is briefly introduced below.

The incident and reflected waves, their diffraction and radiation can be described with potentials. These potentials follow from the boundary conditions. To solve these potentials use is made of Green’s theorem that describes the conversion of a volume integral into a surface integral. This theorem is applied to the surface of the rigid body. In this thesis offshore structures are modeled as static rigid bodies.

DELFRAC is a computer model that solves these potentials. This program is used to give an indication of the influence of a structure on the incoming regular wave. Figure 1.4 indicates in color the amplification of the undisturbed wave for a static four-leg platform as calculated with DELFRAC [14].

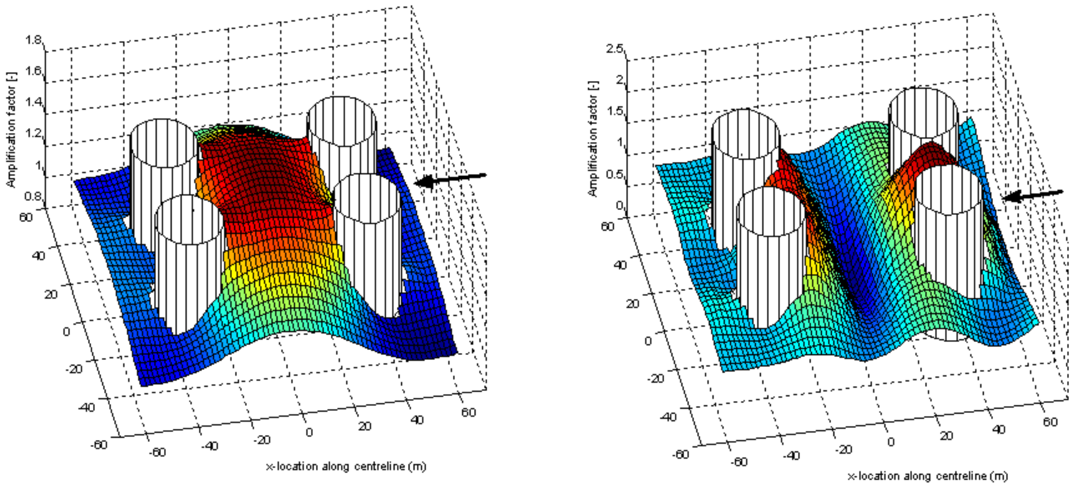

Figure 1.4: Amplification of regular waves under the Sakhalin LUN-A platform.

Why is DELFRAC not used to model the wave impact? DELFRAC has limitations with regard to conditions with high nonlinearity, and it can not simulate wave breaking. DELFRAC uses linear diffraction and radiation potential theory. The surface disturbance (input) can be arbitrary (single valued and continuous) as the surface elevation is decomposed into a frequency domain using FFT. Nonlinear waves can be simulated, but nonlinear radiation and diffraction is neglected.

More important: potential solvers can not simulate the complex wave slam on the top structure, which is the issue of concern.. Navier Stokes solver Comflow can model this and will be used to simulate the impact of extreme waves on offshore structures.

The shape of the wave is of importance to model impact on the offshore structure, therefore a realistic simulation of the design sea condition is desired in Comflow. The nonlinearity of these decisive waves is not modeled sufficiently by Comflow and subject to further study.

1.2. Problem definition

The problem is defined as the difference between the current and the desired capabilities of Comflow, as for the course of this thesis.

Although Comflow is well capable to simulate long, low amplitude waves, the results for high and steep waves are not satisfying. It has been recognized that a relatively fine grid is needed to simulate high and steep waves [10,19]. Currently three causes are thought to be responsible for the high resolution that is needed. These are

- The movement of the free surface,
- Numerical dissipation and diffusion,
- Velocities at the free surface.

These issues are dealt with in the Joint Industry Project (JIP) to develop Comflow. Participants are MARIN, RuG, Force Technology Norway AS, TU Delft and Shell.

Shell EP Projects requires Comflow to be able to simulate the impact of fully nonlinear Newwaves on offshore structures. In order to be a suitable substitute for scale model tests some challenges with respect to numerical modeling of nonlinear Newwaves in Comflow need to be overcome. These are categorized as follows:

1. Inflow boundary conditions
   a. An inflow boundary is desired that is able to describe fully nonlinear Newwaves.
   b. Wave propagation is affected by error waves that are formed at the inflow boundary.

2. Free surface Boundary conditions
   a. Nonlinear waves dissipate energy while propagating. This can be caused by the schematization of the free surface boundary.
   b. Surface velocities and accelerations have not been verified with other codes. These can be a cause of errors in simulations.

3. Outflow boundary condition
   a. A reduction of reflections at the outflow boundary is desired.
   b. The outflow boundary requires a large spatial domain, and therefore considerable computational effort.

4. Initial condition
   a. The time span of the simulation can be reduced if the Newwave can be set as initial condition, while currently the fluid is at rest at the start of the simulation.

5. Newwave focusing
   a. The focal point and focal time using nonlinear Newwave theory can not be determined a priori. Insight is desired in deviations of wave shape, phase and amplitude.
   b. High waves sometimes show breaking and do not focus, possibly due to inflow boundary inconsistencies.

c. The trade-off between grid size, time step, accuracy and computing time can be optimized.

d. Local grid refinement in the vicinity of the offshore structure will increase the accuracy of wave impact and will reduce computational time.

6. Validation

   a. Nonlinear Newwaves in Comflow have not been validated with laboratory tests.

1.3. Objectives

The development of Comflow within the JIP, in which several companies are participating, has been distributed over the participants as follows:

- At the Rijksuniversiteit Groningen two phase flow will be implemented, as well as air entrapment. Moving bodies are implemented and the numerical core is improved such that the simulation of high and steep waves shows better performance. (PhD students T. Helmholt-Kleefsman, R. Wemmenhove).
- TU Delft will develop steep wave generation and propagation (PhD student P. Wellens).
- MARIN will define a new post-processing interface to Comflow, which will make interpretation of the results easier. Laboratory experiments are performed to validate Comflow.
- G.E. Loots, as a RuG financed postdoc at MARIN, will validation Comflow with the laboratory experiments.
- Force Technology Norway AS will develop a users interface to make the program better accessible, and will validate the performance of steep waves in cooperation with MARIN.

The objective of this thesis is to model fully nonlinear Newwaves in Comflow. The developments of Comflow can easily be exchanged among the JIP participants.

The objectives of this thesis are listed below.

1. *To find a nonlinear wave model with which Newwaves can be simulated.* An appropriate numerical model is to describe the inflow of nonlinear Newwaves. Two options are to be considered: Vijfvinkel's model (P.H. Taylor, University of Oxford) and the FEM code Hubris (R.H.M. Huijsmans, MARIN).

2. *Coupling of wave resolving program to Comflow*

   a. To assess the performance of Comflow and the second wave resolving program for modeling nonlinear Newwaves. Experiments are to be done with the considered models. The errors in wave shape, phase and amplitude are to be quantified and interpreted.

   b. To optimize the performance of Comflow by locating problems in simulation of nonlinear Newwaves. Problems may be found in the free surface boundary conditions surface velocities.

c. To couple the nonlinear wave resolving program to Comflow. Alternatives for coupling of both programs are generated and elaborated.

3. *Validation of Comflow simulations of impact of nonlinear Newwaves on structures.* The Comflow simulation of the impact of a fully nonlinear Newwave on the Sakhalin II PA-B platform is to be validated with the scale model tests that were performed at the Canadian Hydraulic Centre.

1.4. Outline

This section concludes the introduction of this thesis. In the next chapters the results of the thesis are presented. Chapter 2 explains the Navier-Stokes equations and the algorithm with which Comflow solves them. The third chapter is an overview of relevant wave physics. The fourth chapter deals with Vijfvinkel, the code that was chosen to create input for Comflow.

In the fifth chapter the results of four experiments are presented. The Beji Battjes experiment is done, as benchmark test case for CFD programs. Three other tests are set up to assess the accuracy of the two programs that are used for this thesis. The tests have increasing relevance for the coupling of Vijfvinkel and Comflow and increasing nonlinearity. Regular waves are considered: firstly, the relative water depth is decreased, secondly, the relative wave steepness is increased to near breaking conditions. In the fourth experiment nonlinear Newwaves simulations are done.

In Chapter 6 the coupling of Vijfvinkel and Comflow is introduced and described. Four coupling alternatives are presented of which the first is executed. Vijfvinkel prescribes the nonlinear Newwave to the inflow boundary in Comflow.

Conclusions and recommendations are formulated in the last chapter.

2. COMFLOW

In this chapter an overview is given of Navier Stokes solver Comflow. First, the governing equations are given. Secondly, the numerical model will be presented that is used to solve the equations.

2.1. Governing equations

The Navier-Stokes equations describe fluid flow and consist of a continuity equation and a momentum balance. An earth bound Cartesian axis system (x,y,z) is used with the origin in the still water level with z positive upwards.

The continuity equation yields that volume is conserved for incompressible fluids:

$$\frac{\partial u}{\partial x}+\frac{\partial v}{\partial y}+\frac{\partial w}{\partial z}=0 \qquad \{1\}$$

In this equation u,v and w are, respectively, the velocities in x,y and z direction, in (m/s).

The Navier-Stokes momentum equation balances inertia with pressure, viscous effects and external forces. The fluid is assumed to be Newtonian. Turbulence modeling is not included in the equations.

$$\begin{aligned}
\frac{\partial u}{\partial t}+u\frac{\partial u}{\partial x}+v\frac{\partial u}{\partial y}+w\frac{\partial u}{\partial z}&=-\frac{1}{\rho}\frac{\partial p}{\partial x}+\frac{\mu}{\rho}\left(\frac{\partial^2 u}{\partial x^2}+\frac{\partial^2 u}{\partial y^2}+\frac{\partial^2 u}{\partial z^2}\right)+f^{b,x}\\
\frac{\partial v}{\partial t}+u\frac{\partial v}{\partial x}+v\frac{\partial v}{\partial y}+w\frac{\partial v}{\partial z}&=-\frac{1}{\rho}\frac{\partial p}{\partial y}+\frac{\mu}{\rho}\left(\frac{\partial^2 v}{\partial x^2}+\frac{\partial^2 v}{\partial y^2}+\frac{\partial^2 v}{\partial z^2}\right)+f^{b,y} \qquad \{2\}\\
\frac{\partial w}{\partial t}+u\frac{\partial w}{\partial x}+v\frac{\partial w}{\partial y}+w\frac{\partial w}{\partial z}&=-\frac{1}{\rho}\frac{\partial p}{\partial z}+\frac{\mu}{\rho}\left(\frac{\partial^2 w}{\partial x^2}+\frac{\partial^2 w}{\partial y^2}+\frac{\partial^2 w}{\partial z^2}\right)+f^{b,z}
\end{aligned}$$

The symbol ϱ denotes the density in (kg/m^3), p the pressure in (N/m^2), μ the dynamic viscosity (Ns/m^2), f^b the external forces (N).

The first term is the local (or time) derivative. The spatial derivatives on the left hand side are the advection (or convection) terms. The first term on the right hand side is the pressure gradient, the central terms are the viscous (diffusion) terms, the rightmost term f^b are the external body forces, such as gravity.

To solve the Navier-Stokes equations boundary conditions and an initial condition need to be applied. The initial condition conisits of the configuration of the fluid, the velocities, accelerations and the pressure distribution. Comflow is used as a numerical wave tank to model wave impact on offshore structures. In this contexts several types of boundary conditions are defined: inflow boundary conditions, outflow boundary conditions, solid boundary conditions, and free surface boundary conditions.

Waves are prescribed at one side of the domain (inflow boundary), and are being absorbed on the opposite side (outflow boundary). The boundaries use the location of the free surface and the velocities at the boundary. At the inflow boundary, these values are prescribed by a selected wave theory. Several types of outflow boundaries exist, e.g. based on the Sommerfeld condition or on hydrostatic pressure.

Two types of solid boundary conditions exist: free slip equation {3} and no slip equation {4}. The numerical wave tank's side walls are impermeable and frictionless (free slip). The bottom and the bodies that are placed in the domain are also impermeable, but do allow shear stress (no slip). In equation {3}, u_n is the velocity normal to the free surface, τ_t the tangential shear stress along the wall (N/m^2). In equation {4}, $\vec{u}$ is the velocity vector at the boundary.

$$\begin{aligned} u_n &= 0 \\ \tau_t &= 0 \end{aligned} \qquad \{3\}$$

$$\vec{u} = 0 \qquad \{4\}$$

The free surface is defined as the fluid-air interface. Three free surface boundary conditions apply, considering the temporal evolution of the free surface {5}, tangential {6} and normal {7} stresses.

The surface is tracked using the following relation, with η the surface elevation in (m).

$$\frac{\partial \eta}{\partial t} + u\frac{\partial \eta}{\partial x} + v\frac{\partial \eta}{\partial y} + w\frac{\partial \eta}{\partial z} = 0 \qquad \{5\}$$

No tangential stress acts on the free surface, with *t* and *n* the tangential and normal direction.

$$\mu\left(\frac{\partial u_n}{\partial t} + \frac{\partial u_t}{\partial n}\right) = 0 \qquad \{6\}$$

The normal stresses at the free surface are given in equation {7}, with p_{atm} the atmospheric pressure (N/m^2), σ the surface tension (N/m) and ϰ the curvature of the surface (1/m). The surface tension in the Comflow runs in this thesis are considered zero, as its influence is negligible. However, in zero gravity applications surface tension can be dominant.

$$-p + 2\mu \frac{\partial u_n}{\partial n} = -p_{atm} + \sigma\kappa \qquad \{7\}$$

2.2. Numerical model

To solve partial differential equations three numerical methods can be categorized:

- Finite difference methods
- Finite volume methods
- Finite element methods

The finite difference method is the most common method to solve partial differential equations. Finite volume methods calculate the values of conserved quantities, mass and momentum, averaged over a control volume. The values of the conserved quantities are considered within the control volume. Finite volume methods can apply to non-uniform grids. Finite element methods approximate continuous quantities as a set of discrete quantities at discrete points. They can be applied to problems with great complexity.

For modeling fluid flows a second categorization can be made. Lagrangian models follow a fluid particle as it moves (moving grid) while Eulerian models have a fixed grid. Eulerian models are better capable to model topological changes.

The Navier Stokes equations are solved with an Eulerian finite volume method. In this method the domain is subdivided using a mesh (grid). Each mesh cell is a control area (two dimensional domain) or control volume (three dimensional domain). For each of the cells the Navier Stokes equations are solved.

The Volume of Fluid (VOF) is the finite volume method that Comflow uses, and was introduced in 1981 by Hirt and Nichols [13]. A variable mesh was introduced. At that time, finite difference methods were well established for modeling free boundary problems. The VOF method provided a simple and efficient method to model fluid flow and is capable to simulate highly complicated free surface flows.

The VOF method is relatively efficient due to the cell labeling procedure. Because the cells are given labels, the solution algorithm can be taylored for cell combinations. Furthermore, each cell has a volume aperture and edge apertures. Volume apertures F indicates the share of the cell being filled with fluid, with F ranging from zero (no fluid) to unity (completely filled). Edge apertures indicate the share of the cell boundaries through which fluid flow is possible. To solve the Navier Stokes equations, first the pressure is calculated, and then the velocities are adjusted.

The pressure in a surface cell is calculated using interpolation from the first subsurface cell and the location of the free surface. For surface cells, the volume aperture is used to construct the shape of the surface; either the downstream cell (Acceptor) determines the shape of the surface or the upstream cell (Donor). First, the slope of the surface is determined. Secondly, the height of the surface is determined. The surface shape is used to compute the fluxes through the surface cells and can be used to apply various boundary conditions. Two stability restrictions apply: the Courant Friedrichs Lewy (CFL) condition {8} and a viscosity condition {9}. In {8} C_r is the CFL number and c the phase velocity.

$$C_r = \max\left(\left|\frac{u\Delta t}{\Delta x}\right|, \left|\frac{w\Delta t}{\Delta z}\right|, \left|\frac{c\Delta t}{\Delta x}\right|\right) < 1 \qquad \{8\}$$

$$v\Delta t < \frac{1}{2}\frac{\Delta x^2 \Delta y^2 \Delta z^2}{\Delta x^2 + \Delta y^2 + \Delta z^2} \qquad \{9\}$$

Reference is made to [7,12,18] for a detailed description of the model.

2.2.1. *Cell labeling and apertures*

The Comflow domain is discretized in a mesh with rectangular cells. A staggered grid is used; the velocities are taken at the center of the cell edges while the pressure is defined at the cell center. The cells are given a label: flow, boundary or exterior. Flow cells can be subdivided into empty cells, surface cells and fluid cells. As noted, these labels make the solution procedure more efficient. The cells are labeled from the top of the domain downward. The first cell that contains fluid becomes a surface cell (S), the cell below the surface cell becomes a fluid cell (F), and boundary cells (B) form the boundary. Accordingly, in order, the cells are:

- Flow cells
    - Empty cells (E)
    - Surface cells (S)
    - Fluid cells (F)
- Boundary cells (B)
- Exterior cells (X)

The cells are given volume apertures and edge apertures. Volume apertures (F_b) indicate the fraction of the cell that can be filled with fluid. Edge apertures (A) indicate the part of the cell surface through which fluid can be transported. Both apertures are dimensionless quantities with values between zero and unity. These apertures make the model efficient, especially when complex rigid bodies are introduced, see Figure 2.1.

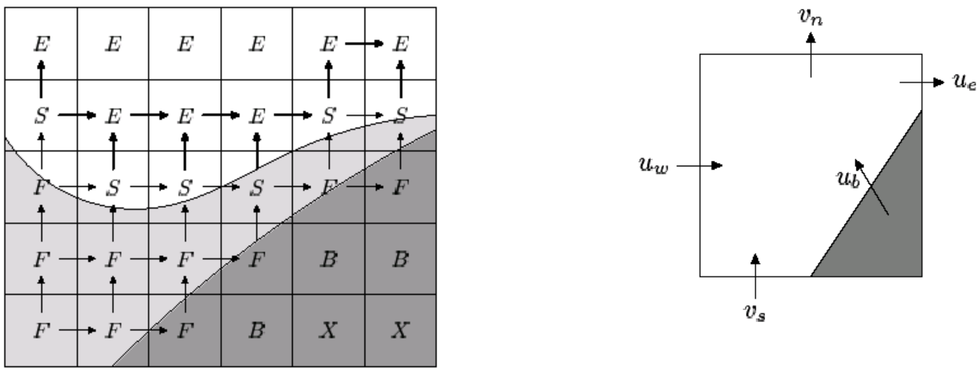

Figure 2.1: The Comflow domain is split in cells; their labels are indicated with capitals.

2.2.2. Discretizatoin of the Navier Stokes equations

Continuity equation

The continuity equation {1} is discretized in each of the F cells. The volume that enters the cell volume must leave the cell or influence the fluid volume in the cell. A two dimensional domain is considered for reasons of clarity. A grid is considered with constant spacing in the vertical and horizontal direction; Δx and Δz are constants. The sides of a single cell are denoted by their orientation, East (*e*), West (*w*), South (*s*), North (*n*), see Figure 2.2.

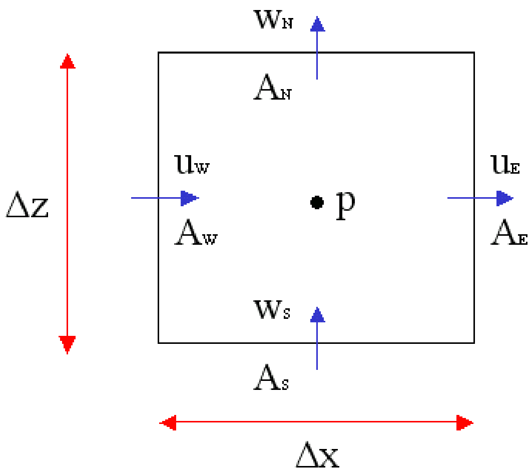

Figure 2.2: Definition of velocities and apertures.

The length of the cell boundary through which fluid can flow is the grid spacing multiplied by the value of the edge aperture (e.g. $\Delta z A_e$.). To obtain the flow through a side boundary this length is multiplied with the velocity in the direction normal to the plane (u_e). The volume of a cell that is open to fluid is the total volume multiplied by the volume aperture ($\Delta x \Delta z F_b$). The discretized continuity equation becomes.

$$\frac{\partial u}{\partial x}+\frac{\partial w}{\partial z}\rightarrow\frac{1}{F_b}\left(\frac{A_e u_e - A_w u_w}{\Delta x}+\frac{A_n w_n - A_s w_s}{\Delta z}\right)=0 \qquad \{10\}$$

Momentum equations

The momentum equations {2} are calculated on the interfaces of FF, FS and SS cell combinations. Information of both cells is used. The discretisation of the momentum equations is explained for the horizontal momentum balance, see equation {11}.

$$\frac{\partial u}{\partial t}+u\frac{\partial u}{\partial x}+w\frac{\partial u}{\partial z}=-\frac{1}{\rho}\frac{\partial p}{\partial x}+\frac{\mu}{\rho}\left(\frac{\partial^2 u}{\partial x^2}+\frac{\partial^2 u}{\partial z^2}\right)+f^{b,x} \qquad \{11\}$$

The local derivative in the momentum equation is discretized in time using explicit forward Euler method.

$$\frac{\partial u}{\partial t}\rightarrow\frac{u_c^{t+\Delta t}-u_c^t}{\Delta t} \qquad \{12\}$$

The advective and the diffusive terms use two cells for discretization. An additional definition of the cell faces is needed for the discretization of the advective terms. Consider two cells that have a vertical interface. The interface forms the central plane (c), the other cell faces are corresponding to their orientation northwest (nw), west (w), southwest (sw), northeast (ne), east (e), southeast (se). Furthermore, u_n is the horizontal velocity, distance Δz above u_c. Similarly, u_s the horizontal velocity distance Δz below u_c. F_w is the volume aperture in the west cell, see Figure 2.3.

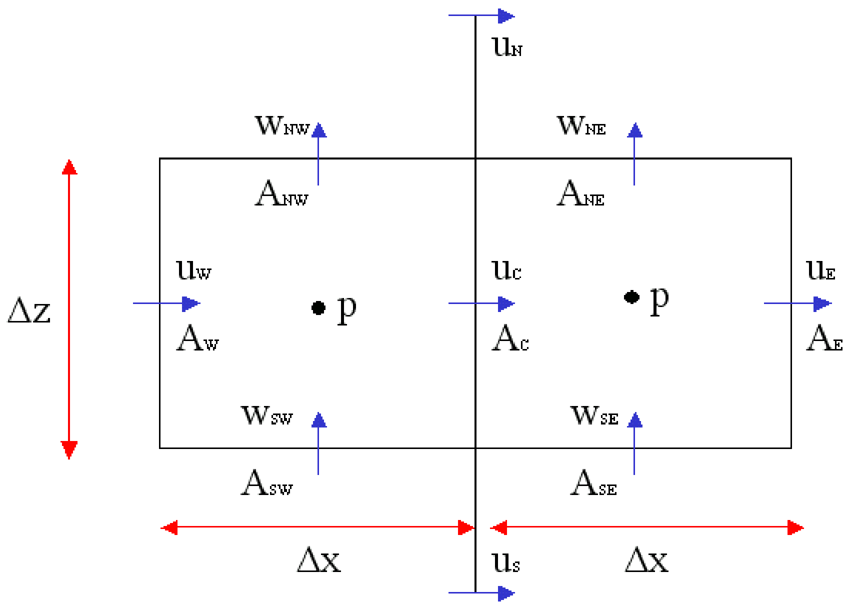

Figure 2.3: Definition of velocities and apertures for two cells.

For the advective term upwind discretization is used.

$$\frac{\partial uu}{\partial x}+\frac{\partial uw}{\partial z}\rightarrow$$
$$\frac{1}{F_w}\left(\frac{A_c u_c u_c - A_w u_w u_w}{\Delta x}+\frac{A_n(u_n+u_c)(w_{ne}+w_{nw})-A_s(u_s+u_c)(w_{se}+w_{sw})}{4\Delta z}\right) \quad \{13\}$$

For Fluid cells the pressure term is discretized using first order central scheme.

$$\frac{\partial p}{\partial x}=\frac{p_e-p_w}{\Delta x} \quad \{14\}$$

The diffusive term is discretized using a central discretization scheme

$$\frac{\mu}{\rho}\left(\frac{\partial^2 u}{\partial x^2}+\frac{\partial^2 w}{\partial z^2}\right)=\frac{\mu}{\rho}\left(\frac{u_e-2u_c+u_w}{\Delta x^2}+\frac{u_n-2u_c+u_s}{\Delta z^2}\right) \quad \{15\}$$

The external forces are discretized similarly.

$$f^{b,x} = g^x \frac{x_e - x_w}{\Delta x} \qquad \{16\}$$

Solution Method

We now have obtained the discretized (indicated with D) continuity equation and the momentum balance in two dimensions.

$$\begin{aligned}
u^{t+\Delta t} &= -w^{t+\Delta t}\frac{\Delta x}{\Delta z} \\
u^{t+\Delta t} &= u^t - \Delta t\left\{\left[\frac{\partial uu}{\partial x} + \frac{\partial uw}{\partial z}\right]_D^t + \frac{1}{\rho}\left[\frac{\partial p}{\partial x}\right]_D^{t+\Delta t} - \frac{\mu}{\rho}\left[\frac{\partial^2 u}{\partial x^2} + \frac{\partial^2 u}{\partial z^2}\right]_D^t + \left[f^{b,x}\right]_D^t\right\} \\
w^{t+\Delta t} &= w^t - \Delta t\left\{\left[\frac{\partial uw}{\partial x} + \frac{\partial ww}{\partial z}\right]_D^t + \frac{1}{\rho}\left[\frac{\partial p}{\partial z}\right]_D^{t+\Delta t} - \frac{\mu}{\rho}\left[\frac{\partial^2 w}{\partial x^2} + \frac{\partial^2 w}{\partial z^2}\right]_D^t + \left[f^{b,z}\right]_D^t\right\}
\end{aligned} \qquad \{17\}$$

The velocity field and the pressures at the next time step are the unknowns. This system of three equations and three unknowns is solved via the expression for the pressure. Substitution yields a Poisson type equation that is solved iteratively with the Gauss-Seidel method with Successive OverRelaxation (SOR). A detailed description is given by [7]. When the pressures at the consecutive time step are known the velocities can be determined.

After the velocities at the new time level are determined the fluid is displaced. First the fluxes through the cell faces are calculated. When the fluxes are known the volume apertures are recalculated with a donor-acceptor algorithm. To reconstruct the free surface of the fluid, [9] concluded the donor-acceptor algorithm with a local height function, as described by [13], yields the best results. Finally cell labels are adjusted.

An upwind parameter is added to the upwind scheme for the momentum equations {13}. The upwind parameter is a weighting factor for the upwind component with value between zero and unity. For an upwind scheme the value of the parameter is unity. Upwind discretization introduces significant artificial damping. If the upwind parameter value is reduced to zero central discretization is obtained, which is unstable. The CFL condition {8} becomes, with α being the upwind parameter:

$$\max\left(\left|\frac{u\Delta t}{\Delta x}\right|, \left|\frac{w\Delta t}{\Delta z}\right|, \left|c\Delta t\right|\right) < \alpha \le 1 \qquad \{18\}$$

An optimum can be found between diffusion and stability, by changing the value of the upwind parameter. In this thesis an upwind parameter of unity is used, having the advection terms as put in equation {13}. At MARIN 2nd order upwind discretization will be implemented.

Free surface

At the free surface the pressure is interpolated, while the velocities are extrapolated. The pressure is determined with the interpolation method proposed by Hirt and Nichols [13]. The velocities at the surface can be split in velocities between surface (S) and empty (E) cells (SE velocities) and velocities between two empty cells (EE velocities). The SE velocities are obtained by constant or linear extrapolation of the velocities in the S cell [7]. Heemskerk [10] made an improvement using quadratic extrapolation of the SE velocities. In the runs in this thesis constant extrapolation is used. The EE velocities are needed in the calculation of the exchange of momentum between two surface cells. The EE velocities are calculated using central discretization of the (no) surface tension boundary condition. The free surface is displaced using Hirt and Nichols method of a local height function [13].

Methods other than presented in [13], have been developed to determine the surface shape and to calculate the velocities and pressures in surface cells. These are subject to further improvement, to optimize the propagation of disturbances through the fluid.

Gerrits [9] made improvements to the free surface reconstruction and advection at the free surface. Fekken [7] made further improvements to the numerical core on how surface velocities and pressures are calculated, to make the model better in line with the physics by reducing the peaky behavior of these parameters.

To simulate waves a relatively fine grid is needed [10,19]. This especially applies to steep waves. Currently three causes are thought to be responsible for the high resolution that is desired. These are:

- The displacement of the free surface.
- Numerical diffusion and dissipation, waves flatten out and energy is lost due to upwind discretization.
- Velocities at the free surface are not interpolated correctly. In the Comflow JIP two phase flow is being developed. Two phase flow simulations will avoid velocity extrapolation.

These issues are dealt with in the JIP, by scientists of MARIN and RuG. The participants of the Comflow JIP are kept up to date with the developments. This thesis focuses on the development of nonlinear Newwave modeling in Comflow.

3. WAVE THEORY

This chapter deals with the wave theories that are relevant for the simulation of nonlinear Newwaves. First, the conditions under which the extreme wave is expected to take place is described in a design spectrum. This spectrum is used to compose the Newwave. Secondly, the wave potential is introduced, as this form the basis of Vijfvinkel's work. Thirdly, Newwave theory is summarized. In appendix A additional information is given on the derivation of the spectrum, nonlinear wave theory and wave kinematics.

3.1. The extreme sea state

A wave field at sea, assumed to be a stationary random process, can be seen as a superposition of numerous regular waves (wavelets) within a certain frequency and directional domain, and with random phases. A sea state is usually described by a variance density spectrum; being a measure for the wave energy distribution over a range of wave frequencies. The spectrum that represents the extreme sea state can be estimated with hindcasts, see Appendix A. The Newwave is derived from the selected spectrum, as will be explained in section 3.5. In this thesis a JONSWAP spectrum is used; it defines the variance density E(ω) as a function of the radian frequency ω.

$$E(\omega) = \frac{320 H_S^2}{T_p^4}\omega^{-5}\gamma^A e^{-\frac{1950}{T_p^4}}$$

$$A = e^{-\left(\frac{\frac{\omega}{\omega_p}-1}{\sigma\sqrt{2}}\right)^2} \qquad \{19\}$$

In equation {19}, the parameter ω_p is the radian frequency of the most energetic wave (rad/s), γ is a peakedness factor equal to 3.3 (-) , and σ (-) a step function, equal to 0.07 for $\omega<\omega_p$ and 0.09 for $\omega\geq\omega_p$.

A discrete spectrum is required to compose the Newwave. In this thesis, the same spectrum is used as Heemskerk [10]. A linear crest height α of 9 (m) is used, the water depth is 30 (m). Once Newwave simulations are modeled correctly the spectrum can be adapted to local design conditions.

Spectrum conversion

Vijfvinkel requires a spectrum that is based on the wave number 1/L, whereas JONSWAP gives the variance density over a radian frequency range. Therefore the linear dispersion relation {27} is substituted in the JONSWAP definition {19}. The spectrum is then discretized in 64 components, with a constant wave number interval Δ(1/L). The spectrum is depicted in Figure 3.1.

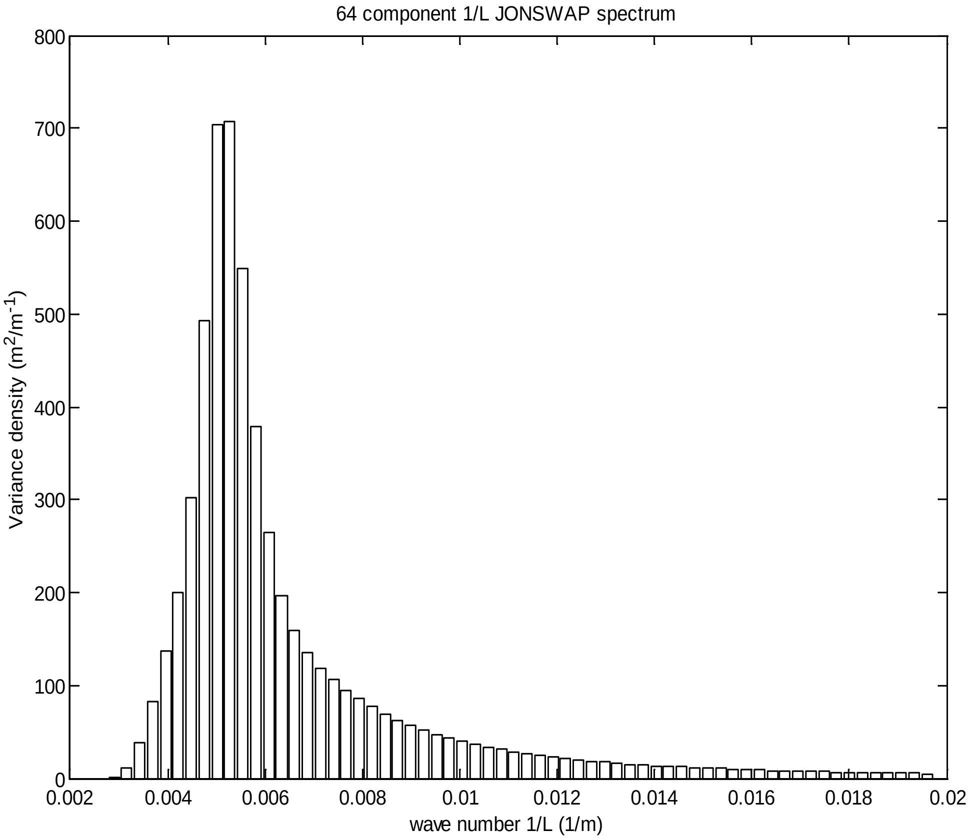

Figure 3.1: Converted JONSWAP spectrum as used for Newwave simulations.

Table 3.1 lists relevant parameters of the discretized JONSWAP spectrum, for the radian frequency based spectrum as well as for the wavenumber based spectrum. In this table, Hs is the significant wave height, M0 the variance, Tp the peak period, ω_{max} the upper cut off radian frequency, ω_{min} the lower cut off radian frequency, $\Delta\omega$ the radian frequency interval. Similarly, $(1/L)_{Peak}$ is the wave number of corresponding to the peak period, $(1/L)_{max}$ the wave number corresponding to the upper cut off radian frequency, etc.

Table 3.1: Discretized JONSWAP spectrum: main parameters.

JONSWAP					
Hs (m)	M0 (m^2)	T_p (s)	ω_{max} (rad/s)	ω_{min} (rad/s)	$\Delta\omega$ (rad/s)
5	1.516	12.87	1.099	0.298	0.0127
JONSWAP discretized over wave number 1/L, d=30 (m)					
	M0 (m^2)	$(1/L)_{Peak}$ (1/m)	$(1/L)_{max}$ (1/m)	$(1/L)_{min}$ (1/m)	$\Delta(1/L)$ (1/m)
	1.516	0.0052	0.0196	0.0029	$2.652\ 10^{-4}$

		L_{peak} (m)	L_{max} (m)	L_{min} (m)	L_{domain} (m)
		189.4	51.0	345.528	3771.1316

The discretization of the spectrum introduces a replication length and period. If the frequency interval Δf is constant, a wave group is created with return period $2\pi/\Delta\omega$. In case of the spectrum presented in section 3.1 the return period is 495 (s). In the runs in this thesis the maximum time span of simulations, 200 (s), is less than half the return period. Similarly, the replication length is $1/\Delta(1/L)$, or 3771 (m).

Applicability wave theories

We have considered a sea state to be described as a stochastically independent process: waves are assumed to be sinusoidal, they can be superimposed and propagate independently. However, wave steepness and the relative water depth influence the shape of the wave and the propagation properties. A linear, sinusoidal, wave in fact only applies for small amplitudes waves in deep water. For high amplitude waves in shallow water, waves have higher harmonics that change the shape of the wave.

Each wave theory has its own range of relative water depth and steepness for which it is applicable. In [21] the wave theory applicability is given as a function of relative water depth d/gT^2 (-) and relative wave steepness H/gT^2 (-).

If waves exceed a threshold value of steepness they break. Wave breaking, solely due to steepness is approximated by the Miche criterion, see equation {20}[21,24]. Parameter k is the wave number in (rad/m), L is the wave length (m), h is the water depth in (m). The wave number usually is defined as $2\pi/L$ with L the wavelength. However, in the context of Vijfvinkel, the wave number is referred to as $1/L$ (1/m), see Chapter 4.

$$\frac{H}{L} \leq 0.14 \tanh(kh) \qquad \{20\}$$

3.2. Wave theory

In this section, an introduction is given to wave theory. Relevant nonlinear wave theories are listed in Appendix A.

The velocity potential φ (m^2/s) is defined as

$$\frac{\partial \varphi}{\partial x} = u \quad , \quad \frac{\partial \varphi}{\partial z} = w \qquad \{21\}$$

With the velocity potential, the velocities, accelerations and displacements can be derived. Substitution of equation {21} in the continuity equation {1} yields the Laplace, or potential, equation.

$$\frac{\partial^2 \varphi}{\partial^2 x} + \frac{\partial^2 \varphi}{\partial^2 z} = 0 \qquad \{22\}$$

To solve the Laplace equation {22} three boundary conditions are introduced; one at the bottom, two at the free surface.

Bottom impermeability states vertical velocity at the bottom is zero, see equation {23}.

$$\frac{\partial \varphi}{\partial z} = 0, \qquad \text{on } z = -h \qquad \{23\}$$

Two surface boundary conditions apply; the kinematic free surface boundary condition and the dynamic free surface boundary conditions. Note that these expressions are both nonlinear.

The kinematic free surface boundary condition tracks the wave surface, the surface water particle velocity equals the surface velocity, see equation {24}.

$$\frac{\partial \varphi}{\partial z} = \frac{\partial \eta}{\partial t} + \frac{\partial \varphi}{\partial x}\frac{\partial \eta}{\partial x} \qquad \text{on} \quad z = \eta(x,t) \qquad \{24\}$$

The dynamic free surface boundary condition describes the interface pressure and is given by the Bernoulli equation (1738). The Bernoulli equation is a combination of the Euler equations and the assumption of irrotational flow ($\frac{\partial u}{\partial z} = \frac{\partial w}{\partial x}$), then integrated in space. The Bernoulli equation expressed in terms of the velocity potential

$$-\frac{\partial \varphi}{\partial t} + \frac{1}{2}\left(\left(\frac{\partial \varphi}{\partial x}\right)^2 + \left(\frac{\partial \varphi}{\partial z}\right)^2\right) + \frac{p}{\rho} + g\eta = 0 \qquad \{25\}$$

The atmospheric pressure is assumed zero at still water level, $p = p_{atm} = 0$. With the dynamic free surface boundary condition the pressure at the free surface is taken equal to the atmospheric pressure.

As these free surface boundary conditions {24}, {25} are nonlinear, no analytical solutions exist. These terms can only be approximated. Linear wave theory (Airy wave theory) neglects the nonlinear terms. Stokes theory use Taylor expansion of the nonlinear terms around the still water level, z=0 (m).

Substitution of the bottom boundary condition {23} and the kinematic free surface boundary condition {24} yields the velocity potential. For linear wave theory the velocity potential becomes, with parameter a being the amplitude:

$$\varphi(x,z,t) = \frac{ag}{\omega}\frac{\cosh(k(h+z))}{\cosh(kh)}\sin(kx-\omega t) \qquad \{26\}$$

The dispersion relation shows the relation between the wave frequency and the wave number. The dispersion relation is obtained by substitution of equation {25} in equation {26}. For linear wave theory the dispersion relation reads:

$$\omega^2 = gk\tanh(kh) \qquad \{27\}$$

3.3. Newwave theory

The Newwave is representative for the design wave [22,23]. Newwave theory is based on both the spectral representation of the extreme sea state, and the statistically determined extreme wave height.

The Newwave theory was developed in 1991 at Shell Research [25,26]. Previously, regular 5th order Stokes wave theory was used to determine water kinematics and dynamics of the ULS design wave. Newwave theory represents the design wave by decomposing the design spectrum in unidirectional wavelets. These wavelets come in phase at the location, time and height of interest. The wave amplitude gradually increases before and decreases after its peak due to the wide range of phase speeds. The height of the Newwave is corrected with a spectral amplification factor, to correspond with the statistically determined crest height. In mathematical terms the Newwave is the autocorrelation function multiplied by the crest height.

Lindgren (1970) made an analysis on the maxima of Gaussian processes and gave a nonlinear mathematical formulation to the shape of an arbitrary crest. Tromans et al. [23] used Lindgren's findings to develop the linear Newwave in 1991. Lingren and Tromans converge as the crest height increases; Lindgren shows better resemblance for small and intermediate size crests while the Newwave gives excellent agreement for high crests [15].

For focusing of a Newwave the surface elevation of the wave is the crest elevation *a*, times the autocorrelation function $\varrho(\tau)$, with τ being the time to focus time.

$$\eta(\tau) = E(\eta_t \mid \eta_0 = \alpha, \frac{\partial \eta}{\partial t}_0 = 0) = \alpha \rho(\tau) \qquad \{28\}$$

With τ = t-t$_0$ (s), X = x-x$_0$ (m), α the crest height (m), $\varrho(\tau)$ the autocorrelation function. The discrete autocorrelation function is defined as:

$$\rho(\tau) = \frac{1}{\sigma^2} \sum_n S(\omega) \Delta\omega_n \cos \omega_n \tau \qquad \{29\}$$

With σ^2 the variance and n the number of spectral components. Substitution of equation {29} in equation {28} yields the linear Newwave surface elevation

$$\eta(X, \tau) = \frac{\alpha}{\sigma^2} \sum_n d_n \cos(k_n X - \omega_n \tau) \qquad \{30\}$$

With d_n the contribution of the wavelet to the variance, σ the variance of the spectrum, X the distance from the focus point in the direction of propagation. The water particle velocities and accelerations are calculated according to linear wave theory, using the amplitude above. As linear theory is only valid up to the still water level a stretching method needs to be chosen. The influence of directional spreading causes a reduction of some ten percent compared to the focusing of a unidirectional wave group.

The linear crest height α is half of the maximum linear wave height H_{max}. With Hs = $H_{rms}\sqrt{2}$ (m) , the relation between the significant wave height, the number of waves N and the linear crest height becomes:

$$\alpha = \frac{H_s}{2} \sqrt{\frac{1}{2} \frac{\ln(N)}{1 - e^{Ne^{-\frac{4\alpha^2}{H_{rms}^2}}}}} \approx \frac{H_s}{2} \sqrt{\frac{1}{2} \ln(N)} \qquad \{31\}$$

Jonathan and Taylor [15.16] extended the Newwave in 1995 to second order by using a linearized second order correction β. Jonathan and Taylor set the second order Stokes term, 0.5ka^2 equal to β. For crests (c) and troughs (t) the second order contributions yields β = 1/2(c+t). The value of β can be estimated from the shape of the spectrum and the wave amplitude. Given a measured time series and thus an estimated value of β, we can reconstruct a linear time series. This is an iterative process for which Creamer found an efficient method using FFT [15.16,25]. This method can also be inverted creating a nonlinear time series from a linear one. A 95% confidence interval graph is available indicating the value of β as a function of linear wave amplitude and a design spectrum shape.

The Tern platform was well equipped with measuring equipment when it was hit by the February 3, 4 storm in 1993 which had a significant wave height of 12 meters and a peak period of 14 seconds. The second order Newwave theory showed good agreement with the measurements taken of these large waves [15,16].

4. VIJFVINKEL

In this thesis, use is made of a method developed by Vijfvinkel [25]. This code was selected to model nonlinear Newwaves as it met the objectives and was available. In this chapter, the numerical method is briefly summarized. A more detailed explanation is given in [8]. In the second section the validation of Comflow and Vijfvinkel are discussed.

4.1. Governing equations

Vijfvinkel simulates the nonlinear propagation of disturbances of the free surface, based on a [5]. The method is one dimensional and applicable for irrotational, time dependent, spatially periodic surface waves in constant depth. Objects can not be implemented. It approximates the Laplace equation {22} using bottom boundary condition {23} and the kinematic and dynamic free surface boundary conditions {24}, {25}. It is a spectral method and switches from a spatial domain to a frequency domain using FFT. A motion that is periodic in the spatial domain *L* is assumed, with U the mean horizontal velocity.

$$\begin{aligned} \eta(x+L,t) &= \eta(x,t) \\ \varphi(x+L,z,t) &= \varphi(x,z,t) + UL \end{aligned} \qquad \{32\}$$

The Dirichlet-Neumann operator, or G(η) operator, is a pivot in the solution algorithm. This operator uses both the value of the velocity potential at the free surface, φ^S, and derivative of this potential at the boundary normal to the free surface.

$$G(\eta)\varphi^S = \frac{\partial\varphi}{\partial z} - \frac{\partial\eta}{\partial x}\frac{\partial\varphi}{\partial x} \qquad \{33\}$$

The velocity potential at the surface can be written as:

$$\frac{\partial\varphi^S}{\partial x} = \frac{\partial\varphi}{\partial x} + \frac{\partial\eta}{\partial x}\frac{\partial\varphi}{\partial z} \qquad \{34\}$$

Substitution of the expression for G(η) in the governing equation results in the following set of equations. The kinematic {24} and dynamic {25} free surface boundary conditions can be written in terms of the G(η) operator:

$$\frac{\partial\eta}{\partial t} - G(\eta)\varphi^S = 0 \qquad \{35\}$$

$$\frac{\partial \varphi^S}{\partial t} + \frac{1}{2(1+(\frac{\partial \eta}{\partial x})^2)}\left((\frac{\partial \varphi^S}{\partial x})^2 - (G(\eta)\varphi^S)^2 - 2\frac{\partial \eta}{\partial x}\frac{\partial \varphi^S}{\partial x}G(\eta)\varphi^S \right) - g\eta = 0 \qquad \{36\}$$

The Dirichlet-Neumann operator plays a central role, it is expanded around the still water level in a Taylor series. The first order approximation returns the linear wave theory. Coifman and Meyer showed that the expression for $G^M(\eta)$ is converging [25].

$$G^M(\eta) = \sum_{j=0}^{M} G_j(\eta) \qquad \{37\}$$

4.2. Numerical model

The governing equations {35} and {36} can be written in vector notation, with $\vec{y}, A, \vec{b}$ defined as follows:

$$\vec{y} = \begin{bmatrix} \eta \\ \varphi^S \end{bmatrix}$$
$$A = \begin{bmatrix} 0 & G(0) \\ -g & 0 \end{bmatrix} \qquad \{38\}$$
$$\vec{b} = \begin{bmatrix} G(\eta)\varphi^S - G(0)\varphi^S \\ \frac{1}{2(1+(\frac{\partial \eta}{\partial x})^2)}\left((\frac{\partial \varphi^S}{\partial x})^2 - (G(\eta)\varphi^S)^2 - 2\frac{\partial \eta}{\partial x}\frac{\partial \varphi^S}{\partial x}G(\eta)\varphi^S \right) \end{bmatrix}$$

The equations reduce to the form:

$$\frac{\partial \vec{y}}{\partial t} - A\vec{y} = \vec{b}(x,t) \qquad \{39\}$$

The solution of this equation is

$$\vec{y}(x,t) = e^{At}\vec{y}(x,0) + e^{At}\int_0^t e^{-As}\vec{b}(x,s)ds \qquad \{40\}$$

The first term on the right hand side of the equation sign is the homogeneous solution, which is the linear wave, and can be solved exactly. The last term of equation {41} is the particular solution and has the nonlinear parts. With the use of the Dirichlet-Neumann operator the governing equations are reduced to a set of equations that have to be solved in time. To approximate this integral a second order Adams Bashforth scheme is used:

$$\int_0^t e^{-As}\vec{b}(x,s)ds \rightarrow \int_0^{\Delta t} e^{-As}ds\left[\frac{3}{2}\vec{b}(x,t)-\frac{1}{2}\vec{b}(x,t-\Delta t)\right] \qquad \{41\}$$

Having G(η) expressed in a Taylor series the set of equations can be solved. The surface elevation and the velocity potential at the surface are obtained at the next time step, t = t+Δt. This method is computationally attractive since FFT can be used for both the surface elevation and velocity potential.

Vijfvinkel [25] modeled regular 5th order Stokes waves as well as focusing wave groups. Laboratory tests done by Baldock at Imperial College showed slightly lower crest heights at the point of focus, but this was caused by friction. A limitation for future extensions to the Craig and Sulem method is that the free surface must be single valued; so breaking waves can not be simulated.

Kinematics

The horizontal and vertical velocities underneath the free surface can be determined using two methods [25]. Both use a record for the free surface elevation in space. In addition, the first method uses a spatial record of the surface velocity potential, while the second method uses the velocities at the surface.

The fluid particle velocities are given by the spatial derivatives of the velocity potential {21}. Substitution in the expressions for the Dirichlet Neumann operator {33} and the velocity potential {34} yield the expressions for the horizontal and vertical velocities at the free surface u^s and v^s.

$$u^S = \frac{\dfrac{\partial \varphi^S}{\partial x} - \dfrac{\partial \eta}{\partial x}G(\eta)\varphi^S}{1+\left(\dfrac{\partial \eta}{\partial x}\right)^2}$$
$$v^S = \frac{\dfrac{\partial \eta}{\partial x}\dfrac{\partial \varphi^S}{\partial x} + G(\eta)\varphi^S}{1+\left(\dfrac{\partial \eta}{\partial x}\right)^2} \qquad \{42\}$$

The velocities underneath the surface can be determined with two methods.

Method 1:

The velocity profile is calculated using a Fourier method proposed by Fenton and Rienecker [8]. The velocity potential becomes:

$$\varphi(x,z,t) = Ux + \frac{1}{N}\sum_{-\frac{1}{2}N}^{\frac{1}{2}N} A_n(t)\cosh(k_n(z+h))e^{ik_n x} \qquad \{43\}$$

The complex coefficients $A_n(t)$ are calculated for the velocity potential at the free surface and the slope of the free surface at time t. Differentiation of the expression above with respect to the horizontal and vertical coordinates gives respectively the horizontal and vertical velocities.

Method 2:

The velocity profile is calculated in a similar way to method 1, however we use a Fourier series for the velocities instead of the potential.

$$\begin{aligned} u(x,z,t) &= U + \frac{1}{N}\sum_{-\frac{1}{2}N}^{\frac{1}{2}N} B_n(t)\cosh(k_n(z+h))e^{ik_n x} \\ v(x,z,t) &= \frac{1}{N}\sum_{-\frac{1}{2}N}^{\frac{1}{2}N} B_n(t)\sinh(k_n(z+h))e^{ik_n x} \end{aligned} \qquad \{44\}$$

Using the surface velocities the complex coefficients B_n can be determined at time t.

The method using the Fourier expression of the velocities {45} shows better numerical behavior in case of steep waves [25]. Small numerical errors in method 1 can result in large deviation of the velocities at near the surface [2,25].

Optimization

The numerical stability is enhanced using a five point smoothing function. This low pass filter smoothes the growth of high wave numbers.

$$\Lambda(k_n,\nu) = \begin{cases} 1 \\ \frac{1}{8}\left(5 + 4\cos\left(\frac{\pi|k_n|}{k_{N/2}}\right) - \cos\left(\frac{2\pi|k_n|}{k_{N/2}}\right)\right) \end{cases} , \quad \begin{cases} |k_n| - 1/|k_{N/2}| \le 1-\nu \\ |k_n| - 1/|k_{N/2}| > 1-\nu \end{cases} \qquad \{45\}$$

In Vijfvinkel's code the filter is applied before inverse FFT operations are performed and at the end of each time step. The expression for the wave numbers that are not affected by the smoothing function are:

$$\nu \leq 1 + L / N\pi - 2n\pi / L \quad \{46\}$$

For $\nu = 0.3$ and domain length 1000 (m) the first 45 wave numbers are unaffected.

The accuracy of Vijfvinkel's code is measured in terms of conservation of energy and momentum

$$\begin{aligned} E &= \frac{1}{2}\int_S \varphi^S G(\eta)\varphi^S + g\eta^2 dx \\ I &= \int_S \varphi^S \frac{\partial \eta}{\partial x} dx \end{aligned} \quad \{47\}$$

Truncation of the Taylor series approximation of the Dirichlet-Neumann operator introduces errors. This error depends on the order of truncation and the magnitude of nonlinear effects in the solution. However, there is an optimal order of truncation M, depending on both the nonlinearity of the case and the number of components. Reference is made to [1] which states the optimal choice of this parameter.

4.3. Validation of Comflow and Vijfvinkel

This section deals with the validation procedures that were used to validate Comflow and Vijfvinkel's code.

Vijfvinkel programmed several wave theories. The programs that are recovered are the Stokes 5 program and the Newwave program. The difference in these programs lays in the prescription of the input and the generation of output. The numerical core is identical. Vijfvinkel used a wave group program to validate his code with wave group experiments done by [1,2] and found good agreement. The deviation from the physical experiments was mainly caused by (physical) damping in the wave tank. In the numerical simulation the energy dissipation was minimal (0.1 % over 30 periods).

Heemskerk [10] validated his Newwave algorithm in Comflow with the results of the wave group simulations of Vijfvinkel. However, the input conditions for the wave group are not in agreement with Newwave theory. Heemskerks validation of the Newwave simulation in Comflow will not be used for the following reasons:

- Baldock uses a wave group that has a different spectrum than the Newwave we consider. 29 wavelets are considered, split equally over a period range [Tb, Te]. The amplitudes of each of the components are the same, being $1/29^{\text{th}}$ of the linear focus elevation. This is not related to the 64 wavelet JONSWAP spectrum we consider in the Newwave.
- The data from the physical experiment done by Baldock are not available. No quantitative comparison can be made with the physical tests.

- Having Vijfvinkel's program, and having it running, the input for the Newwave simulation can be chosen freely. Conditions identical to the cases of interest can be taken to validate.

No experimental data exists with which simulated nonlinear Newwaves can be validated. The validity of the simulations must be derived from logical steps; what is the influence of wave steepness, what is the influence of the water depth, do bound waves remain bound etc. For this reason some experiments are set up to assess the capabilities of Comflow and Vijfvinkel. These are reported in chapter 5.

5. EXPERIMENTS

In this chapter four experiments are presented. The introduction gives the thread of these experiments.

5.1. Introduction

In this chapter the computer models Comflow and Vijfvinkel are subjected to four tests. These tests will show the capabilities of both programs and will be used to indicate the applicability for the desired purpose; extreme wave impact modeling on offshore structures.

The setup of these experiments is the following: first Comflow is subjected to an experiment that is used as benchmark for CFD codes. Then propagation and damping is assessed for low amplitude waves for which nonlinearity plays a minor role. Thirdly the steepness is considered, for which nonlinearity becomes increasingly important. In the last experiment the link is made to nonlinear Newwaves. These nonlinear Newwaves are simulated in Vijfvinkel. With the findings for Comflow regarding propagation and damping (second experiment) and steepness (third experiment) the basis for coupling of these two programs is established. Table 5.1 gives an overview of the experiment, Table 5.2 states the measures that are used.

Table 5.1: Schematic overview of the experiments.

REGULAR WAVES			
Beji Battjes	*Benchmark*		
	water depth	Steepness	Nonlinearity
Sloshing Tank	*Deep-Shallow*	*Small*	*Small-medium*
Steep Waves	*Transitional*	*Small-Large*	*Small-Large*
NEWWAVES			
Newwaves	*Transitional*	*Large*	*Large*

Table 5.2: Measures used for experiments.

	Theory	Comflow	Vijfvinkel	Physical Experiment
Beji Battjes		X		X
Sloshing Tank	X	X		
Steep waves	X	X	X	
Newwaves	X		X	

The following is an introduction to the four experiments that are presented in this chapter:

- The Beji Battjes test simulates the nonlinear generation of higher harmonics as regular waves pass a submerged bar. This test has been performed in a laboratory wave tank and has become a benchmark for wave models. The goal of the computational simulation is to assess the performance of Comflow; is Comflow able to simulate the nonlinear generation of the higher harmonics correctly? It is experienced that especially after the waves have passed the bar, models can show increasing differences with the physical measurements. Several grid resolutions and time steps are used. Vijfvinkel uses a constant depth, so this experiment is not run in this code. The results of the Beji Battjes experiment are presented in section 5.2 and Appendix B.
- The Sloshing Tank experiment is done to assess the propagation and damping characteristics of Comflow, relative to the physical propagation and viscous damping. Several relative water depths are used. A tank is used in which a single sinusoidal wave is set as initial condition, with velocities zero and the crest centered in the tank. The amplitude and period of the standing wave is measured in the center of the tank. The wave frequency equals the tank' second natural frequency. Several grid resolutions and time steps are used. Vijfvinkel uses a homogeneous domain in which impermeable boundaries are not implemented. The results of the sloshing tank experiment are presented in section 5.3 and Appendix C.
- In the third experiment steep, regular waves are simulated in Comflow and Vijfvinkel. Several values for the relative steepness are used, up to the breaking limit. The goal is to assess the performance of both programs of modeling steep waves. The results of the Steep Wave experiment are presented in section 5.4 and Appendix D.
- The fourth experiment simulates nonlinear Newwaves. The goal is to assess the influence of a nonlinear model in comparison to the linear theory, and to assess the applicability of Vijfvinkel's program for Comflow. The time span of the (nonlinear) runs is varied. The simulation of nonlinear Newwaves is presented in section 5.5 and Appendix E.

5.2. Beji Battjes experiment

5.2.1. Goal

The goal of the Beji Battjes [3] test is to assess Comflow's abilities to simulate nonlinear wave formation, propagation and the release of the bound harmonics. The Beji Battjes test serves as benchmark for wave resolving models.

The test is set up to simulate the nonlinear generation of higher harmonics by a submerged bar and the uncoupling of the nonlinear components after the bar is passed [26]. Beji and Battjes performed a laboratory experiment that originally had been used to validate a numerical Boussinesq model [3]. Boussinesq models are in particular designed to simulate waves in relatively shallow water ($kd<<1$) with (near shore) coastal engineering applications. Several authors have since used this as a benchmark to validate numerical models, i.e. [4,20]. In this thesis the data of the original laboratory experiment has been used.

A correct simulation of the generation of nonlinear terms and the nonlinear propagation is essential for the simulation of Newwaves. However, the release of the bound harmonics after the bar has been passed has little relevance with the simulation of the impact of Newwaves on offshore structures. Nevertheless, this is of general interest to gain insight in the capabilities of Comflow.

5.2.2. Experiment setup

The Beji Battjes test consists of a wave tank with a submerged bar and a slope at the end to dampen the waves. The water depth is 0.4 (m) and at the bar 0.1 (m). The wave paddle produces sinusoidal, 0.01 (m) amplitude, waves with a period of 2.02 (s). The time series at the points of measurement are visualized from 30 to 40 (s) after the start of the test from rest, as in the original paper.

The setup of the experiment is visualized in Figure 5.1.

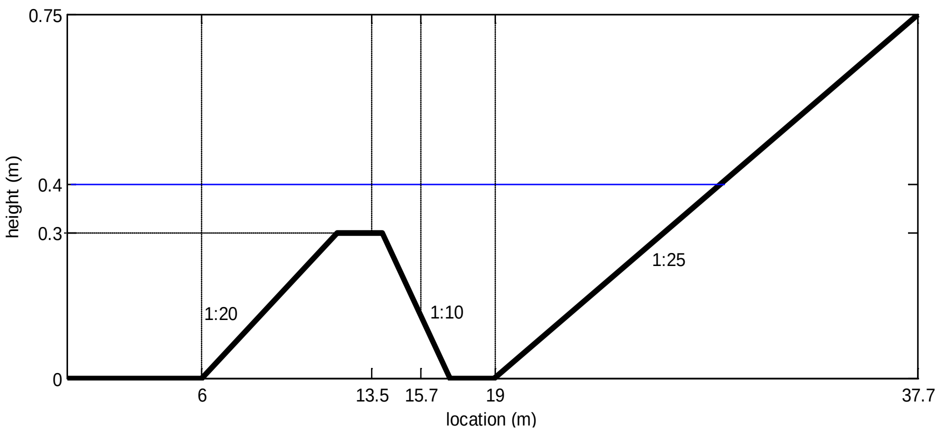

Figure 5.1: Beji Battjes experiment setup.

How does the water depth in the Beji Battjes test relate to the water depth of offshore structures that are subjected to Newwaves? The range of relative water depths of offshore design waves, represented by the Newwave, is classified as deep to intermediate. Typical values of this relative water depth are shown in Table 5.3. The values for the relative water depth at the Tern and Sakhalin platforms are for the most energetic waves. In relatively deep water, nonlinear effects are less pronounced.

Table 5.3: Typical values of relative water depth kd (-).

	kd (-)
Shallow water	< ~0.3
Intermediate water depth	~0.3 < kd < ~3.1
Deep water	kd > ~3.1
Beji Battjes tank	0.67
Beji Battjes bar	0.32

Tern	~1.2
Sakhalin (d=35 m)	~1.1
Sakhalin (d=47 m)	~1.3

5.2.3. Simulations

Several parameters have been changed to obtain insight in their impact on the simulation. The parameters that are changed are the grid size, the time step and the wave theory that is used at the inflow boundary. Four time series are recorded at location 6, 13.5, 15.7 and 19 corresponding with their horizontal coordinate (in meters).

First, general relations of these parameters on the evolution of waves in Comflow are derived. These relations are presented with Comflow runs lasting 200 seconds, starting from an initially undisturbed setup. Secondly the recordings at each of the locations of measurement are analyzed, this is done over the time interval t=(30,40), as is done in the papers on the Beji Battjes test.

The denotation of the grid size and time step in dimensionless terms is the following. The fundamental wave is the wave that the inflow boundary inserts into the Comflow domain. The period of this regular wave is 2.02 (s), the wavelength is 3.738 (m) in water depth of 0.4 (m). The grid is characterized by the distance between two grid points, Δx, relative to the wavelength, L. By inverting this number the number of grid points per wavelength is returned. A similar approach applies to the denotation of the time step. The time step, Δt, is divided over the period of the fundamental wave, T.

Meskers [19] recommends for the simulation of regular waves in Comflow:

- The grid aspect ratio: $\Delta x/\Delta z = 1$ (-).
- The grid size: $\Delta x/L > 1/80$ (-).
- The time step: $\Delta t/T = 1/500$ (-).

In this section the grid size and time step are varied. The grid aspect ratio recommendation is followed, with exception of section 5.3.5 and 5.3.6.

A series of twelve runs were performed using the dimensionless numbers as a base. Runs were performed using $\Delta x/L$ (-) values of 1/50, 1/100, 1/250 and 1/500 and time stepping $\Delta t/T$ (-) of 1/100, 1/500 and 1/1000. This is given in Table 5.4. The simulation time is 200 (s) for all runs. Linear wave theory is used to prescribe the inflow boundary. For each of the twelve runs four time series are registered at the locations of measurement, as indicated in Figure 5.1, making the total number of time series 48.

Table 5.4: Overview Comflow simulations of the Beji Battjes experiment. Indicated is the ratio between computing time over simulated time.

Computing time/ simulation time (-)	$\Delta x/L$ = 1/50 (-)	$\Delta x/L$ = 1/100 (-)	$\Delta x/L$ = 1/250 (-)	$\Delta x/L$ = 1/500 (-)
$\Delta t/T$ = 1/100 (-)	6	36	276	582
$\Delta t/T$ = 1/500 (-)	18	78	318	1338
$\Delta t/T$ = 1/1000 (-)	30	132	456	3294

For the $\Delta x/L$=1/500 (-), $\Delta t/T$ = 1/100 (-) run linear, Stokes 2 and Stokes 5 wave theory was used to prescribe the inflow boundary. For the $\Delta x/L$=1/500 (-), $\Delta t/T$ = 1/1000 (-) linear and Stokes 2 wave theory were used.

The Courant numbers, see equation {8}, of the runs above are indicated in Table 5.5. The phase velocity of the fundamental wave in the deep water is limiting for the Courant condition. The phase velocity of the higher harmonics that are generated and released is equal or smaller. For some runs the capitals A,B or C are added, see Table 5.5. The simulations with the matching capitals are compared in section 5.2.4.

Table 5.5: Courant number for the Beji Battjes simulation. The capitals indicate the runs that are compared in section 5.2.4.

Courant numbers	$\Delta x/L$ = 1/50 (-)	$\Delta x/L$ = 1/100 (-)	$\Delta x/L$ = 1/250 (-)	$\Delta x/L$ = 1/500 (-)
$\Delta t/T$ = 1/100 (-)	0.91	>1	>1	>1
$\Delta t/T$ = 1/500 (-)	0.18	0.36 A B	0.91 A C	>1
$\Delta t/T$ = 1/1000 (-)	0.09	0.18 B	0.45	0.91 C

The time series of these simulations, excluding those of the coarsest grid, are given in Appendix B.

5.2.4. Relations

The following observations were done with regard to the evolution of the waves in the Comflow simulation of the Beji Battjes experiment.

To support the findings of the numerical simulations only the results of two runs are used for clarity reasons. The outcome of the other runs is in agreement with the findings that are represented by these runs. First the grid size is increased while keeping the time step constant. Secondly the time step is made smaller while keeping the grid size constant. Thirdly the Courant number is kept equal, and both grid and time step together are varied.

Grid size (comparison A-A)

To assess the influence of the grid size on the evolution of waves in Comflow the grid was made finer, and the effect on the waves was registered at the locations of measurement. The time step was kept constant at $\Delta t/T = 1/500$ (-), see Table 5.6. The Courant number is larger for the grid with the high resolution.

Table 5.6: Grid size refinement: comparison simulations AA.

Grid size $\Delta x/L$ (-)	Time step $\Delta t/T$ (-)	Courant number
1/100	1/500	0.36
1/250	1/500	0.91

During the time interval in which the results are visualized, the mean water level in location 6 is underestimated, see Figure 5.2. At location 6 no harmonics are formed, as it is just in front of the bar.

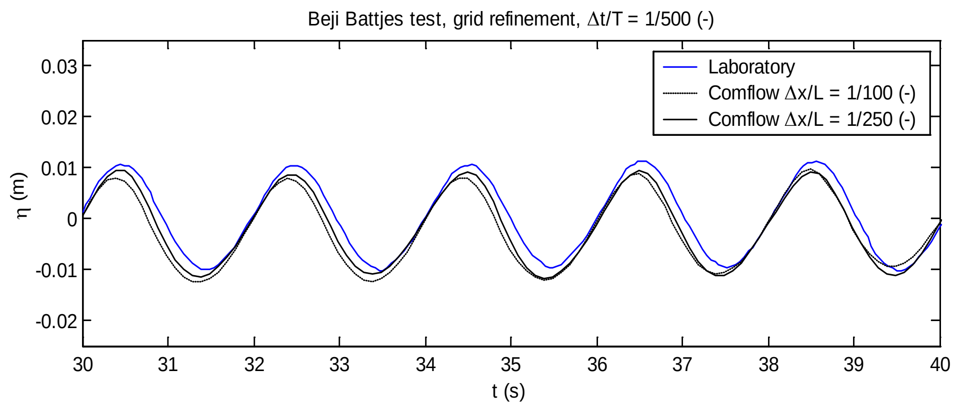

Figure 5.2: Comparison Comflow simulation with laboratory measurements at location 6.

The simulated time span was increased to 200 seconds to see if the lowering of the mean water level is part of a fluctuation of a longer time scale that eventually lead to instability. Both runs fulfill the Courant condition. In Figure 5.3 the minimum and maximum elevation of the simulation over 200 seconds is depicted. The fist 40 seconds of the simulation show a correct wave amplitude but a temporal lowering of the mean water level. After 40 seconds the extremes show variation and wave height decreases slowly. The run with the finer grid spacing shows a more peaked evolution of maxima and minima, see also Figure 5.5.

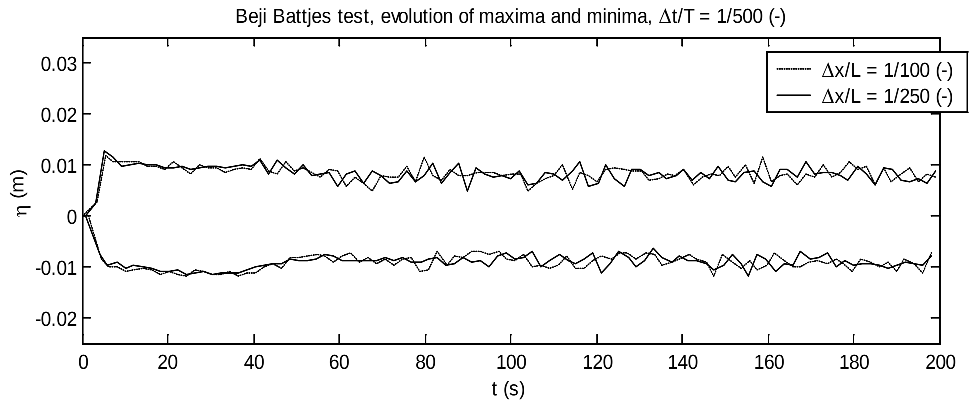

Figure 5.3: Evolution of the local maxima and minima at location 6 with a grid refinement.

The sag in water level is expected to be caused by the method with which regular waves at the domain boundary are prescribed. Initially, the water in the Beji Battjes experiment is at rest. In the Comflow simulation, the wave kinematics and surface elevation are prescribed without a start up procedure. This start up procedure would gradually increase the wave amplitude and velocities. A possible cause of the sag in water level in the first 40 (s) is the transition at the boundary; the sudden start of the wave maker at the domain boundary creates a shock wave that is translated in the sagging water level. This wave is absorbed at the other side of the domain, at the beach.

A start up procedure for regular waves is expected to prevent a sag in water level. Discontinuities in kinematics at the inflow boundary is thought to be responsible for the sag, for the simulations where the fluid initially is at rest.

Time step (Comparison B-B)

The influence of a refinement of the time step on the simulation is now taken into account, see Table 5.7. The grid resolution is kept constant while the time step is made smaller. The Courant number decreases.

Table 5.7: Time step refinement: comparison simulations BB.

Grid size $\Delta x/L$ (-)	Time step $\Delta t/T$ (-)	Courant number
1/100	**1/500**	0.36
1/100	**1/1000**	0.18

Refinement of the time step of the $\Delta x/L = 1/100$ run has little influence, see Figure 5.4. The solid line ($\Delta t/T = 1/500$ (-)) is not significantly different from the dotted line ($\Delta t/T = 1/1000$ (-)). At 80 seconds a local maximum occurs.

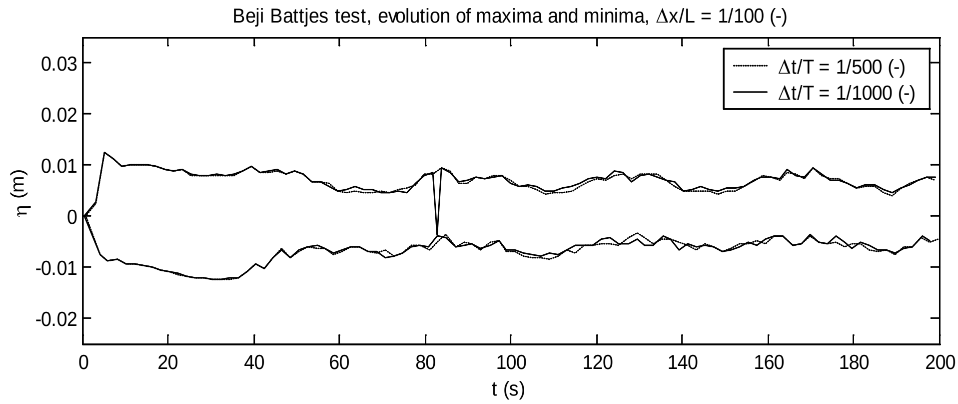

Figure 5.4: Evolution of the local maxima and minima at location 6 with a time step refinement.

Grid and time step refinement (Comparison C-C)

Now the influence is studied of a simultaneous refinement of both the time step and grid spacing. The Courant number is kept equal, see Table 5.8.

Table 5.8: Combined grid size and time step refinement: comparison simulations CC.

Grid size $\Delta x/L$ (-)	Time step $\Delta t/T$ (-)	Courant number
1/250	**1/500**	0.91
1/500	**1/1000**	0.91

The simulation with a finer grid and time step shows a smoother development of minima and maxima, with less damping. This can be seen in the evolution of the minima and maxima, as depicted in Figure 5.5.

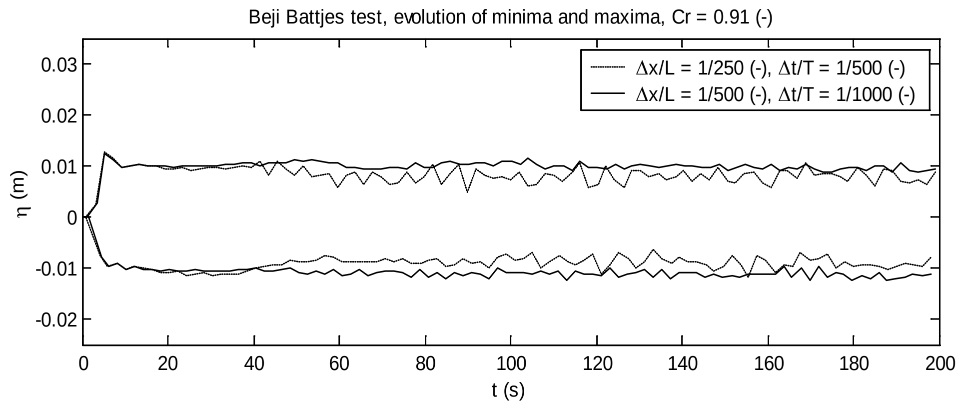

Figure 5.5: Evolution of the local maxima and minima at location 6 with a combined grid size and time step refinement.

Interestingly, the sag in the water level, which was observed in the runs with coarser grids and time steps, is not pronounced, see Figure 5.5. The wave inflow procedure at the boundary is the same for all simulations. The expectation that the sag in water level, as was observed in Figure 5.3 and Figure 5.4 was solely caused by the wave input, is now extended. The combination of the grid and time step is of influence of the sag in water level. The sag in water level as was observed in Figure 5.3 and Figure 5.4, is expected to be related to incorrect simulation of the waves passing the submerged bar.

Wave theory

The wave theory that is used to prescribe the inflow boundary is varied for the run that uses $\Delta x/L = 1/500$ (-), $\Delta t/T = 1/1000$ (-). Linear, second and fifth order Stokes wave theory are used to prescribe the inflow boundary. The relative water depth is classified as intermediate, kd = 0.67 (-). The wave steepness H_0/gT^2 is $5*10^{-4}$ (-), which is small. The linear inflow boundary gives a good representation, and the inflow boundaries prescribed by second and fifth order Stokes wave theory showed no significant improvement, see Figure 5.6.

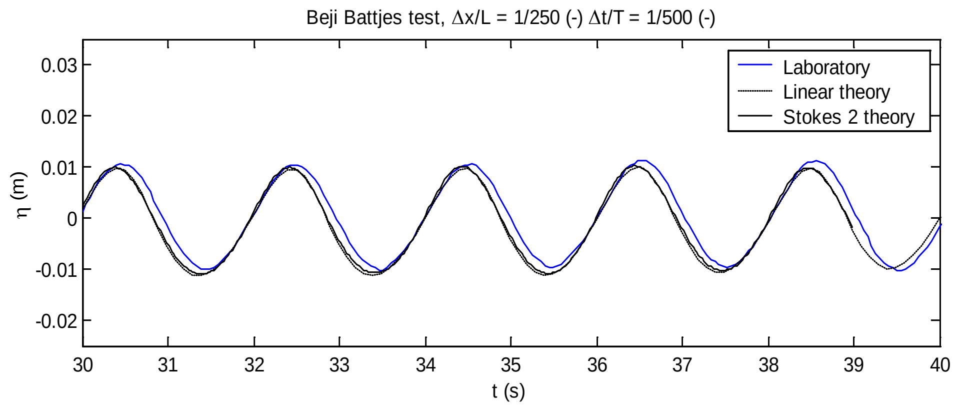

Figure 5.6: Effect wave theory that prescribes the inflow boundary on wave signal at location 6.

Damping

The amplitude of the wave decreases gradually due to artificial damping caused by the first order upwind discretization method, see [11]. The numerical damping can be reduced by changing the upwind parameter from unity (upwind discretization) towards zero (central discretization). However, if the upwind parameter is reduced the model can become unstable. An optimum needs to be found between numerical damping and stability. In this thesis the choice is made for stability: an upwind parameter value of one is maintained.

5.2.5. Analysis

In the previous section local extremes are considered to assess the evolution of waves in Comflow. In this section we focus on the time series that are obtained from one simulation. The time series at the four locations of measurement are analyzed for the runs with the finest grid $\Delta x/L=1/500$ (-)

and time step Δt/T=1/1000 (-). The time series of the Comflow simulation and the Laboratory experiment are depicted in Figure 5.7. The Courant number is 0.91. The time series at the first two locations show reasonable resemblance with the recordings from the laboratory wave tank. The phase shows a small deviation and in the second time series the secondary peak is underestimated. The time series at location 15.7 and location 19 show larger deviation and it can not be judged with the bare eye what is incorrect since several frequencies are represented; only with additional analysis the errors can be extracted.

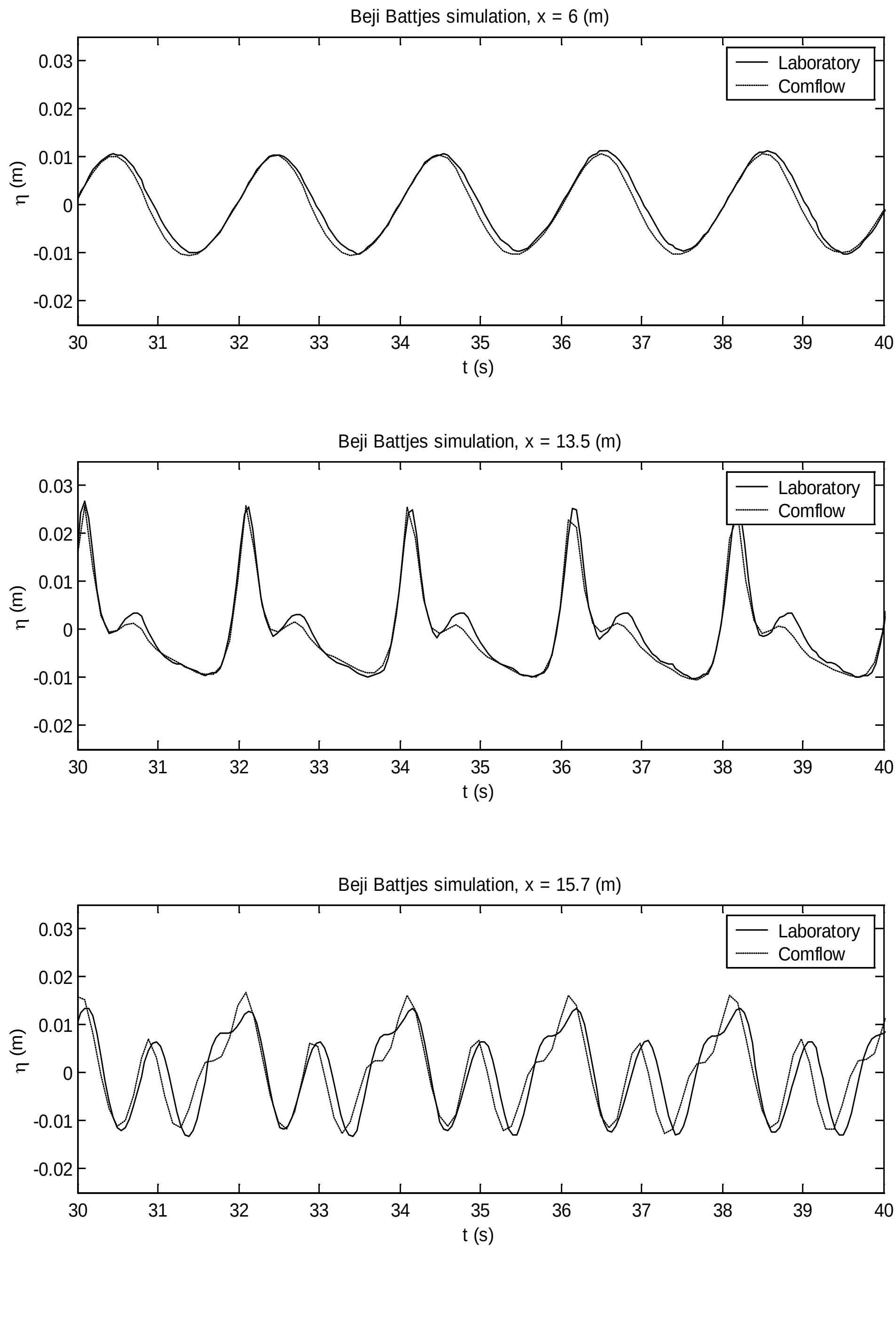

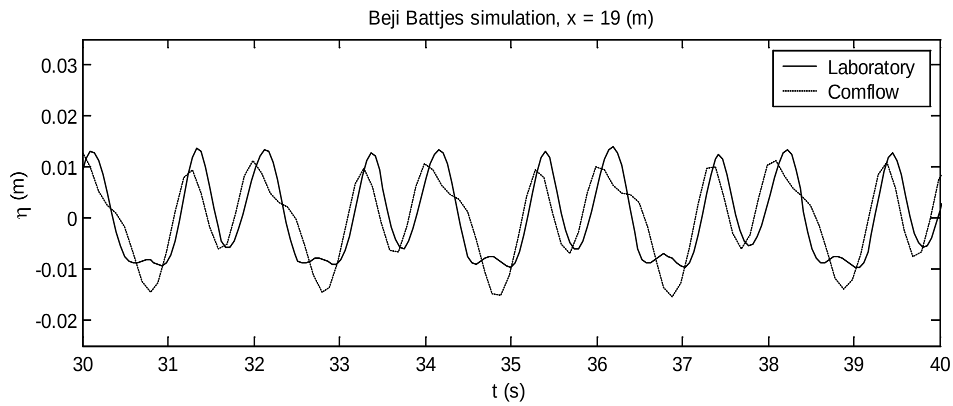

Figure 5.7: Comparison simulation in Comflow with laboratory measurements for finest grid and time step at all locations of measurement.

In the Qqualitative Analysis an indication is given to which harmonic it is expected that Comflow is able to model the generation and release of higher harmonics. In the Quantitative Analysis this expectation is studied, by means of Discrete Fourier Transformations.

Qualitative Analysis

As noted in section 5.2.2 the grid size is defined according to the wavelength of the fundamental wave in the deep part of the wave tank, d=0.4 (m). At the bar the wavelength reduces according to the dispersion relation. The grid is uniform and the number of grid points with which the fundamental wave is described reduces. Waves with a higher frequency, higher harmonics, are generated at the bar that have a smaller wavelength. When these higher harmonics are generated they become bound to the fundamental wave; they propagate with a common propagation velocity. This common phase speed is higher than the natural phase speed of the higher harmonics, which is found using the dispersion relation. After the bar is passed these bound harmonics are released and start to propagate with their natural velocity; their wavelength becomes smaller again. Summarizing, the difference between bound and unbound waves is the phase speed and the wavelength.

To describe waves correctly a sufficiently large number of grid points per wave length and time steps per period should be used. Meskers [19] concluded a regular wave can be modeled correctly in Comflow with acceptable accuracy if around 100, but at least 80, grid points per wavelength are used with the vertical spacing equal to horizontal spacing; $\Delta x/L=\Delta z/L\sim 100$. A time step of $\Delta t/T = 1/500$ is advised.

For accurate simulation of the Beji Battjes test, harmonics of significant amplitude are to be modeled correctly. These higher harmonics should fulfil Meskers recommendations [19]. The effect of the generation of high frequency components at the bar is presented in Table 5.9; it shows that for higher harmonics fewer grid points are available and even the finest grid that is used in the simulations is coarse for the higher harmonics.

How to read Table 5.9, Table 5.10 and Table 5.11? The harmonics are listed in the first column, the frequency, wavelength and propagation velocity, according to the Stokes 5 dispersion relation, are given. The last three columns state the grid size, each standing for a different grid. The finest grid, $\Delta x/L = 1/500$ (-) shows that the fundamental wave is described by 500 grid points in water depth of d = 0.4 (m). For Table 5.9, the waves have shoaled, and are being described by only 263 points. The first harmonic is described by half the number of points, as the harmonic is bound to the fundamental wave. The phase velocity of the bound waves is assumed equal to the phase velocity of the fundamental wave. The wavelength of the bound harmonics is then derived.

Table 5.9: Relative grid size for bound harmonics at the bar.

	F (1/s)	L (m)	C (m/s)	Δx/L	Δx/L	Δx/L
D=0.4 (m)						
Fundamental	0.5	3.738	1.851	1/100	1/250	1/500
D=0.1 (m)						
Fundamental	0.5	1.969	0.975	1/53	1/132	1/263
1st harmonic	1.0	0.985	0.975	1/26	1/66	1/132
2nd harmonic	1.5	0.656	0.975	1/18	1/44	1/88
3rd harmonic	2.0	0.492	0.975	1/13	1/33	1/66
4th harmonic	2.5	0.394	0.975	1/11	1/26	1/53

According to Meskers recommendations, the coarsest grid, $\Delta x/L = 1/100$ (-), is not able to simulate even the fundamental wave passing the bar. The intermediate grid, $\Delta x/L = 1/250$ (-) is only able to simulate the propagation of the fundamental wave. Similarly, the finest grid, $\Delta x/L = 1/500$ (-) can simulate the propagation of the first and second harmonic at the bar.

Behind the bar the bound higher harmonics are released from the fundamental wave. However, in the Comflow simulation this can be modeled incorrectly and the harmonics remain attached to the fundamental. Table 5.10 and Table 5.11 give the relative grid sizes for both scenarios; harmonics remaining bound to the fundamental, and harmonics being released. As the waves remain bound, their wavelength is relatively long, compared to the unbound situation, see Table 5.10. As the waves are decomposed they start to propagate with their natural frequency. The wavelengths become shorter, see Table 5.11.

Table 5.10: Relative grid size for harmonics that remain bound after the bar.

	F (1/s)	L (m)	C (m/s)	Δx/L	Δx/L	Δx/L
D=0.4 (m)						
Fundamental	0.5	3.738	1.851	1/100	1/250	1/500
1st harmonic	1.0	1.869	1.851	1/50	1/125	1/250
2nd harmonic	1.5	1.246	1.851	1/33	1/83	1/167

3rd harmonic	2.0	0.935	1.851	1/25	1/63	1/125
4th harmonic	2.5	0.748	1.851	1/20	1/50	1/100

Table 5.11: Relative grid size for harmonics that are released behind the bar.

	F (1/s)	L (m)	C (m/s)	Δx/L	Δx/L	Δx/L
D=0.4 (m)						
Fundamental	0.5	3.738	1.851	1/100	1/250	1/500
1st harmonic	1.0	1.488	0.737	1/39	1/99	1/199
2nd harmonic	1.5	0.707	0.350	1/19	1/47	1/95
3rd harmonic	2.0	0.398	0.197	1/11	1/27	1/53
4th harmonic	2.5	0.255	0.126	1/9	1/17	1/34

To model free harmonics a finer grid should be used to obtain equal accuracy. The unbound wave situation is limiting. The coarsest grid can only simulate the propagation of the fundamental wave in deep water, the second grid can also simulate the first unbound harmonic, while the finest grid can also simulate the second unbound harmonic.

The period of the waves, regardless of them being bound or unbound, remains constant. The dimensionless time steps are larger for the higher harmonics, see Table 5.12.

Table 5.12: Relative time step of the higher harmonics.

	F (1/s)	Δt/T	Δt/T	Δt/T
Fundamental	0.5	1/100	1/500	1/1000
1st harmonic	1.0	1/50	1/250	1/500
2nd harmonic	1.5	1/33	1/167	1/330
3rd harmonic	2.0	1/25	1/125	1/250
4th harmonic	2.5	1/20	1/100	1/200

The smallest time step $\Delta t/T = 1/1000$ (-) only fulfils Meskers recommendations for the first higher harmonic.

With Table 5.9 to 5.12 it is shown that with the finest grid size, the Beji Battjes test can be simulated accurately up to the second harmonic, however the time step only fulfils Meskers' recommendation for the fundamental wave and the first harmonic. The second harmonic does not agree with the recommendations, but may be shown with reasonable accuracy. Of the grid and time step recommendations the latter is limiting in the considered simulations.

The phase velocity of the higher harmonics, being bound or released from the fundamental wave is not larger than the propagation velocity of the fundamental wave in the deep part of the domain, see Table 5.10 and Table 5.11. The Courant number is thus not affected by the generation and release of the higher harmonics, as the propagation of the fundamental wave remains limiting.

It is expected, that according to Meskers recommendations, a fine grid and time step are needed to simulate the nonlinear formation bound and unbound propagation of higher harmonics. Following on Meskers recommended grid size and time step; the $\Delta x/L = 1/500$ (-), $\Delta t/T = 1/1000$ (-) run will be able to simulate the propagation of the fundamental wave and the generation and release of the first harmonic correctly.

However, Meskers does not include water depth; for shallow water the number of cells in the vertical (cell layers) through which the waves propagate is small. A *cell layer* is defined as the set of grid cells with equal elevation; the top and bottom cell face have a common z-coordinate. If the number of cell layers is small truncation errors are expected to arise. The number of cell layers at the submerged bar are listed in Table 5.13. The grid aspect ratio is unity, making $\Delta x/L$ equal to $\Delta z/L$.

Table 5.13: Number of cell layers in the Beji Battjes simulation.

	$\Delta z/L = 1/100$ (-)	$\Delta z/L = 1/250$ (-)	$\Delta z/L = 1/500$ (-)
D=0.1 (m)	4	9	17
D=0.4 (m)	12	28	56

With the small water depth at the bar the number of cell layers through which the waves propagate is small; the resolution is too low. This is expected to introduce truncation errors as all the information is squeezed though the 17 cell layers, and afterwards expanded again to 56 layers. The errors that are made at the bar are more exposed behind the bar.

Quantitative Analysis

To confirm or reject the hypothesis as put in the qualitative analysis, the data measurements recorded at the simulation with the finest grid and time step are analyzed. To obtain more insight into the modeling of the nonlinear formation, propagation and decompositions of higher harmonics the timeseries at the four locations of measurement are analyzed and compared with the laboratory data. In this analysis, we filter out the amplitude and phase of the fundamental wave and each of the harmonics. This is done with the Discrete Fourier Transform, also denoted as Harmonic Analysis, which can be performed over any single value periodic record. The periodicity condition has impact on the selection of the duration of the time series; it should be chosen such that an integer number of waves is present. Errors are introduced when the periodicity condition is not fulfilled. For fast interpretation of results, the number of registrations for the interval should be a power of 2, such that FFT can be employed. This does not apply to the laboratory dataset, where the frequency of measurement is not coupled to the wave frequency. In the following subsection the time series from the Comflow simulation and the physical experiment are interpreted with Discrete Fourier Transformation, over a timeseries in which ten waves are represented. The

Comflow run has the finest gridding and time step, $\Delta x/L = 1/500$ and $\Delta t/T = 1/1000$. Table 5.14 shows the time series that were used. Note that the frequency of measurement of the time series of the physical experiment is not exactly 1/20 (1/s).

Table 5.14: Time series used for Discrete Fourier Transformation.

	Duration (s)	Frequency of measurement (1/s)	Number of data points	Number of waves
Experiment	20.19	1/20	409	10
Comflow	20.2	1/10	202	10

The most demanding location of measurement is expected to be location 19.0. Experience with other models has shown that at this location the laboratory signal deviates the most with the numerical simulation. It can be seen in Figure 5.7 that Comflow shows deviation at this location. We will therefore focus on this location. The results of the other locations are given in Appendix B.

Results

The amplitude spectrum (Figure 5.8) and phase spectrum (Figure 5.9) are depicted for location 19.0. These spectra are obtained using Discrete Fourier Transformation (Harmonic Analysis). The amplitude spectrum shows that Comflow represents the amplitudes and the frequencies of these amplitudes satisfactory. The amplitudes of all harmonics are well represented. Even though the grid and time step parameters do not fulfill the requirements of Meskers [19], they are modeled well. The deviation that is seen in the time series does not originate from the representation of the amplitudes or frequencies.

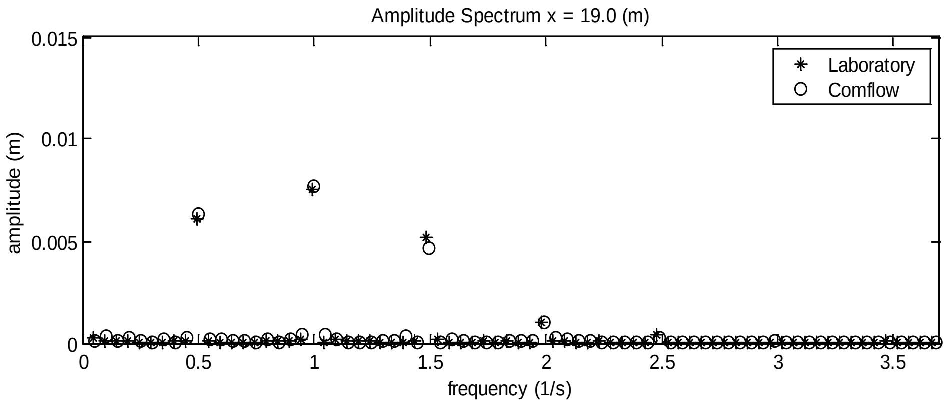

Figure 5.8: Amplitude spectrum at location 19.0.

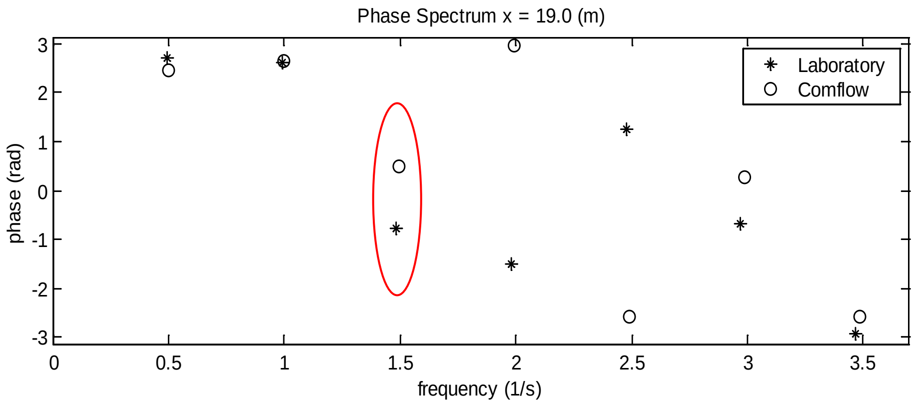

Figure 5.9: Phase spectrum at location 19.

The phase spectrum shows deviations from the second harmonic (f=1.5 (1/s)) up. It seems surprising that the phases of the second, third, fifth, and sixth harmonic are lagging while the phase of the fourth harmonic is leading. However, the phase domain is periodic. The fourth and higher harmonics are expected to have a severe phase lag. The phase velocity causes this phase error. The error in the phase velocity can have two causes:

- The release of the bound harmonics is simulated incorrectly.
- The harmonics are correctly released, but the dispersion is incorrect.

Bispectral analysis is recommended to reveal whether the harmonics are bound or not. Since the second harmonic does fulfill the grid size recommendation and does not fulfill the time step recommendation, the error that is made is expressed in a misrepresentation of the phase velocity. The release of the first harmonic, and its phase velocity are simulated correctly. The first harmonic meets all recommendations.

The second and third harmonics have significant amplitude, which is simulated correctly, but erroneous phase. The phase error is thus the cause of the cause of the difference in the time series.

In general, difference in phase can be caused by numerical lag over the entire wave, or a misrepresentation of single wave frequencies. In case of the Beji Battjes test, the phase spectrum could indicate whether the harmonics are modeled well or not. A phase lag of numerical origin is relevant for simulations that cover a long time span, such as Newwave runs. The numerical lag could become large and could blur the insight in phase representation of separate wave frequencies. A second method is proposed to get better insight in wave phases.

- Time series of physical measurements and numerical simulation use the same starting time.
- The time series of the simulation is shifted in time, such that the phase error of the fundamental wave (Beji Battjes test) or most energetic wave (Newwave) is eliminated.

Since the time series of the laboratory experiment and the Comflow simulation do not show a large phase difference, the first method will be used. In case a longer domain needs to be examined, the benefits of the second method will increase.

Comflow has a lower mean water level at all the locations, see Table 5.15. However, compared to the wave height, 0.02 (m), and cell height 0.0075 (m) the order of magnitude is small. The limited number of data recordings has influence the value of the mean water level. The laboratory tests also have a non-zero mean.

Table 5.15: Mean water level at all locations of measurement.

Mean water level (m)	Location 6	Location 13.5	Location 15.7	Location 19.0
Laboratory	$3.133\ 10^{-4}$	$-2.116\ 10^{-4}$	$-1.119\ 10^{-4}$	$-1.516\ 10^{-5}$
Comflow	$-6.697\ 10^{-4}$	$-8.035\ 10^{-4}$	$-5.495\ 10^{-4}$	$-2.590\ 10^{-4}$

5.2.6. Conclusions

The following can be concluded from the comparison of the Comflow simulation and the wave tank measurements of the Beji Battjes test:

1. Comflow is able to simulate the Beji Battjes test accurately, provided that three conditions are fulfilled, namely the Courant condition, the grid size requirements and time step requirements of Meskers [19]. These requirements make Comflow simulations of the Beji Battjes test computationally demanding. For waves that fulfill the requirements, the propagation, the nonlinear creation as well as their release behind the bar are simulated accuretely.
2. A grid size of $\Delta x/L = 1/500$ (-) and time step of $\Delta t/T = 1/1000$ (-), the finest grid and time step that were used, give the best results. With these parameters, the propagation of the fundamental wave and the generation, release and propagation of the first harmonic are simulated correctly. The computational effort is considerable, with nearly an hour of computing on a Linux 2.4 MHz processor for one second of simulation.
3. The runs with a lower resolution produce a stable solution, however a secondary disturbance influences the wave progression. It is shown that this disturbance is not primarily caused by the sudden start up of the numerical wave maker in the initially undisturbed domain; with the high resolutions this sloshing is not observed. The cause of the disturbance is expected to lay in the incorrect propagation of the fundamental waves over the submerged bar, see conclusion 4.
4. It is expected that, as a result of the limited number of cell layers at the bar, small truncation errors are made, which will be more expressed behind the bar.
5. Linear and 2nd and 5th order Stokes wave theory were used to describe the inflow boundary. No difference in results is observed as the waves conditions at the inflow boundary are linear.
6. The error introduced by having a coarser time step than required is expressed in a misrepresentation of the propagation velocity. Comflow is able to simulate the generation and release of the harmonics that fulfill the Courant condition, the grid size requirements and time step requirements of Meskers [19]. With a grid size of $\Delta x/L = 1/500$ (-) and time step of $\Delta t/T = 1/1000$ (-):

- The first harmonic fulfils all requirements
- The second harmonic does not fulfill the time step requirement, but does fulfill the grid size requirements and Courant condition.

A significant phase error is observed behind the bar (location 19), which indicates the phase velocity is modeled incorrectly.

7. The requirements for a correct simulation of the wave frequency and amplitude are less stringent. The amplitude and frequency of the harmonics that do not fulfill the grid size and time step requirements are represented well.
8. Compared to the sigma layer model of van Reeuwijk [20] the performance of Comflow on the Beji Battjes test is disappointing. The accuracy of the simulation and corresponding time consumption are inferior. The performance of the sigma layer model of van Reeuwijk is accredited to the fact that the pressure is given directly at the surface. The pressure is interpolated over only a few layers, which makes the code efficient.

5.3. Sloshing Tank experiment

5.3.1. Goal

The goal of the Sloshing Tank experiment is to assess the ability of Comflow to simulate waves in relative water depth ranging from deep to shallow.

In the Sloshing Tank experiment a free surface is given an initial sinusoidal elevation with its wavelength equal to the length of the tank. The second natural frequency is excited. Initially the wave crest is located at the center of the wave tank. The initial disturbance will propagate and cause a standing wave in the tank. The period and amplitude that is calculated with the numerical model is compared to the analytical, linear, solution. The relative water depth parameter kd is varied from 100 (deep water) to 0.3 (limit shallow and intermediate water depth). This experiment is done to assess the phase velocity, numerical damping and to analyze the required high resolution and small time step, see section 5.3.3.

Secondly, the influence of the grid resolution and time step is considered. The Courant number remains unchanged.

Thirdly, the influence of a vertical crossing of the fluid surface with a cell border is considered. The number of cells in the vertical is decreased, while in the horizontal direction the grid remains fine. With a correct description of the location of the surface a substantial improvement in accuracy can be expected, see section 5.3.5

Lastly, the influence is shown of a fluid surface being located in a top or bottom cell of the domain. It is expected that Comflow is not able to resolve wave propagation due to the labeling procedure and according solution algorithm.

5.3.2. Experiment setup

The wave amplitude is chosen such that the relative steepness H/L has a value of 0.01 (-). The length of the domain is chosen constant at an arbitrary value of 20 (m), see Figure 5.10. The water depth is varied to obtain the desired kd values. The grid aspect ratio is one with $\Delta x/L = 1/100$ (-). The time step is $\Delta t/T = 1/500$ (-), except for the kd = 0.314 (-) run which has a time step of $\Delta t/T = 1/1000$ (-) to meet the Courant condition. The upwind parameter is unity and constant extrapolation of the surface velocities is used. The time series are measured in the center of the tank. The water depth is changed to obtain the desired wave length-water depth ratio.

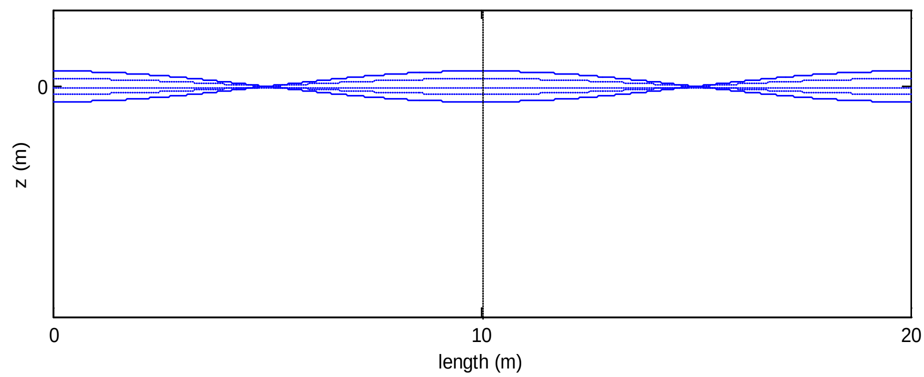

Figure 5.10: Sloshing Tank experiment setup.

5.3.3. Relative water depth

Several runs were done with varying relative water depth kd to track the influence of the relative water depth on the numerical model. The limits between shallow water, intermediate water depth and deep water are given in Table 5.3. The following kd values were tested π/10, 1, π, 10, 100, see Table 5.16.

Having chosen a kd value, the natural frequency of this wave is determined with the linear dispersion relation, due to the low wave amplitude. The Ursell number *Ur* {A9} indicates the applicability range of linear theory. For linear theory the Ursell number should be lower than 25; as indicated in Table 5.16 this is the case. Also indicated in Table 5.16 are the phase speed *C* and the Courant number *Cr*. The simulation can be approximated by linear theory because of the small steepness of the sloshing wave.

Table 5.16: Sloshing Tank simulations: the relative water depth is varied.

Kd (-)	D (m)	T (s)	C (m/s)	U_r (-)	C_r (-)
0.314	1	6.489	3.082	4.0	0.20
1	3.18	4.101	4.878	0.10	0.20
3.14	10	3.586	5.578	$4.0\ 10^{-3}$	0.20
10	31.83	3.579	5.588	$1.2\ 10^{-4}$	0.20

100	318.3	3.579	5.588	1.2 10^{-7}	0.20

At the center of the tank the surface elevation is recorded. The time series for the runs are given in Figure 5.11 to Figure 5.15.

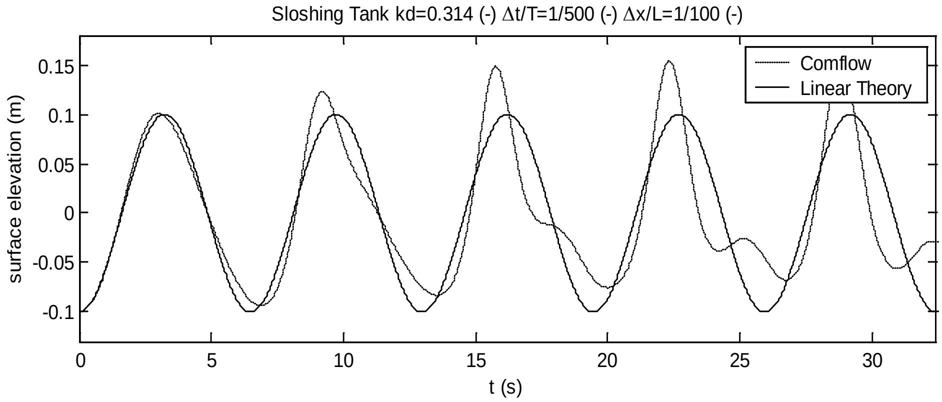

Figure 5.11: Surface elevation, kd = 0.314 (-).

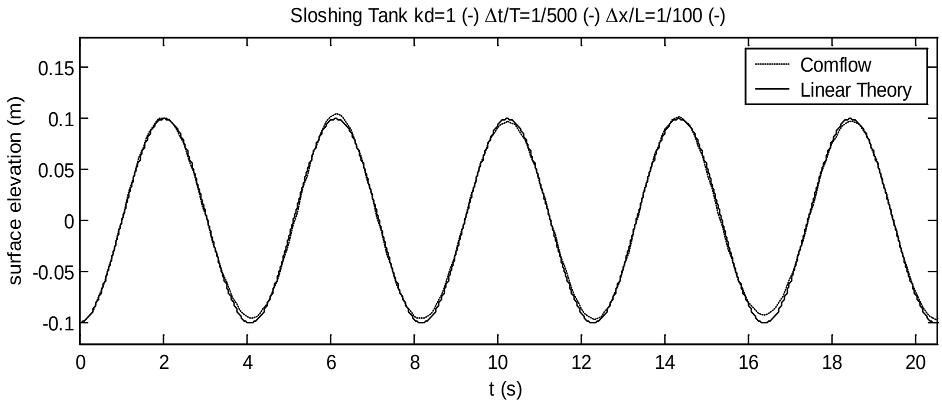

Figure 5.12: Surface elevation, kd = 1 (-).

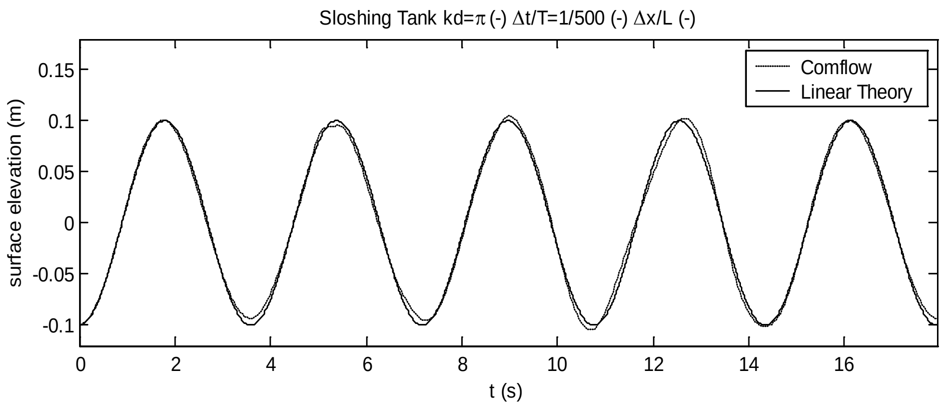

Figure 5.13: Surface elevation, kd = 3.14 (-).

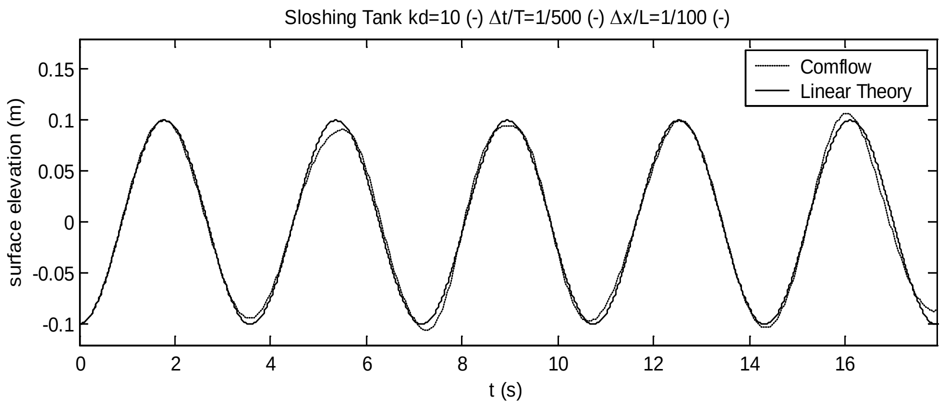

Figure 5.14: Surface elevation, kd = 10 (-).

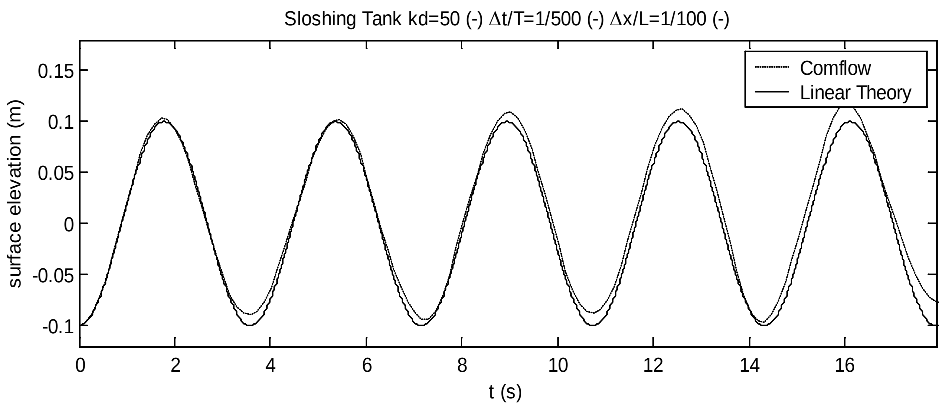

Figure 5.15: Surface elevation, kd = 50 (-).

The waves in relative shallow water show some deviations, possibly leading to instability. A cause of this effect could be the limited number of cell layers; the low resolution introduces errors. The simulation with kd = 0.314 uses only five cell layers to prescribe the standing wave.

5.3.4. Reduction of grid resolution and time step

The grid and time step are made coarser, while the Courant number C_r is kept unchanged. The relative water depth kd is kept at a constant value of 1 (-) and wave steepness H/L = 0.01 (-). The time series of the runs are given in Appendix C, 40 periods are simulated. Table 5.17 gives the grid and time step that is used. Also indicated is the number of cell layer boundaries that are crossed by the free surface, see section 5.3.5. A *cell layer crossing* is defined as the crossing of the free surface through the top or bottom boundary of a cell layer. The elevation of the cell layer boundaries is given in the fourth column of Table 5.17.

Table 5.17: Reduction of grid size and time step.

Δx/L , Δz/L (-)	Δt/T (-)	Number of cell layer crossings (-)	Elevation of cell layer crossing (m)	C_r (-)
1/20	1/100	*0*		0.20
1/30	1/150	*0*		0.20
1/40	1/200	*0*		0.20
1/50	1/250	*1*	*+0.017*	0.20
1/60	1/300	*0*		0.20
1/70	1/350	*1*	*-0.040*	0.20
1/80	1/400	*1*	*+0.067*	0.20
1/90	1/450	*1*	*-0.072*	0.20
1/100	1/500	*1*	*+0.017*	0.20

In the physical situation the viscous damping slowly lowers the wave amplitude. Figure 5.16 and Figure 5.17 show the time series for the coarsest grid Δx/L = Δx/L = 1/20 (-),Δt/T = 1/100 (-) for two time intervals. Results are summarized in Table 5.18.

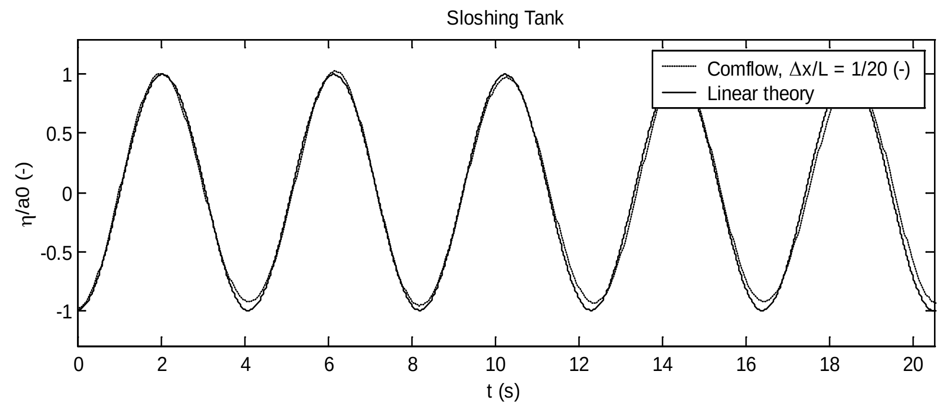

Figure 5.16: Surface elevation for simulation with coarse grid size and time step for first five periods.

After 35 periods it is observed that both the amplitude and the phase of the Comflow simulation deviate from the analytical solution, see Figure 5.17.

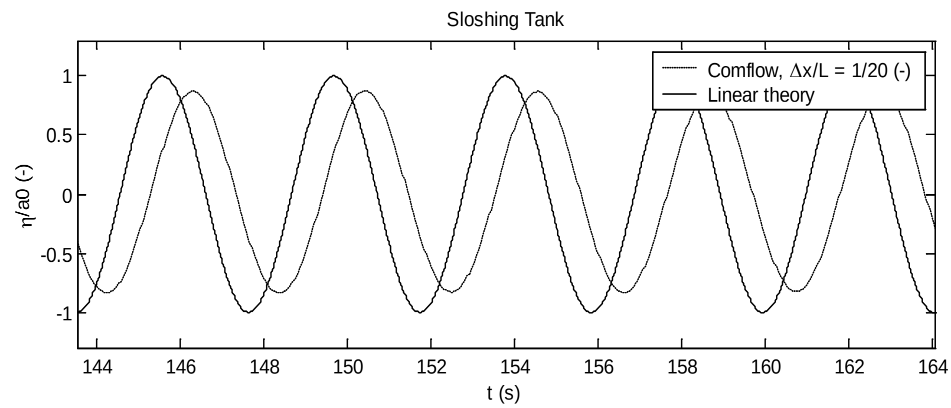

Figure 5.17: Surface elevation for simulation with coarse grid size and time step after 35 periods.

To assess numerical damping, the extreme surface elevations are taken, see Figure 5.18.

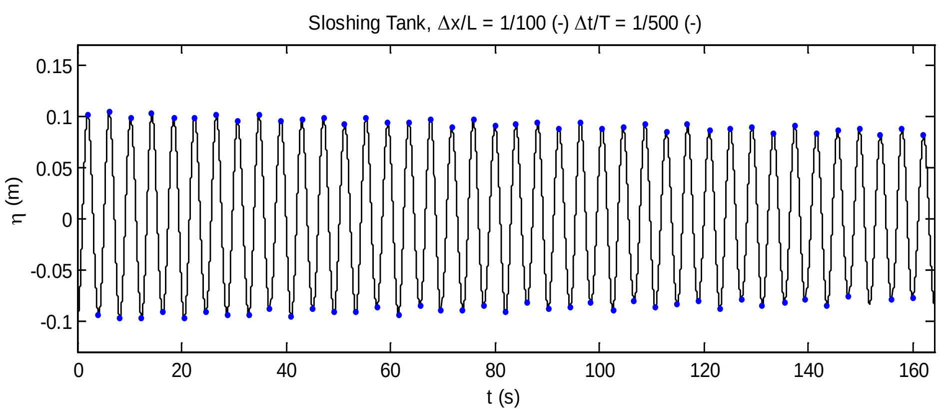

Figure 5.18: Surface elevation over 40 periods: damping is clearly visible, the extreme values are highlighted.

The damping of the sloshing wave in Comflow is defined as an artificial viscous term, K (m^2/s). The values of K for each of the runs is calculated with exponential curve fitting around the extreme values with the least square method, see Figure 5.19. Table 5.18 indicates that two simulations unexpectedly show an increase in amplitude (negative damping).

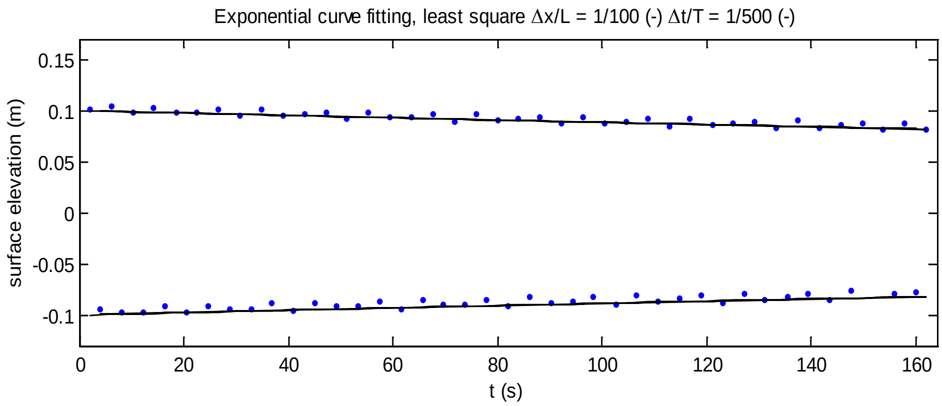

Figure 5.19: Exponential curve fitting to assess artificial viscosity.

For water the kinematic viscosity ν is 10^{-6} (m^2/s), artificial damping is approximately a factor 100 larger, see Table 5.18. The phase velocity is calculated using the time it takes before 40 cycles are observed, theoretically the phase velocity of waves with this steepness, wavelength and water depth is 4.878 (m/s). The phase velocity is overestimated for the simulations that use a coarse grid and time step.

For the calculation of the velocities in the surface cells constant extrapolation method is used; taking the velocities at the free surface equal to the velocities in the first cell below the surface. Linear extrapolation of the velocities shows less damping, however, this is not beneficial if wave structure interactions are simulated, which is the objective of this thesis. The extrapolation method is expected to be of influence on the damping of the waves in the simulations above.

Table 5.18: Results Sloshing Tank simulations with coarse grid and time step.

Δx/L, Δz/L (-)	Δt/T (-)	Phase velocity (m/s)	K (m^2/s)
1/20	1/100	*4.975*	*9.060 10^{-4}*
1/30	1/150	*5.019*	*1.709 10^{-3}*
1/40	1/200	*5.000*	*5.814 10^{-4}*
1/50	1/250	*4.752*	*1.799 10^{-3}*
1/60	1/300	*4.878*	*5.967 10^{-5}*

1/70	1/350	*4.876*	*-3.438 10^{-4}*
1/80	1/400	*4.875*	*7.224 10^{-4}*
1/90	1/450	*4.878*	*-6.554 10^{-5}*
1/100	1/500	*4.875*	*1.224 10^{-4}*

The phase velocity is underestimated with less than 1% for simulations with a grid finer than Δx/L = 1/60 (-) and Δt/T = 1/300 (-). It is questionable if this is significant.

The artificial kinematic viscosity is of the order of 10^{-4} (m^2/s). However, the simulations with 70 and 90 grid points per wavelength show an increase in amplitude; negative damping. Both runs with increase in amplitude have a cell layer crossing below the mean water level. The fluctuations in damping indicate that other, unidentified, aspects plays a role in the simulation of the Sloshing Tank experiment in Comflow. The effect of the layer crossing is investigated in the next section, where runs with and without cell level crossing are compared.

5.3.5. Cell layer crossing

It is investigated what the influence is of a cell layer crossing on the simulation of the Sloshing Tank experiment. In the previous section it is observed that the grids that include a cell crossing below the mean water level show an increase in wave amplitude (negative damping). This observation is studied in this section.

The same experiment setup is used, with kd = 1 (-) and H/L = 0.01 (-), however the grid is changed. A horizontal spacing is of Δx/L =1/100 (-) and time step of Δt/T = 1/500 (-) is used, but the vertical spacing varied; the grid aspect ratio is no longer unity. The number of cell layers is strongly reduced. The number of cells from the bottom to the mean water level is varied from 1.5 to 16, with equidistant spacing and at least two cells above the fluid surface. When the number of cell layers is 16 the grid aspect ratio is approximately unity again. The time step is Δt/T = 1/500 (-). Simulations are performed over 40 periods.

Two cases are considered:

- *Cell layer crossing* There is a cell layer boundary in the mean water level. The number of cell crossings, with the given wave amplitude, is one. The number of cells below the mean water level is an integer. Figure 5.20 shows an example for a grid with two cell layers under the mean water level, with one cell layer crossing. The amplitude of the disturbance is less than half of one cell height.

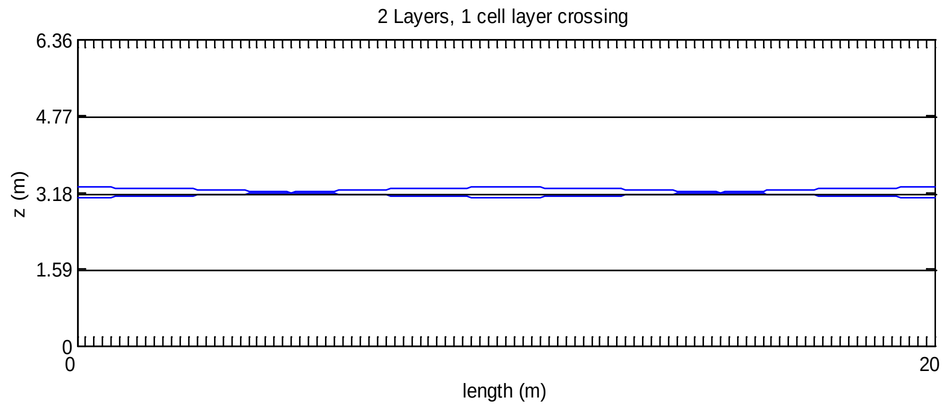

Figure 5.20: Example grid with a *cell layer crossing*:

- *No cell layer crossing* The mean water level is the center of a cell layer. There are no cell crossings as the amplitude of the disturbance is less than half the height of a cell. Figure 5.21 shows an example of a 1.5 layer grid with one cell layer crossing. There are one and a half cell layers under the mean water level. The wave amplitude is less than half the cell height. There are no cell crossings, but in case there are 15.5 layers underneath the mean water level, the wave almost reaches both cell layers' boundaries; there are almost two crossings.

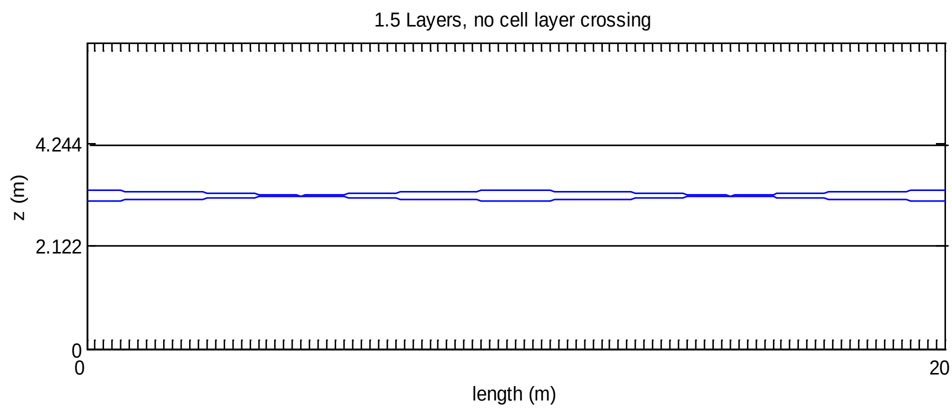

Figure 5.21: Example grid with *no cell layer crossing*:

The number of cell layers below the mean water level is listed in Table 5.19 and Table 5.20. The depth of the Sloshing Tank is 3.18 (m), since the kd value is 1 (-). The Courant condition {8} is met. Table 5.19 and Table 5.20 indicate the cell height and the relative grid size.

Table 5.19: Sloshing Tank simulations with a *cell layer crossing*.

Cell layers	Cell height (m)	Δz/L (-)
2	*1.592*	*1/13*

3	*1.061*	*1/19*
4	*0.796*	*1/25*
5	*0.637*	*1/31*
7	*0.455*	*1/44*
10	*0.318*	*1/63*
13	*0.245*	*1/82*
16	*0.199*	*1/101*

Table 5.20: Sloshing Tank simulation with *no cell layer crossing*.

Cell layers	Cell height (m)	$\Delta z/L$ (-)
1.5	*2.122*	*1/9*
2.5	*1.273*	*1/16*
3.5	*0.909*	*1/22*
4.5	*0.707*	*1/28*
6.5	*0.490*	*1/41*
9.5	*0.335*	*1/60*
12.5	*0.236*	*1/85*
15.5	*0.205*	*1/97*

Results

The time series are given in Appendix C. Figure 5.22 shows the time series of the 16 and 15.5 layer runs over the first 5 periods. The 16 layer run has one cell layer crossing, the 15.5 layer none, but is close to crossing two cell layers. Both simulations match linear theory quite accurately. The difference between the 16 layer run and the 15.5 layer run is marginal, for the first five periods.

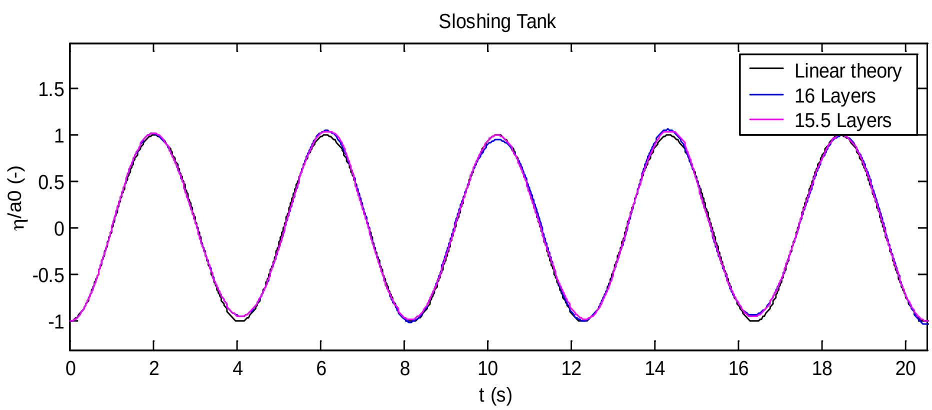

Figure 5.22: Sloshing Tank simulations with 16 and 15.5 layers for first five periods. Both simulations match linear theory.

After 35 periods the signal of the 16 layer run shows small disagreements in surface elevation and phase, see Figure 5.23. The crest of the last depicted wave (t=164 (s)) is clearly lower, and it seems that a secondary wave travels through the domain. This remains visible for runs with a cell layer crossing at the mean water level. The 15.5 layer run still is representative, it only has slightly shallower troughs than the analytical solution. The phase shows good agreement.

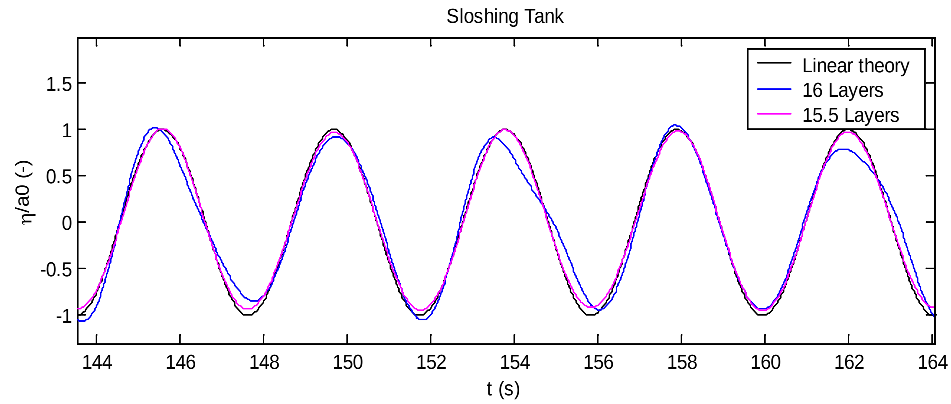

Figure 5.23: Sloshing Tank simulations with 16 and 15.5 layers after 35 periods. The 16 layer simulation shows inferior results.

As the number of cell layers below the mean water level is decreased, the magnitude of the secondary, erroneous waves seem to increase. We jump to the simulation using 4.5 cell layer grid, where another interesting observation is made. Figure 5.24 shows the time series over the 40 periods of simulation for the 5 layer and 4.5 layer simulations. Reduction of number of layers results in a high peak and low trough for the run with 4.5 cell layers. The 4.5 layer run shows a high crest after 77.2 seconds, and a low trough at t=131 (s). The height of the extreme crest is 0.353 (m), the surface elevation of the extreme trough reaches –0.139 (m). The evolution of the standing wave after the extreme crest and trough goes surprisingly well. The 5 layer shows that the crests are less high than expected according to linear theory.

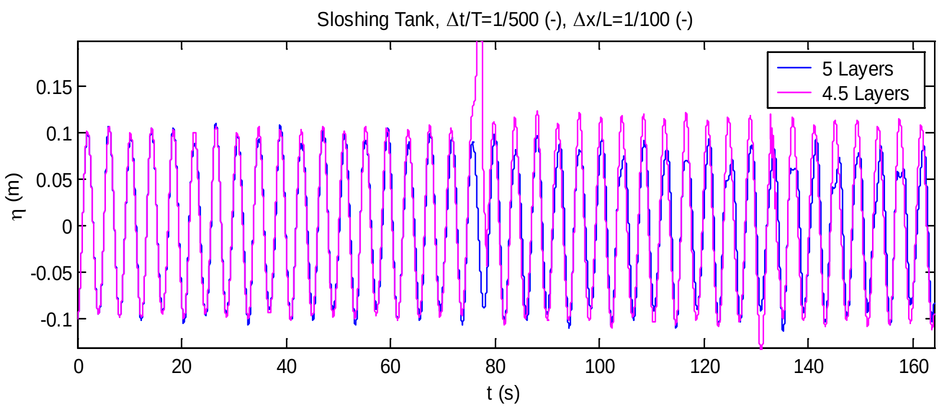

Figure 5.24: Sloshing Tank simulations with 5 and 4.5 layers over 40 periods. The 4.5 layer simulation shows interesting cusps.

What is happening? The high peak at t= 77.2 (s) is the result of a local cusp caused by a focusing of high frequency error waves. This is depicted in Appendix C, showing that the size and duration of these cusps is very limited. The rest of the standing wave is not significantly affected. The trough at t = 131 (s) has similar cause. The formation of these cusps has only been observed for the 4.5 layer run.

Further reduction of the number of layers causes a break down the standing wave after approximately 15 periods. The amplitudes and phases until this time are represented with small error. This is shown in Figure 5.25, indicating the evolution of the standing wave simulation with 4 and 3.5 cell layers. The standing wave decomposes in several frequencies.

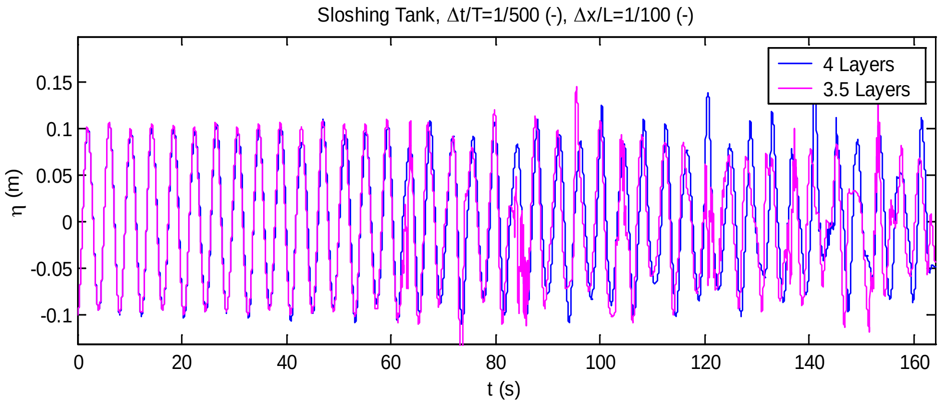

Figure 5.25: Sloshing Tank simulations with 4 and 3.5 layers over 40 periods. Both simulations show a decomposition in multiple frequencies.

In contrast to the findings for a simulation with 4 and 3.5 layers, the simulations with less than 3.5 layers an evolution is observed that is stable in time. The runs with a cell layer crossing now show a strong reduction of the amplitude. The damping is largest for the simulation with only two cell layers. This is shown in Figure 5.26. The simulations without cell layer crossing have good performance throughout the duration of the simulation, except for a phase error. The number of layers cannot be reduced further because the solution procedure requires a cell above and under the surface cell, see section 2.2 and section 5.3.6.

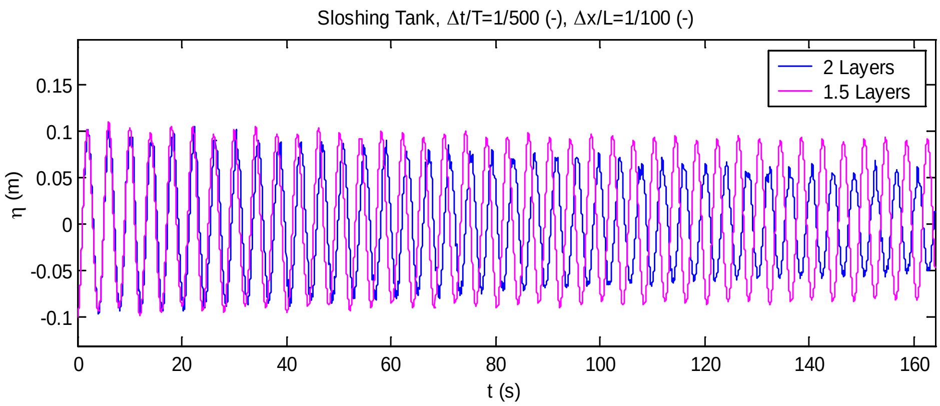

Figure 5.26: Sloshing Tank simulations with 2 and 1.5 layers over 40 periods. The 2 layer simulation shows strong damping.

Zooming in to the time series of the runs with 2 and 1.5 cell layers we do the following observations. The run with no cell layer crossing (1.5 layers) shows an erroneous phase speed, expressed by the phase difference after some periods. The phase speed for this simulation with coarse grid is overestimated, which is in line with the findings presented in Table 5.18. The 2 layer run shows small error waves, even in the first 5 periods, see Figure 5.27. The run with no cell layer crossing shows an erroneous phase speed, expressed by the phase difference after some periods. The figure depicts the first five standing waves.

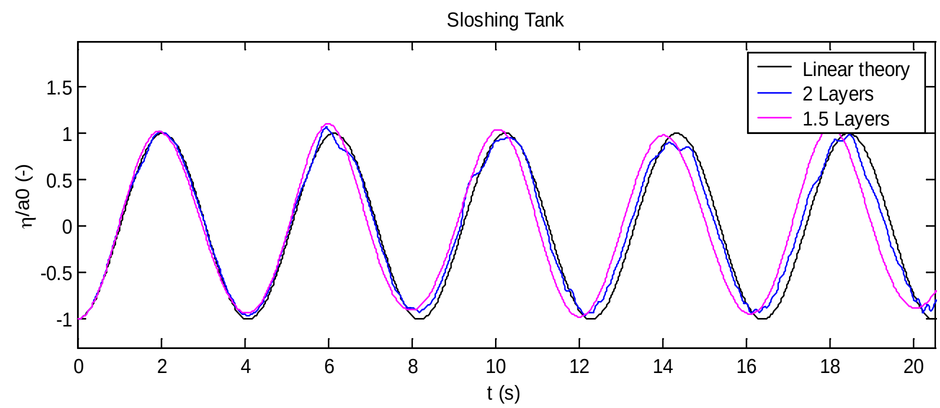

Figure 5.27: Sloshing Tank simulations with 2 and 1.5 layers over the first five periods. The 2 layer simulation shows error waves, while the 1.5 layer simulation shows overestimation of the phase speed.

After 35 periods the effects are extrapolated, see Figure 5.28, showing the time series of the 2 and 1.5 layer simulation between 35th and 40th period. The amplitude has decreased slowly for the 2 layer run and the standing wave clearly is not a smooth sine any more, in contrast to the 1.5 layer run. Both runs cope with significant artificial damping and phase error.

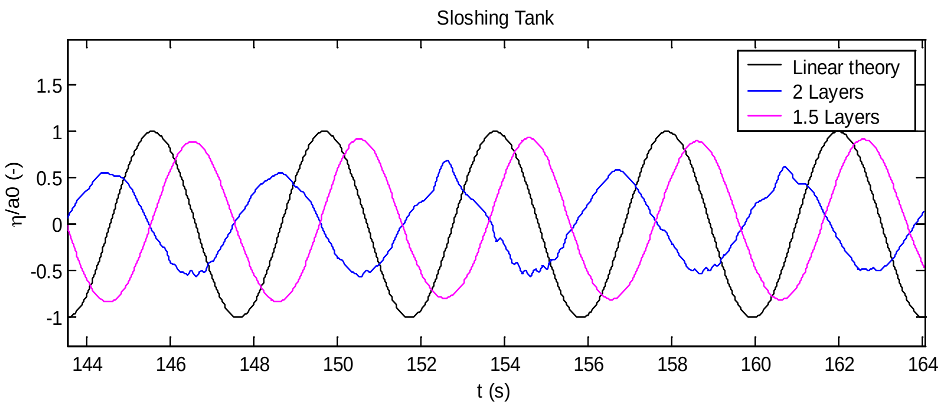

Figure 5.28: Sloshing Tank simulations with 2 and 1.5 layers after 35 periods. The effects observed in Figure 5.27 are more expressed.

In overview, the following is observed:

- The runs with a cell layer crossing at the mean water level have problems with secondary, erroneous, disturbances that result in an inferior evolution of the standing waves in comparison with the simulations that were performed with no cell layer crossing.
- The fewer layers are used in the simulation the more the effects show.

How can this be explained? The inferior performance of the runs with a cell layer crossing is expected to originate in the surface velocity algorithm. The labels of the cells in the simulation with a cell layer boundary in the main water level change as the surface passes the mean water level twice per period. It is shown that the switch between the two cell layers introduces these error waves. It is expected that the errors originate in the velocity extrapolation method. It has shown that the extrapolation method has significant impact on artificial wave damping. The location of the cell layer boundary, at which the vertical velocities are calculated influences the length over which needs to be extrapolated. Possibly the transition between maximum extrapolation length (the surface is just below a cell layer boundary), and no extrapolation (the free surface is at the cell layer boundary), is responsible for the generation of error waves. As the cell layer height is increased, see Table 5.19, the height over which needs to be extrapolated is increased, and this transition at the cell layer boundary is increased, making the error waves of more impact. These small high frequency error waves that arise at the cell boundary have increasing impact as time progresses.

A more accurate velocity extrapolation method, such as using the spline function, is recommended to reduce the generation of error waves. Extrapolation of the velocities to determine the u_n velocities (see Figure 2.3) can reduce the error waves that are expected to originate in the transition between the extrapolation and exact determination.

Exact prescription of the pressure at the free surface would reduce artificial damping or wave excitement. The error of pressure interpolation is expressed in artificial damping or excitement. A correct prescription of the pressures, exactly at the surface, would eliminate the artificial influence of the pressure on the wave propagation.

5.3.6. Bottom and top boundary cells

The solution algorithm of Comflow uses cells that are above and under the surface cell. If the cell in which a free surface is located is a bottom or top boundary cell Comflow fails in simulating wave propagation. This is demonstrated in this section.

The same domain specifications are used as in section 5.3.5; the relative water depth kd = 1 (-), a grid using $\Delta x/L = 1/100$ (-) and dimensionless time step $\Delta t/T=1/500$ (-). The number of cell layers is 16; a cell layer boundary is located in the mean water level.

First we consider a grid with 16 cell layers below the mean water level. The cell height is less than the amplitude of the standing wave, see Table 5.19. Two cell layers are added on top of the 16 layers. The top cell layer remains empty throughout the duration of the simulation. This is the same case as was presented in section 5.3.5.

Now the top cell layer is taken off. Only one cell layer remains above the mean water level, in which the free surface will move. In this experiment the free surface comes into the top cell layer after one second; Figure 5.29 shows that the simulation goes reasonably well until the top cell layer should be entered.

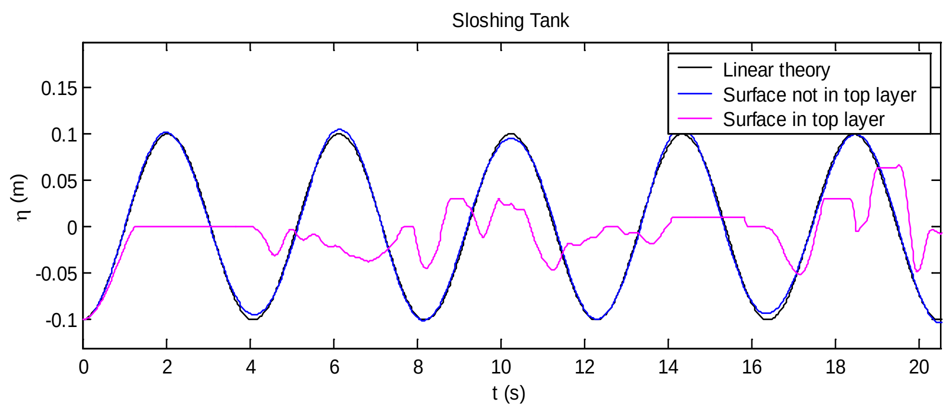

Figure 5.29: Sloshing Tank simulation fails with the free surface in top cell layer.

Conversely, what happens if the surface is located in the bottom cell layer? The number of cell layers below mean water level is reduced from 2 (see Table 5.19) to 1. The effect is again as expected, see Figure 5.30.

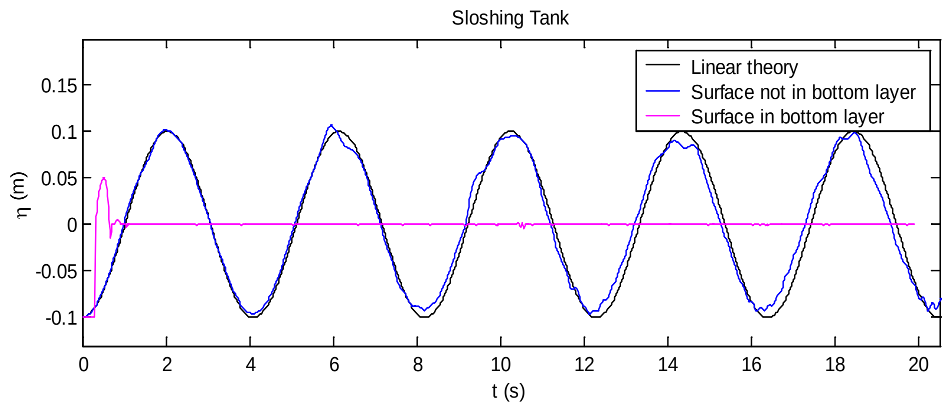

Figure 5.30: Sloshing Tank simulation fails with the free surface in bottom cell layer.

The cause of the erroneous performance is again the labeling procedure of Comflow. As explained in Chapter 2 the cells are labeled from the top of the domain downwards. First the empty cells are given (E), the first cell that contains the free surface becomes a surface cell (S) and underneath the surface a fluid cell (F) is given. If the cell that contains the free surface forms a boundary cell the propagation algorithm is distorted.

5.3.7. Conclusions

The following can be concluded from the simulation of the Sloshing Tank experiment in Comflow:

1. In Comflow, the propagation of low crested regular waves can be modeled accurately from an intermediate relative water depth kd of 1 (-) upwards with a grid aspect ratio of unity. However, the grid configuration is of influence on the performance; some interesting observations are presented.
2. The run with the smallest kd value, which forms the limit between shallow water and intermediate water depth, shows the formation of secondary waves. These erroneous waves are expected to be the result of truncation errors originating from the small number of cell layers (five).
3. The damping coefficient differs interestingly per simulation, if the grid size and time step are made coarser proportionally, for a relative water depth kd = 1 (-). The artificial kinematic viscosity is of the order of magnitude 10^{-3} to 10^{-5} (m^2/s). However, for grid configurations with a cell layer crossing below the mean water level the resulting damping is negative; the wave amplitude increases. It is expected that both the velocity extrapolation and pressure interpolation are of influence.
4. The Sloshing Tank experiment shows results that resemble the analytical solution with a grid with $\Delta x/L = \Delta z/L = 1/40$ (-) and time step $\Delta t/T = 1/200$ (-). The performance of the simulation in general, improves as the resolution is increased with according time step.
5. The phase velocity in the Sloshing Tank experiment does not deviate significantly for grid and time step finer than $\Delta x/L = \Delta z/L = 1/60$ (-) and time step $\Delta t/T = 1/300$ (-).
6. A grid with a cell layer center located at the mean water level is better able to simulate the wave propagation in the Sloshing Tank experiment. The cell height was varied such that either a cell boundary was located in the mean water level (the surface disturbance crosses

one cell layer) or the cell center was is the mean water level (the surface disturbance remains in the surface cell layer).

7. Grid configurations with a cell layer boundary at the mean water level cause the generation of surface disturbances. These secondary waves affect the standing wave.
8. Grid configurations with a cell layer center in the mean water level, and no cell layer crossing, show the generation high frequency error waves that cause local cusps that do not affect the standing wave significantly.
9. Conclusion 7 becomes more visible if the number of cell layers is reduced, down to the minimum of 2 layers.
10. Conclusion 8 becomes more visible if the number of cell layers is reduced to 4.5 layers. The simulation with 3.5 cell layers below mean water level shows a chaotic wave pattern. A transition is observed if the number of cell layers is further reduced to 2.5 and 1.5 cell layers. The simulation produces a steady solution, but with larger damping.
11. The velocity extrapolation method is expected to cause surface disturbances as the free surface crosses a cell layer boundary. Here a transition takes place between the extrapolated velocity and the calculated velocity.
12. The pressure interpolation method is expected to be the cause of an artificial decrease or increase in wave amplitude.
13. It is demonstrated that at least one cell layer must be above and below the cells that contain the free surface.

5.4. Steep Wave experiment

5.4.1. Goal

The goal is to examine the ability of Comflow and Vijfvinkel to simulate steep, regular waves.

First, the steepness of the regular wave is varied from low crested to near breaking. In Comflow, three separate wave theories are used to prescribe the inflow boundaries: linear, 2nd order Stokes and 5th order Stokes. It is shown that these wave theories can not prescribe near breaking regular waves as boundary effects have an impact on the wave simulation. A higher order nonlinear inflow boundary in Comflow will enhance the accuracy of modeling steep waves in Comflow, see section 5.4.3.

Secondly regular 5th order Stokes waves are simulated in Vijfvinkel. This is presented in section 5.4.4.

Thirdly the results of both programs are compared. It is shown that Comflow has difficulty with producing a solution and damping becomes increasingly important for steep waves, see section 5.4.5.

5.4.2. Experiment setup

The experiment setup is shown in Figure 5.31. The length of the wave tank is equal to five wavelengths, and relative water depth kd equal to 2 (-). Measurements taken at one and two wavelength from the inflow boundary.

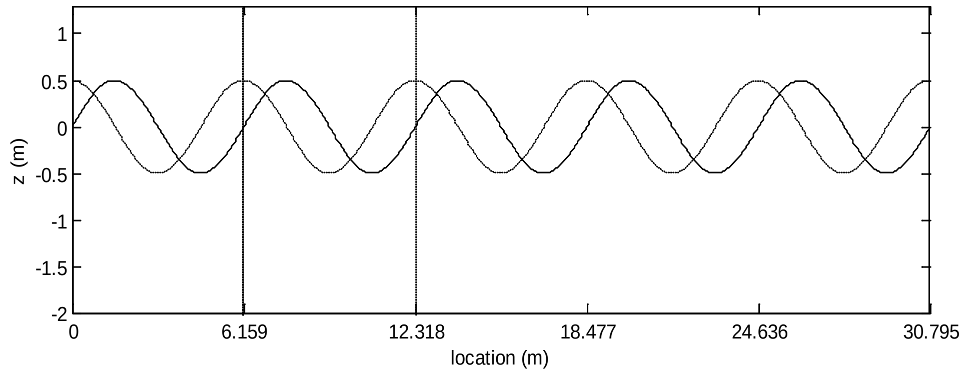

Figure 5.31: Steep Wave experiment setup.

Table 5.21 gives the wave parameters that remain constant for all Steep Wave simulations. The same wave period is taken as is used for the Beji Battjes test, T=2.02 (s). The linear dispersion relation is used.

Table 5.21: Wave parameters as used in the Steep Wave simulation.

T (s)	D (m)	Kd	L0 (m)	L (m)	C (m/s)	Cg (m/s)
2.02	2.00	2.040	6.371	6.159	3.049	1.735

The boundary conditions and initial condition differ for Comflow and Vijfvinkel as the programs are set up differently. Comflow uses an inflow boundary to prescribe the waves, it is initially at rest and has a Sommerfeld outflow boundary. Vijfvinkel has fifth order Stokes waves set as initial condition, no in and outflow boundaries exist as the domain is spatially periodic.

Wave steepness is increased to near breaking conditions. The breaking criterion (due to wave steepness) is given by Miche, see equation {20}. The Miche breaking criterion yields that dimensionless steepness parameter H/gT^2 should be equal to, or less than 0.023 (-).

In textbooks, i.e. [21,24] wave theory applicability is related to the wave steepness parameter $H0/gT^2$ (-) and relative water depth parameter d/gT^2 (-). For the latter parameter a value is chosen of 0.05 (-), for this value Stokes theory is recommended up to the breaking limit. Three values are considered for the steepness parameter in both Comflow and Vijfvinkel simulations, 0.0001 (-) for which linear theory is recommended, 0.001 (-) for which Stokes 2 theory is recommended and 0.01 (-) for which Stokes 5 theory is recommended.

Comflow

Table 5.22 lists the simulations that are performed in Comflow; the wave theory that prescribes the inflow boundary is varied, as well as the wave steepness, expressed in dimensionless terms $H0/gT^2$ and H/L.

Table 5.22: Steep Wave experiment: wave steepness and wave theory to prescribe inflow boundary.

$H0/gT^2$ (-)	0.0001	0.001	0.01	0.02
H/L (-)	$6.28\ 10^{-4}$	$6.28\ 10^{-3}$	$6.28\ 10^{-2}$	$1.26\ 10^{-1}$
Linear	Appendix D	Appendix D	Figure 5.32	Figure 5.34
Stokes 2	Appendix D	Appendix D	Figure 5.32	Figure 5.34
Stokes 5	Appendix D	Appendix D	Figure 5.32	Figure 5.34

The spatial gridding is $\Delta x/L=\Delta z/L=1/100$ (-) and $\Delta t/T=1/500$. The Courant number is 0.20 (-). The simulation is started from rest (initial surface elevation and velocities are zero).

A Sommerfeld outflow boundary is used. The group velocity of the fundamental waves allows us to measure from t=(0,28.4) seconds before a reflection of equal wave period from the outflow boundary is expected at the second point of measurement. The group velocity of the fundamental waves is such that the outflow boundary is reached after 17.75 (s). A reflected wave with the same period as the fundamental wave takes 10.65 seconds to return to the second location of measurement. The total time span in which the undisturbed wave can be measured in location 2 is equal to the sum of the two times; t=(0,28.4). Again, this is under the assumption the fundamental wave does not generate larger period, thus faster propagating, reflections at the outflow boundary. The second location of measurement is reached 7.1 (s) after the start of the experiment. The effective time interval becomes t=(7.1,28.4) seconds. To minimize possible disturbances at the boundaries of this effective times series, t=(10,20) seconds, is used for interpretation.

Vijfvinkel

In the Comflow simulation, the fluid initially is at rest and a boundary condition is used to prescribe the waves. Since Vijfvinkel's domain is periodic no outflow or inflow boundaries are used. The waves are prescribed as initial condition using 5th order Stokes theory.

The simulations are listed in Table 5.23. The table gives the wave steepness, linear amplitude, rate of filtering (ν), order of truncation of the nonlinear terms (M), grid parameters and Courant number. The steeper the waves, the more instability can arise due to the generation of high frequency (erroneous) waves [25]. Stability is maintained by increasing the filter coefficient, or by reduction of the number of grid points, which eliminates high frequency error waves by the Nyquist criterion. Reference is made to [25] for detailed information on the filtering method.

Table 5.23: Input values for Steep Wave simulation in Vijfvinkel.

$H0/gT^2$ (-)	H0/L0 (-)	A0 (m)	N	M	Δx/L	Δt/T (-)	Cr (-)
0.0001	$6.283\ 10^{-4}$	0.002	0	10	1/26	1/50	0.52
0.001	$6.283\ 10^{-3}$	0.02	0	10	1/26	1/50	0.52
0.005	0.0314	0.1	0.1	10	1/26	1/50	0.52
0.01	0.0628	0.2	0.3	10	1/26	1/100	0.26
0.015	0.0942	0.3	0.35	10	1/26	1/200	0.01
0.02	0.126	0.4	0.5	8	1/26	1/1000	0.002
0.02	0.126	0.4	0.25	10	1/13	1/100	0.13

5.4.3. Inflow boundary wave theory in Comflow

The influence of the wave theory that prescribes the inflow boundary on the performance of Comflow is investigated. It is expected that free error waves, that are generated by a simplification (such as linear theory) of the physics, will reduce if a higher order nonlinear inflow boundary is used. This effect will show increasingly for higher wave steepness.

Results

The time series and amplitude spectra of the Comflow simulations are given in Appendix D. For the two lowest wave steepnesses, $H/gT^2 = 0.0001$ (-) and $H/gT^2 = 0.001$ (-), the wave theory that describes the inflow boundary does not influence the simulation. No deviations are observed between the three theories that are used.

Figure 5.32 shows the time series of the waves with steepness $H0/gT^2 = 0.01$ (-). A difference is seen for the time series with linear wave theory at the inflow boundary. High frequency, low amplitude surface waves influence the wave. Also the mean water level seems to go down slowly.

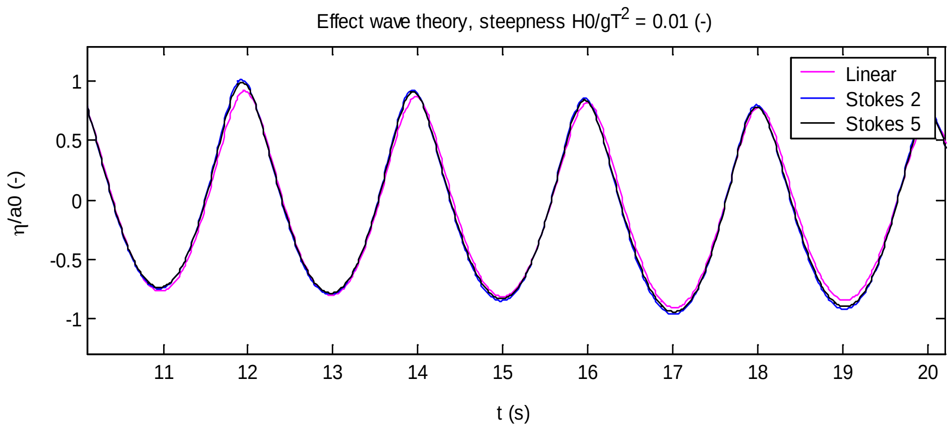

Figure 5.32: Steep Wave simulation in Comflow, $H0/gT^2 = 0.01$ (-).

The amplitude spectrum (Figure 5.33) shows that there is a significant contribution of the second order component. As this component is not prescribed at the inflow boundary Comflow generates free error wave to overcome this. This is an explanation for the deviation in the simulation that uses linear wave theory to prescribe the inflow boundary.

The apparent sag in water level is represented in the first component of the amplitude spectrum, which has significant contribution, see Figure 5.33. The same observation was done in the Beji Battjes test (section 5.2) for the run with equal (and coarser) grid parameters and time step. The cause of the sag was expected to lie in the sudden transition between the initial condition and the wave input at the boundary. However, when the wave steepness was increased, the lowering of the water level was decreased, see section 5.2.6. This sag in water level is more pronounced in the steepest simulation, $H0/gT^2 = 0.02$ (-).

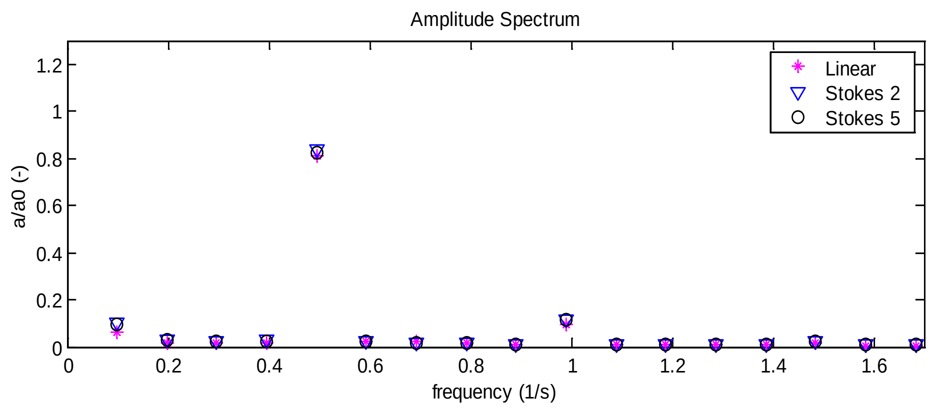

Figure 5.33: Amplitude spectrum of Steep Wave simulation in Comflow, $H0/gT^2 = 0.01$ (-).

For near breaking waves the difference between the wave theory at the inflow boundary is clearly visible. Figure 5.34 shows the time series of the waves with steepness $H0/gT^2 = 0.02$ (-). None of the wave theories that are used at the inflow boundary result in a steady solution, and have significant skewness. Free error waves disturb the simulations that use linear and Stokes 2 wave theory. The sag in the water level is, as discussed above, even more pronounced.

However, a clear difference is seen between the three runs with different wave theory. The runs that use linear and Stokes 2 wave theory at the inflow boundary show lower crests with high frequency error waves. The simulation that uses Stokes 5 wave theory to prescribe the inflow boundary has the highest crests and has the smoothest surface.

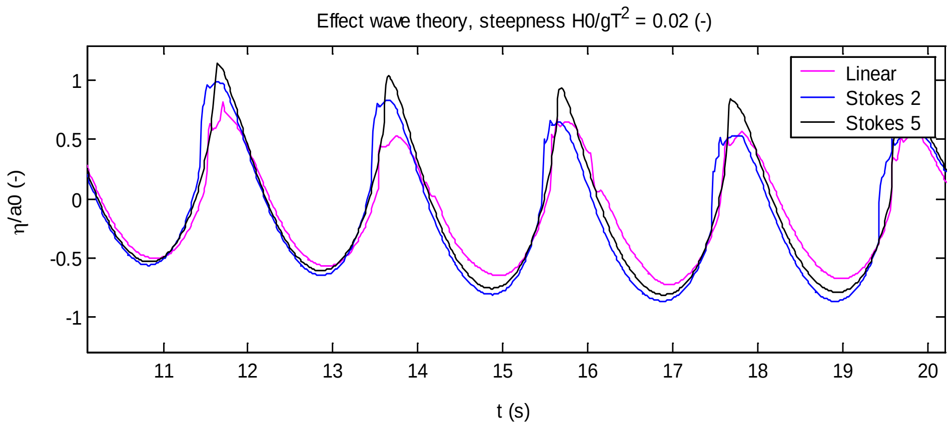

Figure 5.34: Steep Wave simulation in Comflow, $H0/gT^2 = 0.02$ (-).

The amplitude spectrum (Figure 5.35) shows that numerous harmonics are measured. The amplitude decreases as the frequency increases. The first natural frequency has significant contribution as the mean water level sinks. To what order does our wave theory need to be to model near breaking waves correctly? In Figure 5.35 the 6th order harmonic has significant amplitude, so Stokes 5 theory implies the generation of error waves.

Harmonics up to the 5th or 6th order have measurable amplitude, while the inflow boundary only produces 5th order waves. By prescribing the inflow boundary in Comflow with Stokes 5 wave theory error waves are generated. A fully nonlinear inflow boundary would avoid the question as all harmonics are incorporated.

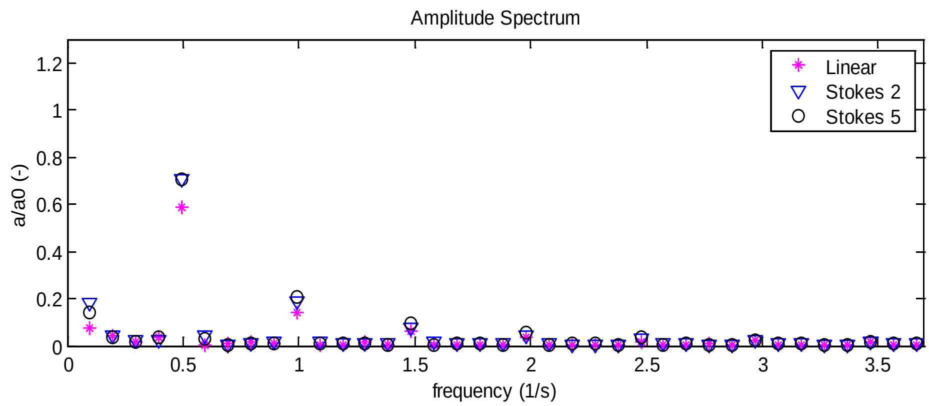

Figure 5.35: Amplitude spectrum of Steep Wave simulation in Comflow, $H0/gT^2 = 0.02$ (-).

5.4.4. Regular waves in Vijfvinkel

In Vijfvinkel waves of various steepness are simulated. The performance is expected to be better than Comflow. The Nyquist limitation, and the impact on the simulation is discussed, as is the influence of the input that Vijfvinkel requires.

The time series of the Steep Wave experiment simulation are listed in Appendix D. The most demanding simulation, that of near breaking waves, is depicted in Figure 5.36. The number of grid points in the domain of length equal to five wavelengths is 64; per wave length the number of grid points is $\Delta x/L = 1/13$. The time step $\Delta t/T = 1/100$ (-) and the linear amplitude is 0.4 (m). Figure 5.36 shows that Vijfvinkel is able to produce a steady solution, even in these conditions.

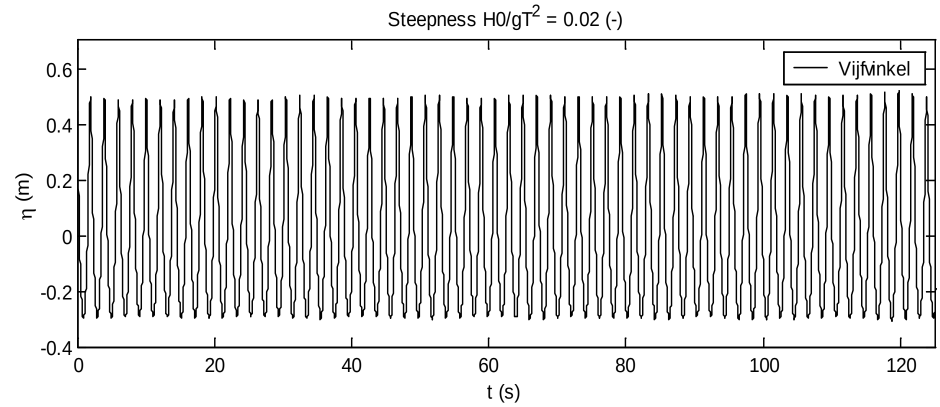

Figure 5.36: Vijfvinkel run of $H0/gT^2 = 0.02$ (-).

The used parameters in Vijfvinkel are given in Table 5.23. The results for all Steep Wave simulations that were done in Vijfvinkel are listed in Table 5.24.

Table 5.24: Results Steep Wave simulation in Vijfvinkel.

Input		Output			
$H0/gT^2$ (-)	H0/L0 (-)	T (s)	Max(A)/a0	$H0/gT^2$ (-)	H/L (-)
0.0001	$6.283\ 10^{-4}$	2.000	1.001	$5.097\ 10^{-5}$	$6.494\ 10^{-4}$
0.001	$6.283\ 10^{-3}$	2.000	1.012	$5.097\ 10^{-4}$	$6.495\ 10^{-3}$
0.005	0.0314	2.000	1.067	$2.548\ 10^{-3}$	0.03264
0.01	0.0628	1.960	1.138	$5.307\ 10^{-3}$	0.06534
0.015	0.0942	1.930	1.224	$8.210\ 10^{-3}$	0.09883
0.02	0.126	1.840	1.513	$1.204\ 10^{-2}$	0.1265
0.02	0.126	1.820	1.296	$1.231\ 10^{-2}$	0.1285

The last two runs ($H0/gT^2$ =0.02 (-)) are done with identical amplitude but with different grid. Instability can arise due to the generation of high frequency error waves. Two strategies are used to maintain a stable solution for the simulation with $d/gT^2 = 0.02$ (-), see Table 5.24.

- The rate of filtering is increased which flattens the high frequency waves. In addition, a lower order of truncation is used.

- The grid is made coarser such that the high frequency waves are excluded due to the Nyquist limitation. The coarse grid has limitations regarding the representation of the nonlinear terms as the Nyquist limitations only allows a 6^{th} order harmonic to be represented. However, error waves may be translated to lower frequencies that can be modeled.

For the simulation of near breaking waves instability can arise due to high frequency error waves. Stability can be maintained with a filter or by reduction of the number of grid points, which transfers the effect to lower frequency waves. In contrast to the high frequency error waves, low frequency error waves have less influence on stability. The frequency of the error waves is expected at, and just below the Nyquist frequency. The wavelets that compose the Newwave, and their higher harmonics (to the 6^{th} order) can be modeled with the chosen grid. Change of the required input (see recommendation 2.5), and improvement of the initial condition (see recommendation 2.6) will prevent the generation of high frequency error waves.

The effect of Vijfvinkel's input; a S(k) spectrum

The initial condition in Vijfvinkel is constructed in accordance to the wave numbers that need to be given as input. This applies to the simulation of regular waves. For Newwave simulations the input consists of a spectrum, giving the variance over a range of wave numbers. When Vijfvinkel coded up his findings he chose for wave numbers as input, instead of the wave periods. However, from a physical point of view this is inconvenient.

From a mathematical point of view the input of wave numbers is appropriate. The wave number is inversely related to the wavelength. Having the wavelength it can easily be checked if the wave is periodic in the spatial domain; this is beneficial for the FFT algorithm on which Vijfvinkel's pseudo-spectral method is based.

From a physical point of view the input of wave frequency is appropriate. Using a frequency as an initial condition is straightforward when modeling a spectrum, since spectra are defined in a frequency domain. Frequency based spectra, such as the JONSWAP spectrum that is used in this thesis to model Newwaves, need to be transformed into a wave number based spectra.

The dispersion relation links the wavelength and frequency. For nonlinear irregular wave groups the dispersion relation is unknown a priori.

The implication is demonstrated for the regular waves that are simulated in the Steep Wave experiment. In Table 5.24 it is shown that the wave periods are underestimated. The linear dispersion relation (which is also applicable for Stokes 2 theory) was used to transform the wave frequency into a wavelength. However, significant error was introduced by this transformation, as the returned wave period is shorter.

Using the Stokes 5 dispersion relation {A14} the dispersion relation includes the wave steepness. As for the linear dispersion relation, the wavelength of the regular waves can be calculated iteratively; the resulting wavelengths are shown in Table 5.25.

Table 5.25: Effect nonlinear dispersion on wavelength for Steep Wave experiment.

$H0/gT^2$ (-)	L Linear wave theory (m)	L Stokes 5 (m)
0.0001	6.159	6.160
0.001	6.159	6.161
0.005	6.159	6.216
0.01	6.159	6.389
0.015	6.159	6.677
0.02	6.159	7.063

The initial condition of the simulation of the Steep Wave experiment in Vijfvinkel, with the highest wave steepness, is done using the linear dispersion relation and the Stokes 5 dispersion relation. The latter returns the desired wave frequency. This is shown in Figure 5.37. The frequencies of the simulation that uses the 5th order Stokes dispersion relation show less deviation from the desired wave frequency, 0.5 (1/s).

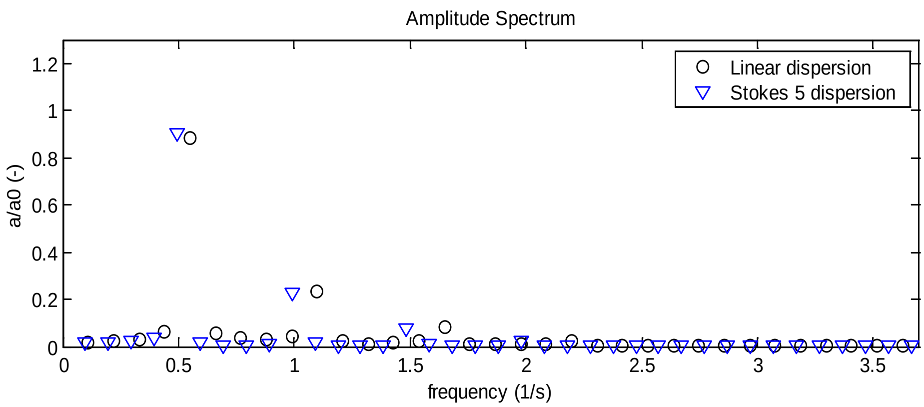

Figure 5.37: Amplitude spectra for the Vijfvinkel runs with steepness $H0/gT^2$= 0.02 (-), using linear and Stokes 5 dispersion relation.

For nonlinear, irregular waves, such as the Newwave, the dispersion relation is not known a priori as waves of a range of frequencies interact. How to deal with the translation between a frequency based spectrum and wave number based spectrum? When modeling Newwaves in Vijfvinkel the initial condition is chosen such that the wave heights are as low as possible. The error originated in the influence of wave steepness and irregularity on the dispersion is then minimalized.

In this thesis the transformation between the frequency spectrum and wave number spectrum is done using the linear dispersion relation. The initial condition is chosen such that the wave heights are minimal, which reduces the error.

It is recommended that a frequency based spectrum can be used as initial condition in Vijfvinkel. Vijfvinkel needs to include a nonlinear dispersion code, taking into account local steepness. The spatial domain should be adapted accordingly, to maintain the periodicity condition.

5.4.5. Comparison Comflow and Vijfvinkel

In Figure 5.38 the results of both models are visualized. The propagation characteristics of Vijfvinkel are superior to Comflow, especially with regard to steep waves. Comflow has difficulty with producing a stationary solution, the waves have skewwness, and shows more damping as waves get steeper; aspects that are not observed in the Vijfvinkel simulation.

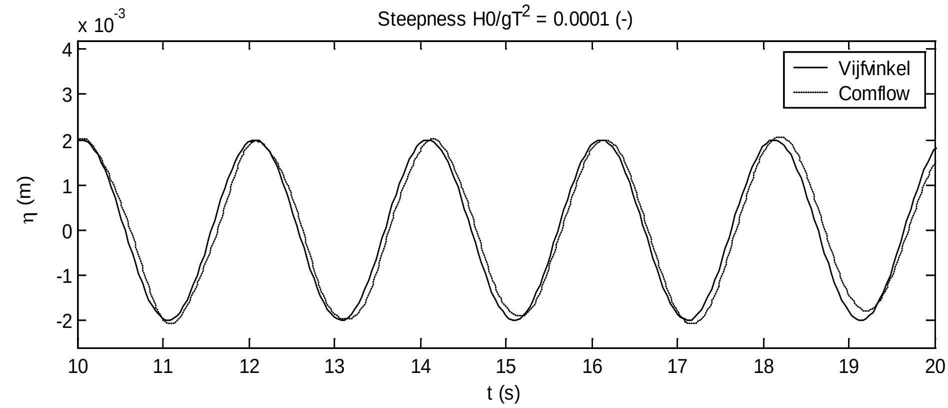

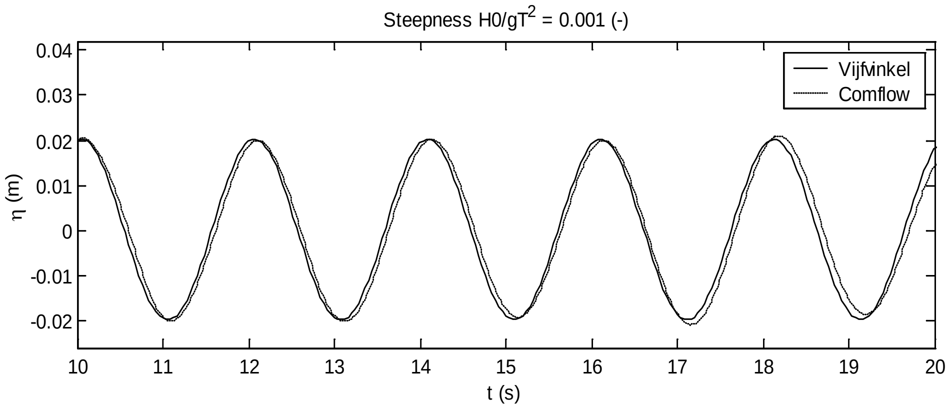

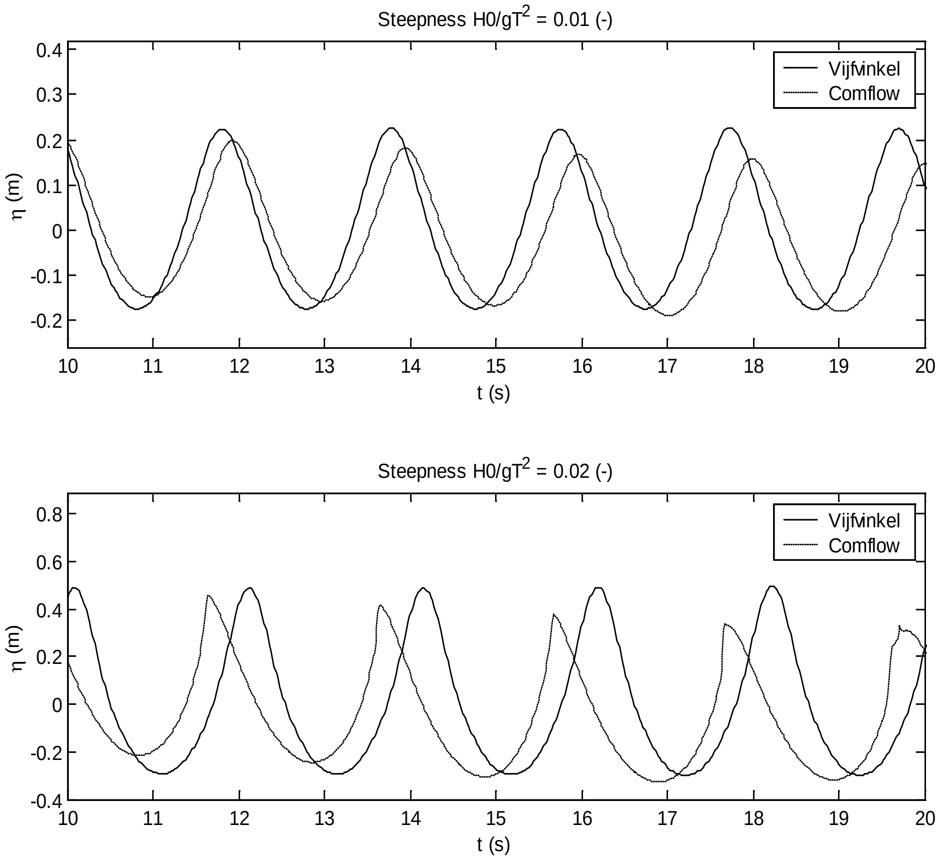

Figure 5.38: Comparison Steep Wave simulations in Vijfvinkel and Comflow.

5.4.6. Conclusions

The following can be concluded from the simulation of the Steep Wave experiment in Comflow and Vijfvinkel:

1. Vijfvinkel gives superior results for the simulation of regular waves, compared to Comflow. In Comflow, damping is large if the wave steepness is close to the limit steepness. Comflow shows increasing damping and unsteadiness if steep waves are modeled. Vijfvinkel is able to simulate waves of high steepness and produces a stationary solution for the chosen parameters.

2. Error waves are created in Comflow if a wave theory is used to prescribe the inflow boundary that is not representative for the nonlinear conditions of the wave steepness and relative water depth. For waves with steepness $H0/gT^2 = 0.01$ (-) at least a second order theory should be used. For waves of steepness $H0/gT^2 = 0.02$ (-) a fully nonlinear theory is recommended as Stokes 5 is not representative.

3. The desired input for Vijfvinkel requires the knowledge of the dispersion relation for the waves that are modeled. The Vijfvinkel input is given in term of wavelength instead of wave frequency, which is sensible from a mathematical point of view, as it is easy to comply with the spatial periodicity condition. However, from a physical point of view it is inconvenient. The transformation of a wave spectrum in to a Newwave requires knowledge of dispersion of wavelets within a nonlinear wave group.

5.5. Simulation of nonlinear Newwaves

5.5.1. Goal

The goal of this experiment is to simulate nonlinear Newwaves, to compare these with linear Newwaves theory, and to indicate the applicability for Comflow.

5.5.2. Experiment setup

Nonlinear Newwaves are generated in Vijfvinkel, which uses the linear Newwave theory as initial condition. The domain specifications are listed in Table 5.26. The begin time is varied for several runs.

Table 5.26: Domain specifications of nonlinear Newwave simulation in Vijfvinkel.

Domain length (m)	Grid points (-)	Δx (m)	Order of Truncation M (-)	Filter (-)	Δt (s)	End time (s)
3771.1	512	7.380	10	0.3	0.01	70

The 64 component JONSWAP spectrum (see section 3.1) is used to compose the Newwave; the wave number interval, Δ(1/L), over which the contribution to the variance is calculated is constant. The length of the Vijfvinkel domain is taken equal to the recurrence length of the Newwave, see Table 3.1 and Table 5.26.

$$L_{dom} = \frac{1}{\Delta\left(\frac{1}{L}\right)} = 3771.1(m) \qquad (-)$$

Exactly one wave group is represented in the domain. The interval between the wave length of each of the 64 components is such that each component is exactly represented once more than the previous component (starting from the lower wave numbers): the spectral component with the longest wave length is represented 10.914 times in the domain, the next component 11.914 times, the third component 12.914 times etc. If a different domain length is chosen, the interval between the number of waves represented in the domain would not be equal to one. Preferably the number of waves in the domain is an integer. However, the restriction that Vijfvinkel has is that the spectrum is defined having an equally spaced Δ(1/L) interval. Now the number of waves in the domain is not an integer, but we are close; and the closer it is, the better the FFT performs. Having the number of waves close to an integer (.914) , for all 64 spectral components (by having adding an entire wavelength for the next component; 10.914, 11.914, 12.914 etc.), yields less error in the FFT procedure of Vijfvinkel than having the number of waves distributed randomly.

Ideally, the domain length is chosen such that the number of waves is an integer. However, this is not possible with the used spectrum as this would result in a domain that is considered too large.

5.5.3. The effects of nonlinearity

One of the effects of nonlinearity is the shape of the wave: higher and peaked crests and shallower long troughs. For irregular waves it is also noted that waves interact. A surface depression accompanies the wave group.

Linear Newwave as initial condition

In Linear Newwave theory a focus time and location are chosen with which the surface elevation in time and place can be reconstructed, using the linear dispersion relation, and the superposition of the wavelets of which the spectrum is composed. Using a linear model, focus takes place with no time lag, and at the (linear) focus height. The independent propagation, which is used in the linear model, is not applicable for nonlinear modeling.

With a nonlinear solver these initially superimposed components interact, and this influences the focus time and location. The shape of the wave changes: the crests get higher and peaked, and the troughs shallow and long. Waves interact and a surface depression accompanies the wave group.

Parameters that affect the nonlinear effects include the number of waves, the direction of the waves, the relative steepness and relative water depth etc. Of these parameters, the starting time of the Newwave simulation in Comflow is varied; all other parameters are kept constant. Figure 5.39 shows three different initial conditions that characterize three Newwave simulations.

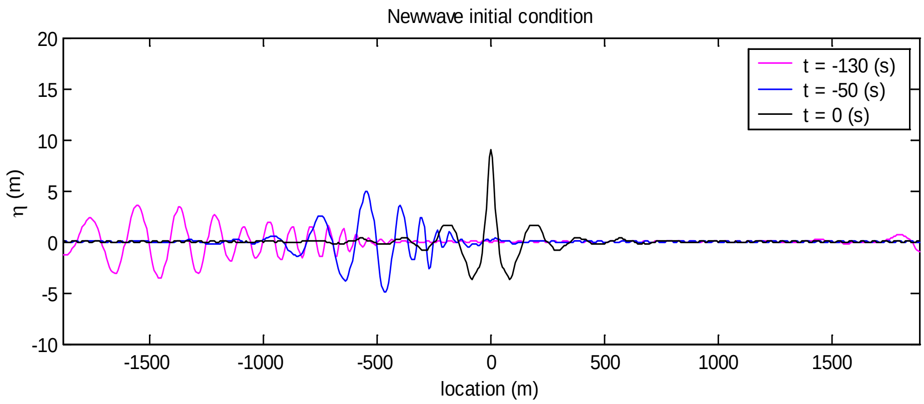

Figure 5.39: Nonlinear Newwave simulations in Vijfvinkel are done with several starting times.

The starting time of the nonlinear Newwave simulation is bound by two issues: numerical damping (upper boundary) and the development of the nonlinear terms (lower boundary). It is observed that the waves steepen quickly, this is an indication that nonlinearity is expressed quickly. The Steep

Wave experiment showed that Vijfvinkel has marginal numerical damping, even for steep waves in transitional water depth (see section 5.4); the start time of the Vijfvinkel simulation could be large.

For irregular waves the wave steepness is defined as the difference in elevation between a crest and the mean of the neighbouring troughs, divided by the distance between the two troughs, see Figure 5.40. The wave steepness is considered for the wave with the highest crest.

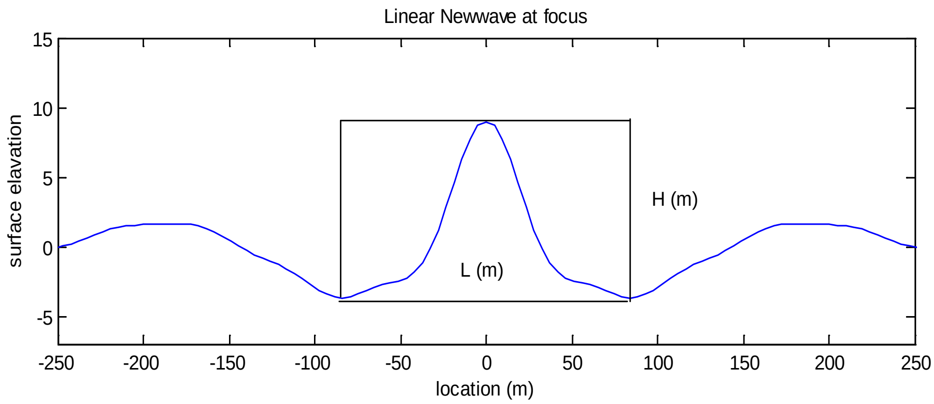

Figure 5.40: Definition of steepness of an irregular wave.

Table 5.27 gives relevant parameters of the linear Newwave that is imposed as initial condition in the performed Vijfvinkel simulations. The starting time of the simulation is varied for the different simulations.

Table 5.27: Relevant parameters of input for Newwave simulations in Vijfvinkel. Linear Newwave theory is used to compose the initial conditions.

T_{start} (s)	Crest height (m)	Location of crest (m)	Steepness H/L (-)
-130	5.893	-1560.8	0.0625
-75	6.489	-741.67	0.0749
-50	7.183	-549.8	0.0798
-25	7.413	-188.2	0.0932
-20	6.424	-291.5	0.0755
-15	6.825	-210.3	0.0939
-10	7.398	-136.5	0.1057
-5	8.259	-62.7	0.1016
0	9.000	3.7	0.0849

Quasi-nonlinear Newwave as initial condition

Vijfvinkel implemented a method to improve the propagation of a nonlinear wave that is defined using linear wave theory. This method, known as Creamers method, modifies the linear initial condition to a quasi-nonlinear condition by adding higher order terms. The transformed initial condition is better representative for nonlinear simulation and reduces the generation of free error waves [25]. Creamers method uses the Hilbert transform of the surface elevation to calculate higher order contributions. It is recommended [25] that the initial condition for Newwave simulations in shallow water is transformed with Creamers method to reduce the generation and influence of freely propagating error waves. This recommendation is followed. The Creamer transformed initial conditions are listed in Table 5.28. Note that only higher harmonics are added, while the extension to lower harmonics is expected to be beneficial for wave group simulations.

Table 5.28: Relevant parameters of input for Newwave simulations in Vijfvinkel. Creamer transformed Newwaves are used as initial conditions.

T_{begin} (s)	Crest height (m)	Location of crest (m)	Steepness H/L (-)
-130	6.478	-1560.8	0.0628
-75	7.286	-741.7	0.0758
-50	8.109	-549.8	0.0810
-25	8.530	-188.2	0.0951
-20	7.259	-121.8	0.0978
-15	7.652	-210.3	0.0931
-10	8.392	-136.5	0.1060
-5	9.607	-62.7	0.1060
0	10.641	3.7	0.0911

The difference between the linear initial condition and the initial condition that is transformed with Creamer's method is shown in Figure 5.41 and Figure 5.42. The surface elevation is given over a part of the domain. As expected the initial condition that uses Creamer's method shows a peaked and higher crests and shallower and longer troughs. This effect is larger if the surface elevation is large; the Creamer method contribution increases as the wave steepness increases. For the simulation with starting time t = 0 (s) this is evident: the linear crest height of the initial condition that uses Creamer's method exceeds the theoretical linear focus height of 9 (m), see Figure 5.41, Figure 5.42 and Table 5.28

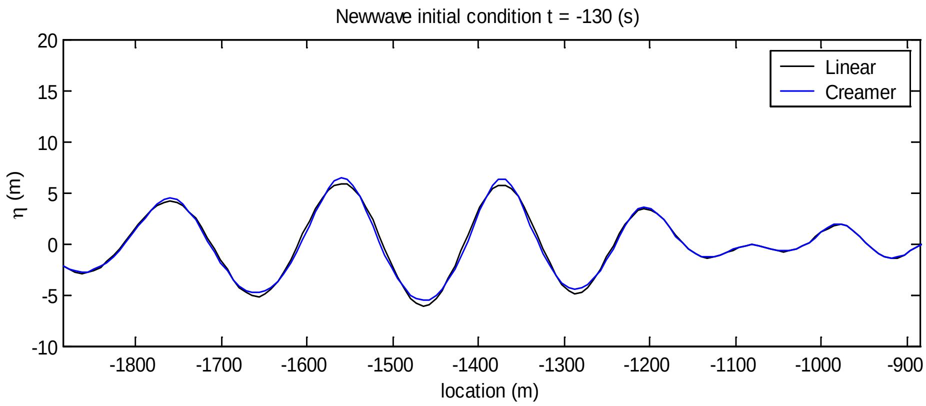

Figure 5.41: Comparison initial surface elevation using linear Newwave theory and Creamer transformed Newwave for waves of low steepness.

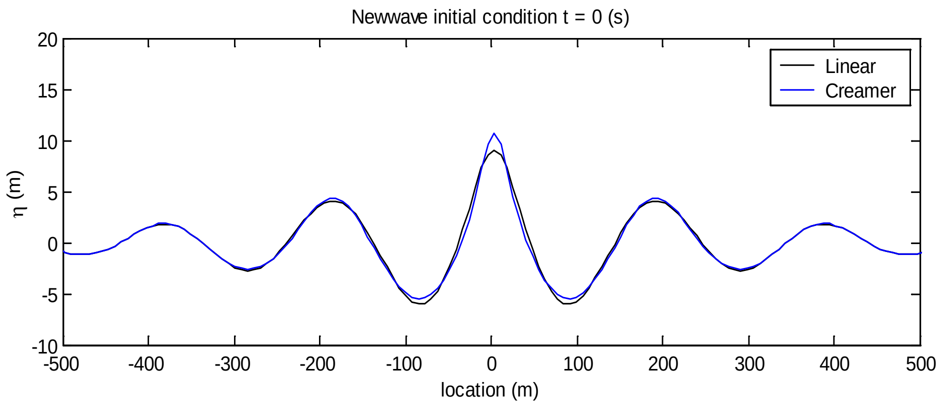

Figure 5.42: Comparison initial surface elevation using linear Newwave theory and Creamer transformed Newwave for waves of low steepness.

The Creamer transformed initial conditions will be used for Newwave simulations.

Results

The influence of nonlinear simulation of Newwaves on the location, time and height of focus is given in Table 5.29, listing the time and the height of the maximum surface elevation. In Appendix E the surface elevation is plotted in space and time.

Table 5.29: Nonlinear Newwave peak, closest to the linear focus location and time.

T_{begin}	Focustime (s)	Focuspoint (-)	Crestheight (m)	H/L (-)
-130	7.4	121.8	8.836	0.0642
-75	4.3	92.2	10.014	0.0733
-50	5.1	114.4	11.718	0.0958

-25	0.8	40.6	13.902	0.127
-20	3.3	77.5	15.549	0.167
-15	0.9	40.6	15.573	0.0943
-10	2.5	62.7	15.731	0.084
-5	10.8	188.2	15.477	0.083
0	15.6	254.6	13.177	0.095

Nonlinear Newwaves show multiple peaks

A first observation is that the runs covering a longest time spans, with start time t=-130, t= -75 and t=-50 (s) show multiple peaks well in front of the linear focus point. Similar observations were done by [25]. These maximum peak height is the first peak, these take place approximately 18 seconds after the start of the simulation, for the three runs covering a relatively long time span, see Table 5.30.

Table 5.30: Nonlinear Newwave highest peak.

T_{begin}	Focustime (s)	Focuspoint (-)	Crestheight (m)
-130	-114.7	-1317.3	10.214
-75	-57.3	-645.7	11.733
-50	-32.9	-276.7	14.307

The maximum surface elevation (regardless of the location) is plotted in Figure 5.43. In this Figure, the Newwave simulation starts at t = -130 (s). The focus peak is considered to be the peak at t = .4 (s), which is indicated with an arrow. The maximum surface elevation is at t = -114.7 (s).

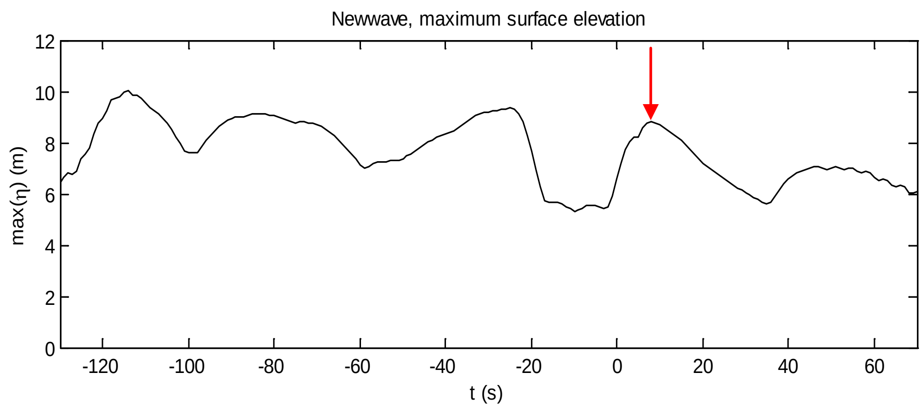

Figure 5.43: Maximum surface elevation in time for nonlinear Newwave simulation with start time t = -130 (s).

The time of the first focus, after the run has started, is approximately 18 seconds. This is an indication that nonlinear terms are fully developed. Despite the previous focuses, these runs do have an extreme crest height close to the theoretical focal point. The crest height at the focal point is lower than the first peak, but is close to the linear focal height.

For the runs that have a starting time close to the linear focus time have the first peak near the linear focus point and time. The surface elevation is larger than for the long runs, see Table 5.29. The largest surface elevations are recorded at a location down wave of the linear focus point and time.

In linear Newwave theory all spectral components come in phase at the location and time of focus; at this spot and moment the phases of all component show no variation. With a nonlinear model the definition of the focus point is not strictly met. Having a nonlinear solver and a wave group composed of a variety of wavelets, the propagation velocity of the wavelets will be changed by nonlinear interaction. Having modified phase velocities the phases at the linear focus point will not all be equal; in the nonlinear model, the phases at the (linear) theoretical focal point and time show variation. The larger the nonlinear effects and the more these have developed, the larger this variation will be at this point and time. For the runs covering a long time span (Table 5.28) the phases of the energetic frequencies show larger agreement at the first peak than near the linear focus time. The nonlinearities show quickly, the wave group gets bound and translates steadily, compare the linear Newwave (Figure 5.44) and the nonlinear Newwave (Figure 5.45). The small wiggles in these figures originate in the plotting procedure; the waves in fact have a smooth surface.

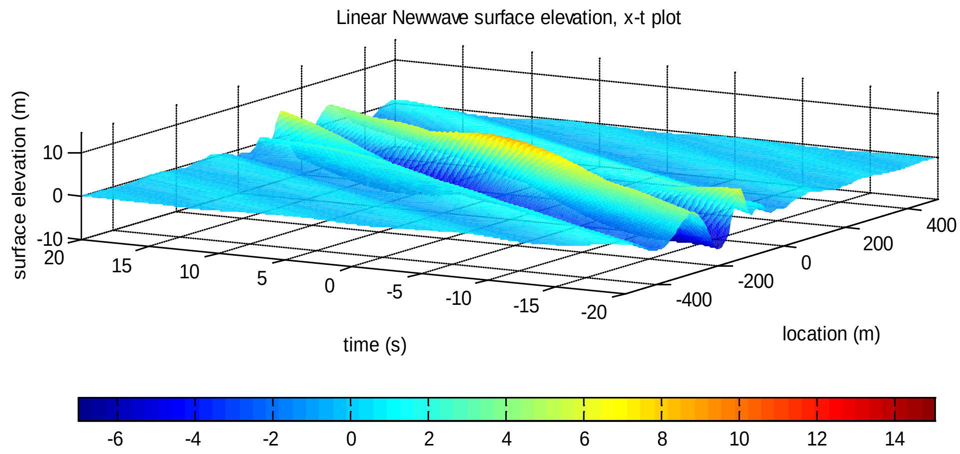

Figure 5.44: Linear Newwave.

The focusing of linear and nonlinear Newwaves is depicted in Figure 5.45.

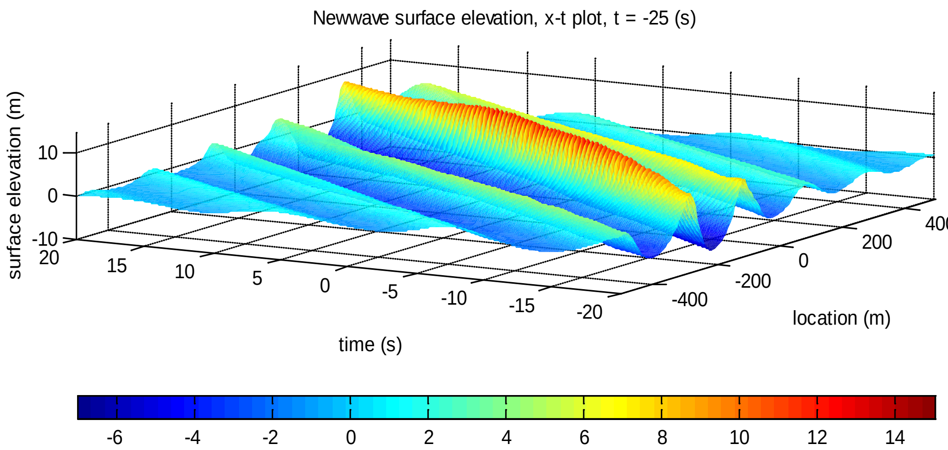

Figure 5.45: Nonlinear Newwave with start time t = -25 (s).

Figure 5.45 shows that, despite the observations regarding the multiple peaks and the surface depression, the nonlinear Newwave shows resemblance with the linear Newwave. The aspects that are expected are indeed observed: the sharpening of the crests, the stretching of the troughs, the shift of the location and time of focus. The wave group propagates bound, the design crest does not emerge out of the blue (color) as in the linear Newwave. It needs to be studied if the nonlinear Newwave is representative for the extreme wave, as the crests of the wave group are maintained for a longer time interval.

A surface depression that accompanies the Newwave is generated and released

Wave groups are accompanied by a surface depression of the length of the same order as the wave group. This surface depression can be seen as a relatively long wave that is bound to the wave group. In Vijfvinkel a relatively long, erroneous wave is observed, that propagates freely (unbound to the wave group). The influence of this long wave is depicted in Figure 5.46. This Figure shows the development of the variance density spectrum in time. Note that the spectrum is given per wave period; as in Figure 3.1. With the arrow the generation of the low frequency wave is indicated. The variance of this wave increases steadily. The peak of the JONSWAP spectrum that was used as initial conditions slowly moves to a lower wave number and the peak flattens out. Also in the higher wave numbers, close to the first harmonic, near $1/L = 0.01$ (1/m), wiggles are observed. These are indicated with the ellipse.

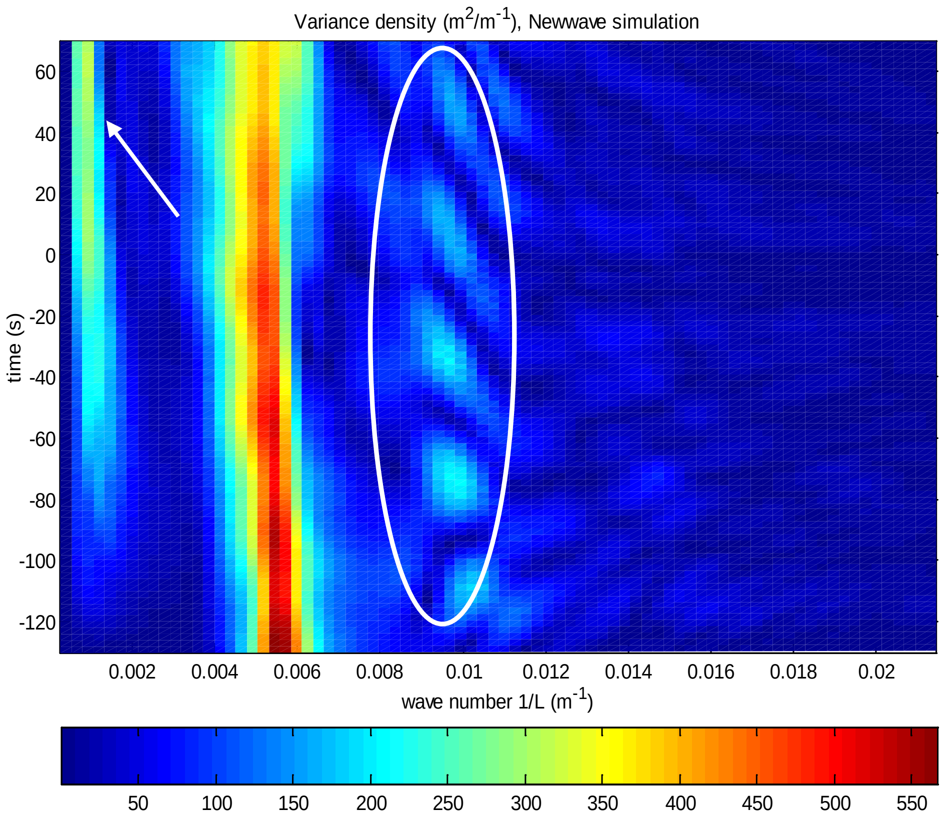

Figure 5.46: Variance spectrum development in time for a nonlinear Newwave simulation with start time t=130 (s).

From Figure 5.46 it can not be derived if the low frequency wave is bound to the wave group or not. Bispectral analysis can indicate this. Figure 5.47 shows the surface elevation at the end time of the simulation. The still water level is indicated with the dotted line. Figure 5.47 shows a wave with a long wave length (and low frequency) that leads the wave group (indicated with an arrow). The long wave has propagated independently and has entered the left side of the domain, as the spatial domain in Vijfvinkel is periodic.

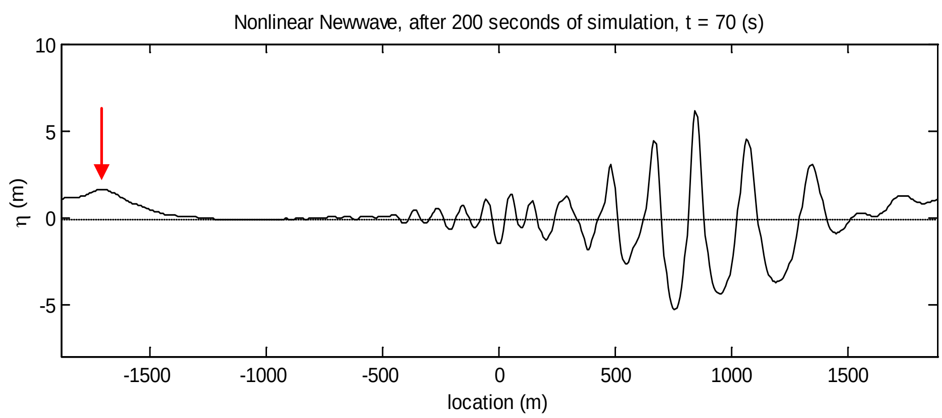

Figure 5.47: Surface elevation at the end time of the simulation t = 70 (s).

It is expected that the generation of this erroneous long wave can be prevented. Extension of the Creamer method by including a correction for lower harmonics can reduce the generation of the erroneous unbound wave.

5.5.4. Preparations for Comflow implementation

One difficulty for Comflow is the simulation of steep waves. Steep waves in Comflow show significant damping, (see section 5.4). Two issues are considered in this section:

1. The steepness of Newwaves at the location of the inflow boundary of Comflow. This is done for both linear and nonlinear Newwaves, based on the same input spectrum. The crest height of the nonlinear solution is higher, while the troughs are shallower that the linear Newwaves.
2. The consequence of the nonlinear surface depression that is released from the wave group, as discussed in section 5.5.4.

The steepness of the Newwave is considered at the boundary of the Comflow domain. The Comflow domain starts at x = -500 (m). The closest node in the Vijfvinkel run is located at x = -498.2 (m). Here a time series is recorded for the surface elevation and velocity potential. The wave steepness is calculated using the dimensionless d/gT^2 and H/L steepness parameters. The definition of the wave steepness (see Figure 5.40) also is applied to the time series; only the length axis is changed for the time axis. The linear dispersion relation this is rewritten in terms of the wavelength in the considered water depth of 30 (m). Maximum values are listed in Table 5.31 for each of the Newwave runs. The runs that start short before focusing are not given since the main part of the wave group has already passed the location of measurement.

Table 5.31: Extreme values of wave parameters at x = -498.2 (m).

T_{begin} (s)	Crest height (m)	Time of crest (s)	Steepness H/gT^2 (-)	Steepness H/L (-)
-130	7.589	-48.34	0.0067	0.0597
-75	9.629	-47.63	0.0094	0.0778
-50	8.654	-34.13	0.0114	0.0856
Linear				
	5.105	-46.67	0.0080	0.0611

In Figure 5.48 and Figure 5.49 the time series are shown of the surface elevation and velocity potential at the location where Vijfvinkel prescribes the inflow boundary of Comflow. The Comflow inflow boundary is located at x = -500 (m). Two simulations are depicted, with starting time t = -130 (s) and t = -75 (s) respectively. In Figure 5.48 the linear Newwave is also depicted (magenta line) for comparison. The inflow boundary for Comflow requires the surface elevation and a velocity profile. The velocity profile can be calculated with record of the surface elevation and velocity potential.

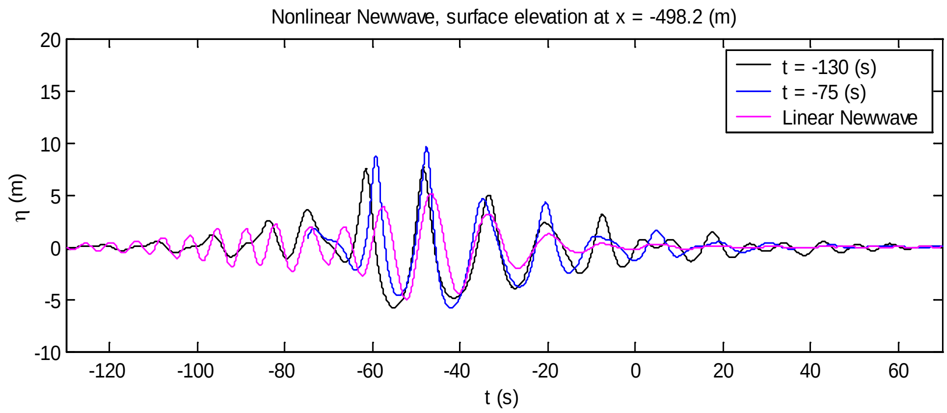

Figure 5.48: Nonlinear Newwave, surface elevation at x = -498.2 (m).

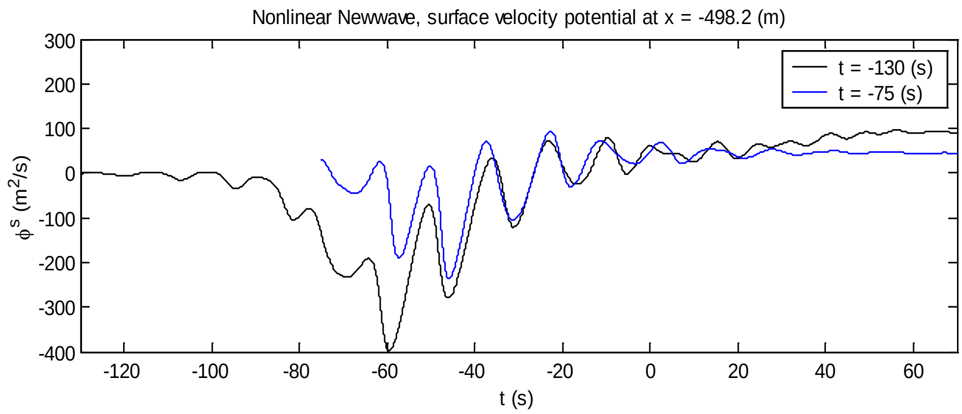

Figure 5.49: Nonlinear Newwave, surface velocity potential at x = -498.2 (m).

Figure 5.50 shows a the surface elevation at x = -498.2 (m) for the nonlinear Newwave simulation with starting time t=-130 (s). The still water level is indicated with the dotted line. The waves preceding the design wave have a slightly lower mean water level, while the waves following up on the extreme wave seem to have lifted, based on visual interpretation of Figure 5.50. The influence of the erroneous long wave (see section 5.5.3) is expected to be limited at this location during the considered time interval. The surface depression under the most energetic wavelengths seems minor. It is expected that extension of the Creamer method to correction for lower harmonics would reduce the influence of the unbound long wave.

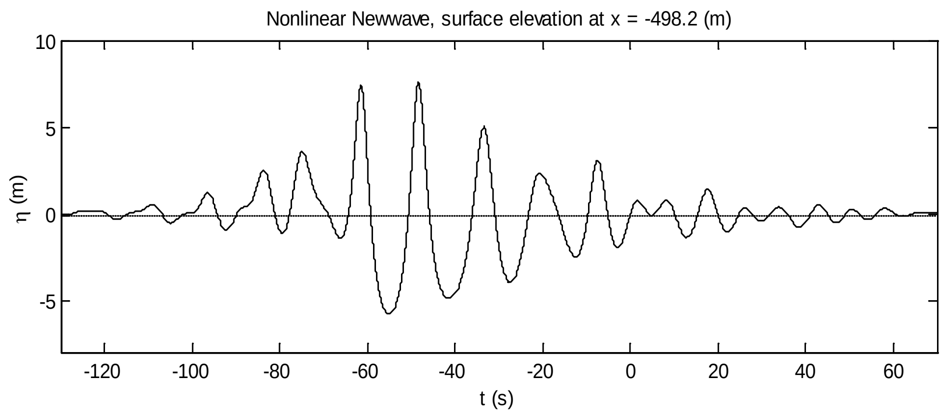

Figure 5.50: Surface at the Comflow inflow boundary, x =-498.2 (m).

5.5.5. Conclusions

The following can be concluded from the simulation of nonlinear Newwaves in Vijfvinkel:

1. The Vijfvinkel domain length must be chosen such that the spectrum is most suitable for FFT operations, on which Vijfvinkel's algorithm is based. The ideal domain length should represent an integer number of waves for all the spectral components. This domain would be impracticable, as it is extended to a computationally demanding length.
2. Newwaves can be simulated with a method that adds nonlinear contributions to the linear Newwave that is set as initial condition in the Vijfvinkel domain. The method that is used for this purpose is Creamer's method [25]; it reduces the generation of free error waves and enhances the stability of the solution. The Creamer transformed initial condition is used for Newwave simulations.
3. The starting time of the simulation influences the focusing of the nonlinear Newwave in Vijfvinkel. The shape of the wave train, the time, height and location of focus are affected, as expected.
4. The Newwaves that have a start time of 25 (s) and less before the linear focus time show a crest height increase of approximately 70 %, relative to the linear crest height.
5. Newwave simulations in Vijfvinkel that have starting time of 50 seconds and more before the linear focus time have several peaks before the focus time and location. The extreme surface elevation takes place at the first peak, approximately 18 seconds after the start of the simulation. Near the linear focus time and place the Newwave crest height is close to the linear crest height.
6. A long wave is generated and is released from the wave group. The importance of this long wave increases, and is clearly visible after 200 seconds of simulation.
7. The variance spectrum indicates the varying contribution high frequency waves, relative to the most energetic frequencies of the spectrum representing the extreme sea state.
8. Despite conclusions 6 and 7, the nonlinear Newwave shows resemblance with the linear Newwave, taken into account the expected influence of wave shape, height, focus location and time. It is recommended that the validity of the nonlinear Newwave is verified.

9. The estimates of the steepness of the Newwaves at the location of the inflow boundary in the Comflow domain indicate that at least a second order inflow boundary is required.

6. COUPLING OF VIJFVINKEL TO COMFLOW

Vijfvinkel is used to prescribe the inflow boundary to Comflow. The propagation performance of Vijfvinkel is used to improve the wave modeling in Comflow, which has the strength to accurately simulate wave impact on structures.

In this chapter the coupling between Vijfvinkel and Comflow is presented. After an introduction, several alternatives are presented how this can be established. An alternative is chosen and elaborated.

6.1. Introduction

Comflow

A 2nd order Newwave has been implemented in Comflow as boundary condition using Sharma and Dean theory for the kinematics. With Newwave simulations the deviations due to artificial damping were recognized. A higher order theory, or even a fully nonlinear method is recommended [10].

Vijfvinkel

A linear Newwave has been implemented in Vijfvinkel. Using the Creamer method this linear initial conditions is corrected with higher order terms to reduce the generation of free error waves at the start of the simulation. Vijfvinkel is a nonlinear solver and has shown superior results in the simulation of wave propagation compared to Comflow.

Goal

The goal of the coupling of Vijfvinkel to Comflow is to obtain the simulation of fully nonlinear Newwaves in Comflow. To start with, and following [10], the Newwaves are prescribed as a boundary condition.

Outline

Several alternatives are presented of making a coupling between Vijfvinkel and Comflow. Vijfvinkel can be used to prescribe initial and boundary conditions, or an interactive coupling of the two programs can be made. In this thesis the nonlinear Newwave simulation as described in chapter 5.5 is used to prescribe the inflow boundary in Comflow. This can later be extended to a an interactive coupling.

Besides the opportunity that fully nonlinear Newwaves can be modeled in Comflow, the coupling of the programs yields another opportunity. The location of the inflow boundary, for the fully nonlinear case, can be made closer to the location of focus. Also, the time span of the simulation can be shortened. For the existing Newwave inflow boundary a long spatial domain and time span of simulation are necessary as all the spectral components needed to be prescribed separately. In contrast, by using a second program to prescribe the Newwave, these components are not prescribed individually, but the wave group as a whole is prescribed. This saves domain length and time span of simulation. The benefit of a shorter Comflow domain has the following implications:

- A finer grid can be used. Given a maximum computational capacity implies that, with a shorter domain, a finer grid can be used. Geometries can more accurately be represented, and the wave impact better simulated. The results become more accurate.
- There is less damping. As Comflow shows more numerical damping, relative to Vijfvinkel, a shortening of the spatial domain implies less artificial damping. This enhances the results.
- Given a required grid and time span, a shortening of the domain and time step implies less computational time. Results are obtained quicker.

The computational effort currently limits the application of wave impact simulation. Numerical damping has undesired effects on the wave height. At Rijksuniversiteit Groningen the propagation characteristics of Comflow are being developed; as soon as improvements are achieved, nonlinear Newwaves simulation in Comflow will be less time consuming and will show less artificial damping.

The nonlinear Newwave simulations as presented in section 5.5 are used as basis for nonlinear Newwave simulation in Comflow. The programs can be coupled. Four alternatives are presented in section 6.2.

6.2. Alternatives for coupling of Vijfvinkel and Comflow

Alternatives are generated to use this property for wave impact modeling in Comflow. Four alternatives to combine the strength of Vijfvinkel and Comflow are introduced:

1. Vijfvinkel's Newwave model is used to create an inflow boundary for Comflow. A registration is made of the surface elevation and the velocity potential at the surface. This is used to calculate the particle velocities at the surface. A velocity profile is constructed. For each time step the surface elevation and the velocity profile are read by Comflow and enforced at the inflow boundary.

   Figure 6.1 shows the Vijfvinkel domain and the Comflow domain. The red circle denotes the location of registration. Note that the velocity potential and the surface elevation in the Comflow domain initially are assumed to be zero.

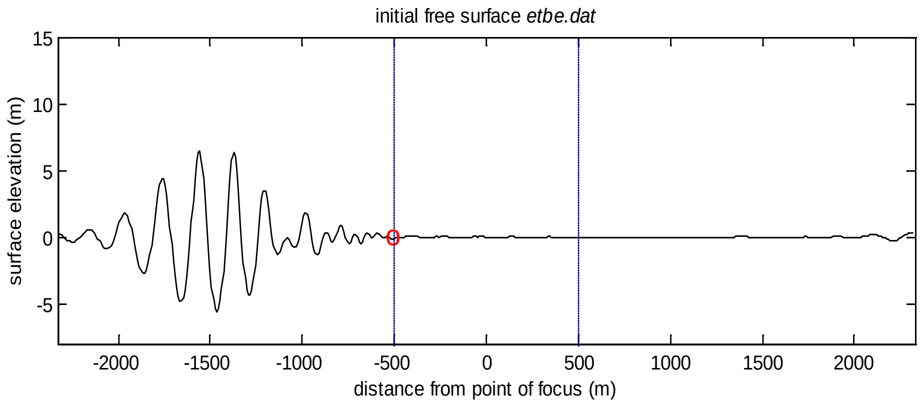

Figure 6.1: Coupling alternative 1.

2. Vijfvinkel's surface elevation and surface potential 'just' before focusing occurs as the initial velocity field and surface elevation in Comflow. The same method is used to determine the inflow boundary as in alternative 1. The fluid in the Comflow domain is initially not at rest. The velocity field and the surface elevation are prescribed by Vijfvinkel, see Figure 6.2.

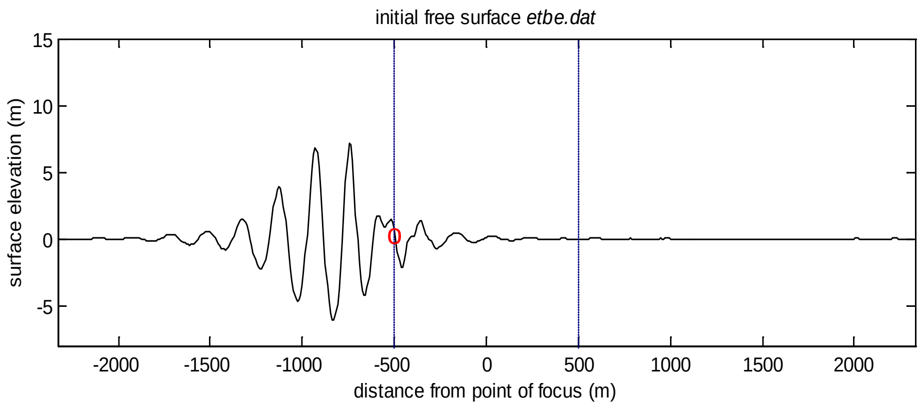

Figure 6.2: Coupling alternative 2.

3. Vijfvinkel's solver will be used in the part of the Comflow domain that is only affected by the undisturbed, propagating, Newwaves in the time span of the run.
4. Complete coupling of Vijfvinkel's solver to Comflow.

The question is how to benefit from the advantages from Vijfvinkel's program the most, without the loss of capabilities of Comflow. The alternatives have increasing complexity to implement. The alternatives relate: alternative 2 is an extension of alternative 1, alternative 3 is an extension on alternative 2 etc. Alternatives one and two are one-way couplings, alternatives three and four are interactive coupling. Alternatives 1 and 2 do not contribute to a more efficient solving procedure in

Comflow, but do prescribe a fully nonlinear Newwave to Comflow. Heemskerk recommendation states alternative 1 [10]. Considering these issues, a start is made by implementation of alternative 1.

6.3. Coupling of Vijfvinkel to Comflow: alternative 1.

Vijfvinkel is used to prescribe the fully nonlinear Newwave as inflow boundary to Comflow. What does Comflow require at the boundary?

- The surface elevation at each time step.
- The vertical and horizontal velocities for each cell at each time step.

How is this established? Vijfvinkel uses the surface elevation and the velocity potential at the surface. The surface elevation and the surface velocity potential are recorded at the Vijfvinkel node closest to the Comflow inflow boundary. The Comflow domain chosen equal to the one Heemskerk has used, starting at 500 meters before the linear focus location. With the Newwave simulation as presented in section 5.5 the node closest to the inflow boundary is located at x = -498.2 (m).

Surface elevation

The surface elevation is directly taken from the Newwave simulation in Vijfvinkel, at the location of Comflow's inflow boundary, see Figure 5.50

Velocity profile

The horizontal and vertical velocities can be derived from the record of the surface velocity potential using equations {43}. The surface elevation and the surface velocity potential throughout the domain are needed for each time step to calculate the velocity profile.

The record of the surface velocity potential and the surface elevation in time at the location of the Comflow inflow boundary is given in Appendix F.

The surface elevation, as given in Figure 5.50, can directly be used to prescribe the surface elevation in Comflow. However, to calculate the velocity profile, the surface elevation throughout the domain is needed for all time steps. With the complete record of the surface velocity potential and surface elevation, the velocity profiles can be calculated at a chosen location. Vijfvinkel's program was modified in such way that the grid that is used in Comflow can be used as input. The depth and height of the Comflow domain as well as the number of cells in the vertical direction is given as input. Vijfvinkel's program now calculates the horizontal velocities at half the height of each cell and the vertical velocities at the elevation of the cell top and bottom. The x coordinate where this is done is the same.

Figure 6.3 is a close-up of the data that is prescribed to the Comflow inflow boundary. It shows the surface elevation (solid line) and the velocities (arrows) in time. The cell layer boundaries are given with a dotted line. The vertical velocities are prescribed at these boundaries, the horizontal velocities are prescribed halfway each cell. It can be seen that the z-coordinate of the horizontal and vertical velocities are correctly specified. In this Figure the velocities are given every 0.5 second for clarity reasons, while in a coupled simulation every 0.01 (s) a new velocity profile is prescribed.

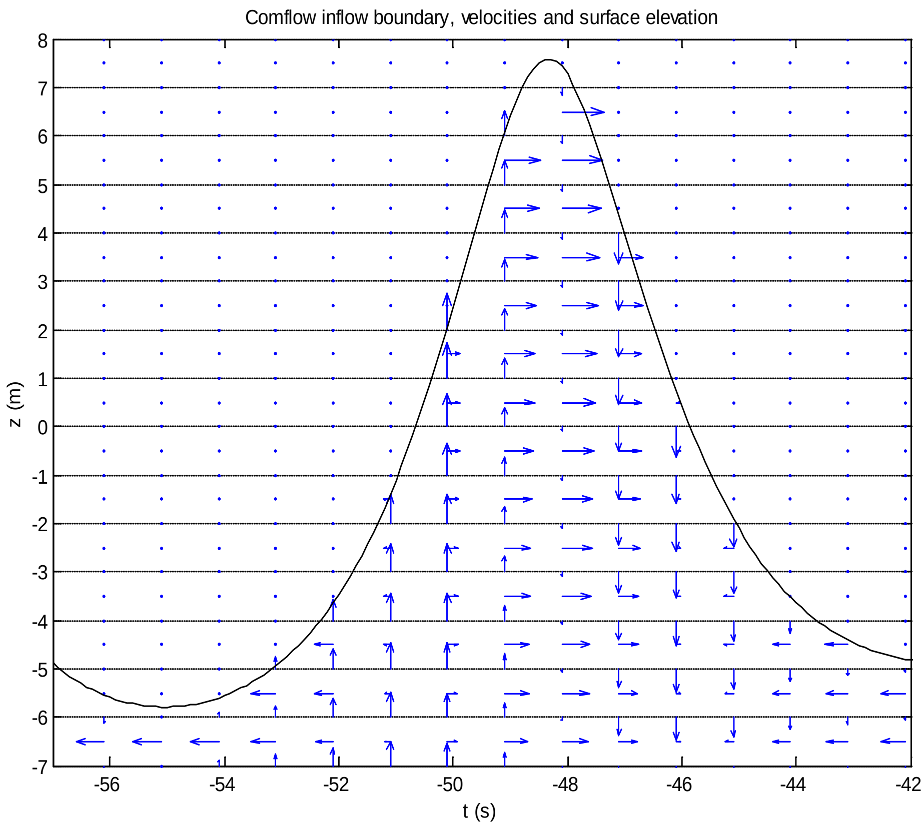

Figure 6.3: Surface elevation and velocities as prescribed by Vijfvinkel to Comflow (schematically).

The coupled Newwave run

The inflow boundary as described in the previous section is implemented in Comflow. The Comflow domain has the following parameters, see Table 6.1.

Table 6.1: Parameters used in coupled simulation (alternative 1).

x_{min} (m)	x_{max} (m)	z_{min} (m)	z_{max} (m)	i_{max} (-)	k_{max} (-)	Δt (s)
-500	500	-30	12	1000	42	0.01

The Comflow simulation with the new inflow boundary shows that the Newwave breaks at x = -280 (m).

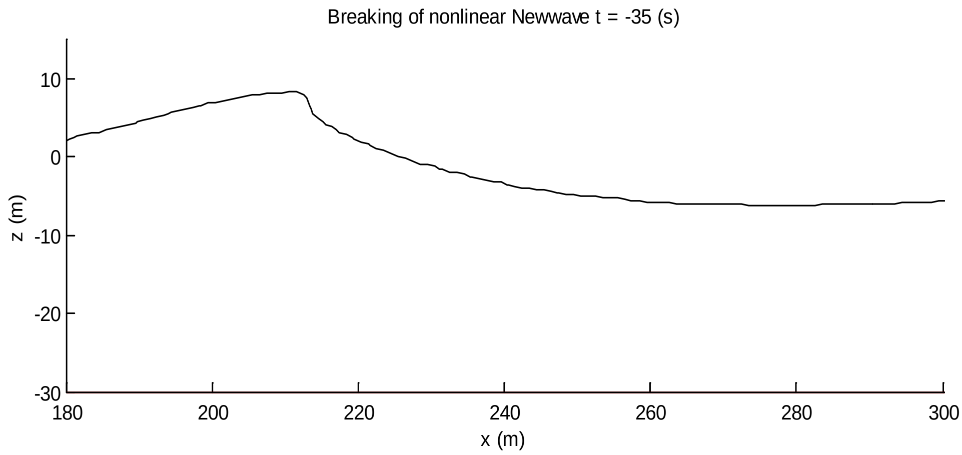

Figure 6.4: Breaking of nonlinear Newwave in Comflow.

The three dimensional simulation of a nonlinear Newwave impact on an offshore structure

A three dimensional simulation is performed in which Vijfvinkel prescribes the nonlinear Newwave to Comflow as an inflow boundary. Two legs of an offshore platform are inserted to model the impact of the nonlinear Newwave. The structure has been removed form the linear focus location to the location where the nonlinear Newwave breaks. The domain length has been to reduce computational effort. Relevant parameters of the Comflow domain are listed in Table 6.2

Table 6.2: Parameters used in 3-D nonlinear Newwave simulation.

x_{min} (m)	x_{max} (m)	y_{mix} (m)	y_{max} (m)	z_{min} (m)	z_{min} (m)
-500	-100	-35	35	-30	30

i_{max} (-)	j_{max} (-)	k_{max} (-)	Δt (s)
400	70	60	0.01

Figure 6.5 shows a snapshot of a Comflow simulation of the impact of a nonlinear Newwave on an offshore structure.

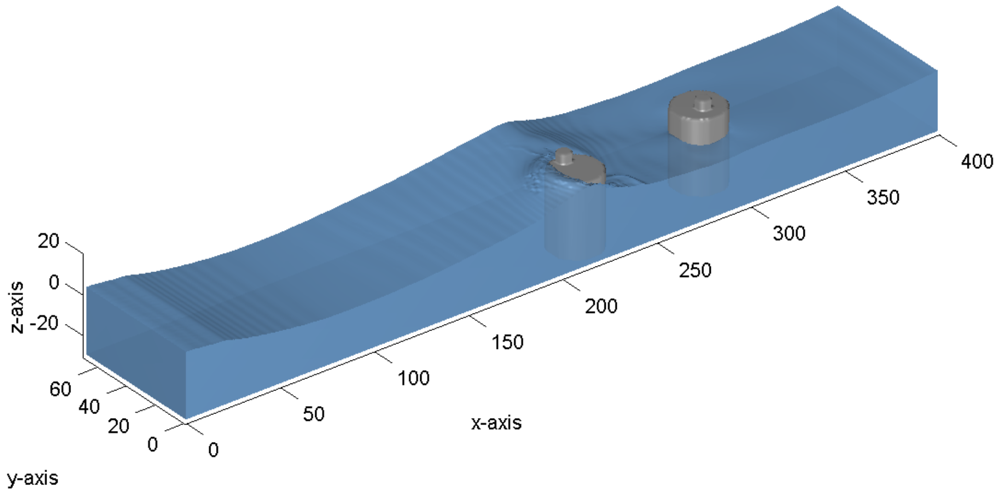

Figure 6.5: Comflow simulation of a wave impact on two legs of a platform.

6.4. Conclusions

1. Fully Nonlinear Newwaves have been successfully implemented in Comflow, by using the Vijfvinkel code to prescribe the inflow boundary in Comflow
2. A new inflow boundary is created in Comflow that enables any arbitrary flow with a single surface to be prescribed.
3. Construction of the velocity profile has been achieved, vertical staggering was implemented, horizontal staggering not yet. The error made is expected to be small, as the time step at which the velocities are calculated 0.01 (s) is, the cell width and height is 1 (m). This error could be anticipated on with interpolation in space, or via a dispersion relation.
4. The nonlinear Newwave as prescribed by Vijfvinkel breaks in Comflow at x=-280 (m).

7. CONCLUSIONS AND RECOMMENDATIONS

7.1. Conclusions

The thesis concerns the numerical modeling of the impact of nonlinear Newwaves on offshore structures, the objectives are:

1. To find a nonlinear wave model suitable for nonlinear Newwave simulation.
2. To couple the selected nonlinear wave resolving program to Comflow.
    2.1. To assess the performance of Comflow for nonlinear waves.
    2.2. To optimize the performance of Comflow for nonlinear waves.
    2.3. To couple the selected nonlinear wave code to Comflow.
3. To validate the coupled version of Comflow with scale model tests.

The development of Comflow is ongoing in cooperation with a Joint Industry Project where the contributions of several parties will be integrated. Objectives 2.2 is dealt with by PhD students from TU Delft and Rijksuniversiteit Groningen (RuG). MARIN will facilitate a RuG postgraduate study to validate Comflow.

Based on the research that is presented in this thesis the following conclusions are drawn.

1. Nonlinear wave model: Vijfvinkel.
    1.1. A method to describe the propagation of fully nonlinear waves as developed by E. Vijfvinkel was used to model fully nonlinear Newwaves. The method, based on a spectral method as described by Craig and Sulem [25], has a one dimensional, spatially periodic domain using a constant depth. It is based on Taylor expansion of the Dirichlet-Neumann operator, which is substituted in the governing equations. This operator is the pivot in the solution algorithm, with which the elevation of the free surface and the velocity potential at the free surface are calculated. Vijfvinkel had coded this method in Fortran 77, however the remains of this code contained errors and was incomplete.
    1.2. The Vijfvinkel programs that model 5th order Stokes waves and Newwaves were revitalized. The code to prescribe the particle velocities was debugged and adapted to prescribe a velocity profile in depth at a location and during a time span of choice.

2. Coupling Vijfvinkel to Comflow.
    2.1. Assessment of the performance for nonlinear waves.
        2.1.1. Four tests were set up to assess the performance of Comflow relative to Vijfvinkel and theory and laboratory measurements. These test show the capability of both computer programs and indicate the applicability for modeling fully nonlinear Newwaves.

2.1.2. The Beji Battjes simulation highlighted the high computational demands of Comflow, due to the required fineness of the grid size and time step. Comflow is able to simulate the propagation of regular waves, the nonlinear generation of higher harmonics if the grid and time step requirements [19] are fulfilled. Even the finest grid, using three days of computation, showed deviation in phase of the second and higher harmonics, behind the submerged bar. The phase velocity is simulated incorrectly for the harmonics that do not fulfill the requirements. In contrast, the frequency and amplitude do show correctly.

2.1.3. The Sloshing Tank experiment showed that the propagation of regular waves with low steepness can be simulated from a relative water depth close to shallow water, kd=1 (-). A grid with 60 nodes per wavelength and 300 time steps per wave period showed a deviation in phase velocity of 0.06 %. However, interesting findings were made with regard to wave damping. Simulations that have a cell layer boundary just below the mean water level show an increase in wave amplitude. The grid configuration relative to the location of the free surface influences the accuracy of simulation; simulations where the free surface does not cross a cell layer show superior performance in comparison to grids where the free surface crosses a cell layer. The number of cell layers was minimized. The Sloshing Tank experiment was unstable for grids with 5, 4,5, 4 and 3.5 layers below mean water level. Further reduction of the number of cell layers to 3, 2,5, 2 and 1,5 layers showed a stable solution, but with increased damping.

2.1.4. The Steep Wave experiment in Comflow proved that error waves originate at the inflow boundary if the wave theory at the inflow boundary is not compatible with the (nonlinear) physical conditions, such as wave steepness and water depth. Vijfvinkel is able to simulate the propagation of steep regular waves, whereas Comflow shows instabilities and damping.

2.1.5. The simulation of Newwaves in Vijfvinkel uses a linear initial condition that is transformed using the Creamer method, which adds nonlinear terms to reduce the generation of error waves. The location, time and height of focus are clearly affected by nonlinear simulation. Spectral components, of which the wave group initially is composed, become bound. The shape of the wave group becomes fixed, and the wave group seems to translate steadily. An erroneous long wave is generated that is released from the wave group. Several peaks are recorded, of which the first is the highest. Only for the simulations over a short time span is the first peak equal to the focus peak. For these runs, the wave focusing is shifted forwards in time and space. The height of the resulting peak is increased. In contrast, simulations with a start time well before the theoretical focus time show a peak close to the theoretical focal point and time, with a crest height close to the linear crest height. The wave steepness of the nonlinear wave group, at the location of the inflow boundary in the Comflow domain, requires at least a second order wave theory.

2.2. Optimization of Comflow for nonlinear waves.

2.2.1. Several interesting questions have arisen and have been presented and documented to be basis to further research by PhD students in Delft and Groningen.

2.3. Coupling Vijfvinkel to Comflow.

2.3.1. Four alternatives were formulated with which use is made of the strengths of Vijfvinkel and Comflow. Two alternatives use Vijfvinkel to prescribe the inflow boundary condition and initial condition, the other two alternatives are interactive couplings as information is looped between Comflow and Vijfvinkel. One alternative is selected and further elaborated: Vijfvinkel prescribes the surface elevation and velocities at the Comflow inflow boundary cells. The velocities are prescribed at the correct height, but no differentiation has been used yet for the horizontal coordinate. A coupled, three dimensional simulation of a nonlinear Newwave impact on an offshore structure was successfully made.

3. Validation of coupled Vijfvinkel-Comflow with scale model tests.

   3.1. The simulations have not been validated with scale model tests. However, the simulated experiments each highlight an aspect of Newwave modeling separately. The conclusions drawn from the simulation of each of these separate experiments indicate the validity of the simulation of nonlinear Newwaves. Newwaves have not been modeled in a laboratory setup, and it is expected to be difficult to model these waves with great precision.

It is concluded that the development of the numerical core of Comflow is essential to obtain a model that is better capable to prescribe the physics, with less computational effort. The high number of grid cells that is required to model progressing waves and the deviation from reality indicates that improvements are welcome to let Comflow become a substitution for scale tests of wave impact studies on offshore structures.

7.2. Recommendations

The recommendations are:

1. Numerical core

   1.1. Development on the solution algorithm for the surface cells. With the Sloshing Tank experiment it was shown that the grid configuration has impact on the accuracy of the simulation, see conclusion 2.1.3. The cause of these differences is expected to lie in:

   - The calculation of the free surface velocities.
   - The cell labeling and solution algorithm.

   These issues are to be studied.

   1.2. Implementation of a local grid refinement holds the opportunity to greatly reduce the computing time. This will make detailed three dimensional impact simulations in Comflow possible.

2. Nonlinear Newwaves

   2.1. Further study is recommended to indicate if the nonlinear Newwave is representative for the extreme wave, as the crests of the bound wave group are maintained for a longer time interval. The influence of the nonlinear propagation of the Newwave on the wave focusing location, time, height and the shape of the wave group needs to be analyzed.

   2.2. It is observed that a wave group with a high crest maintains this high crest due to nonlinear propagation, see conclusion 2.1.5. This increases the probability that an extreme wave is occuring at a certain location. The effect of nonlinear wave propagation on wave statistics is to be studied.

2.3. Bispectral analysis is recommended to reveal whether waves are bound or not.

2.4. The coupling of Vijfvinkel to Comflow needs to be validated and extended. Vijfvinkel is to prescribe the initial fluid configuration in Comflow, and a dynamic coupling can be made.

2.5. A frequency based input spectrum needs to be implemented in Vijfvinkel. Vijfvinkel needs to include a nonlinear dispersion code, taking into account local steepness. The spatial domain should be adapted accordingly, to maintain the periodicity condition.

2.6. The Creamer method needs to include a correction for lower harmonics. When this is implemented, the transformation of the linear initial condition to the quasi-nonlinear initial condition in Vijfvinkel is expected to reduce the influence of the long, unbound wave, especially for runs covering a long time span.

3. Validation

3.1. Comparison of Newwave impact simulations in Comflow with scale tests will indicate the validity of Comflow.

REFERENCES

1. **Bateman WJD, Swan C, Taylor PH.** *On the efficient Numerical Simulation of Directionally Spread Surface Water Waves* Journal of Computational Physics 174, p. 277-305, 2001
2. **Bateman WJD, Swam C, Taylor PH.** *On the Calculation of the water particle kinematics in a directionally spread wavefield* J. of Computational Physics 186, p. 70-92, 2003.
3. **Beji S, Battjes JA.** *Numerical simulation of nonlinear wave propagation over a bar* Coastal Engineer 23, p. 1-16, 1994.
4. **Casulli V, Stelling GS.** Numerical simulation of 3D quasi-hydrostatic, free-surface flows Journal of Hydraulic Engineering, p.678-686, 1998
5. **Craig W, Sulem C.** *Numerical Simulation of Gravity Waves* J. of Computational Mechanics 108, p 73-83, 1993.
6. **Dean RG, Dalrymple RA.** *Water Wave Mechanics for Engineers and Scientists* Prentice-Hall, New Jersey, 1984.
7. **Fekken G.** *Numerical Simulation of Free-Surface Flow with Moving Rigid Bodies* PhD thesis, RuG, 2004.
8. **Fenton JD, Rienecker MM.** *A Fourier method for solving nonlinear water-wave problems: application to solitary-wave interactions* J. Fluid. Mech 118, p 411-443, 1982.
9. **Gerrits J.** *Dynamics of Liquid-Filled Spacecraft* PhD thesis, RuG, 2001.
10. **Heemskerk JM.** *Implementation of a Non-Linear New Wave in the Numerical Wave Tank "Comflow"* SIEP, Rijswijk, 2004.
11. **Helmholt-Kleefsman T.** *Report on the implementation of waves in Comflow*, RuG, 2003.
12. **Helmholt-Kleefsman T.** *Safeflow Manual Comflow V1.0.5E and V1.1.5* RuG, 2004
13. **Hirt CW, Nichols BD.** *Volume of Fluid (VOF) Method for the Dynamics of Free Boundaries* Journal of Computational Physics 39, pag. 201-225, 1981.
14. **Ieperen EJ van.** *Amplification of waves by a Concrete Gravity Substructure* SIEP, Rijswijk, 2003.
15. **Jonathan P, Taylor PH.** *Irregular, non-linear waves in a spread sea* SIEP, Rijswijk, 1995.
16. **Jonathan P, Taylor PH.** *On irregular, nonlinear waves in a spread sea* Journal of Offshore Mechanics and Arctic Engineering 119, p.37-41, 1997.
17. **Leibovich S, Seebass AR.** *Nonlinear Waves* Cornell University Press, Ithaca, 1974.
18. **Loots E.** *Fluid-Structure Interaction in Hemodynamics* PhD thesis, RuG, 2003.
19. **Meskers G.** *Realistic inflow conditions for numerical simulation of green water loading* MSc thesis, TUDelft, 2002.
20. **Reeuwijk M van.** *Efficient simulation of non-hydrostatic free-surface flow* MSc thesis, TUDelft, 2003.
21. **Sarpkaya T, Isaacson M.** *Mechanics of Wave Forces on Offshore Structures* Van Nostrand Reinhold, New York 1981.
22. **Taylor PH.** *On the kinematics of large ocean waves* Shell Research, Rijswijk, 1992.

23. **Tromans PS, Anaturk AR, Hagemeijer R.** *A new model for the kinematics of large ocean waves* SIEP, Rijswijk, 1991

24. **Tucker MJ** *Waves in ocean engineering* Ellis Horwood, UK, 1991.

25. **Vijfvinkel EM.** *Focused wave groups on deep and shallow water* SIEP, Rijswijk, 1996.

26. **Whitham GB.** *Linear and Nonlinear Waves* John Wiley & Sons, 1974

APPENDIX A: Wave theory

Derivation of a spectrum

From wave measurements to wave theory

Before an offshore structure is designed the height of the decisive wave and the sea state in which this wave occurs are estimated. A sea state can be decomposed into single sinusoidal waves each with a different amplitude, frequency and phase. This can be represented in spectra showing the distribution of the variance, amplitude or phase over a frequency range. From buoy measurements the surface elevation over a certain time span (time series) can be derived. From these time series a statistical maximum wave height can be calculated. This only applies if sufficient data is assumed to be available; in most cases hindcasts are made.

Maximum wave height

With hindcasts sea states can be reproduced. Hindcasts are based on atmospheric pressure measurements that have been taken for many decades, in contrast to wave measurements. With the pressure fields the wind fields can be calculated, with corrections for local effects, like thermal winds in near shore locations. The obtained wind field is used as input in wave modeling programs (e.g. WAM). This hindcast produces relevant wave parameters, like significant wave height, peak period, zero-crossing period. With the obtained knowledge the significant wave height and peak period of the 1:100 year storm are estimated. Directional spreading is often not considered in the calculation of the extreme wave height. It is assumed that these conditions are, by far, more demanding than the second fiercest storm. The duration of the extreme sea state conditions during this most severe storm are estimated. With the wave period and duration of these decisive conditions a total number of waves, N, that pass the location of interest are calculated. From the significant wave height and the number of waves the maximum wave height can be derived.

The significant wave height has empirical background, being 'the' observed wave height. However it can be seen as the mean of the top one third wave heights, and is proportional to the variance via $H_s=4m_0^{0.5}$. The variance m_0 (m^2) of a time series with n registrations and elevation η_i (m) and mean elevation $\overline{\eta}$ (m) is defined as:

$$m_0 = \mathrm{var}(\eta) = \frac{1}{n}\sum_{i=1}^{n}(\eta_i - \overline{\eta})^2 \qquad \{A1\}$$

The central limit theorem states that the sum of a large number of stochastically independent variables has a Gaussian probability density function (distribution). The Gaussian probability density function $p(\eta)$ is dependent on the mean and the variance:

$$p(\eta) = \frac{1}{\sqrt{2\pi m_0}} e^{-\frac{\eta^2}{2m_0}} \qquad \{A2\}$$

For timeseries that can be represented by a Gaussian distribution, the probability of maxima is Rayleigh distributed. The maximum surface elevation is only dependent on the variance.

$$p(\eta_{\max}) = \frac{\eta_{\max}}{m_0} e^{-\frac{\eta_{\max}{}^2}{2m_0}} \qquad \{A3\}$$

It follows that the expected value of the maximum wave height H_{max} in the 'one in a hundred year' storm, is calculated using, with $H_{rms} = (8m_0)^{0.5}$ and N the number of waves.

$$E(\max H) = \sqrt{\frac{\ln(N)}{1 - e^{Ne^{-\frac{H2}{H_{rms}^2}}}}} H_{rms} \qquad \{A4\}$$

Spectrum

A sea state can be decomposed into sinusoidal waves with each a distinct amplitude, frequency and phase. A decomposition in wavelets can be done by switching from a time domain to a frequency domain using Fourier Transformation. A spatial domain can also be described in a frequency domain but requires a relation between wave length and period (dispersion relation). The result of this analysis is often depicted in spectra. One spectrum type that is often used in the variance density spectrum, showing the distribution of the variance over a range of frequencies. The area of this spectrum returns the variance; this is the zeroth order moment (m_0). Using the peak period and the zero crossing period, some information is given about the distribution of the variance over the various wave frequencies, as higher order moments can be returned (m_1, m_2). From these limited parameters a representative spectrum is chosen. Usually the highest waves in near shore conditions occur when the wind speeds are strong and the sea is nearly (fully) developed. Standardized spectra like, JONSWAP or Pierson-Moskowitz are often used.

Nonlinear wave theory

There are a number of nonlinear wave theories such as Stokes theory, Stream theory, cnoidal theory, hyperbolic wave theory and solitary wave theory. This section highlights some theories, more extensive elaboration can be found in textbooks such as [7,20,24,28]

These theories are all based on expansion of the kinematic and dynamic boundary conditions {23}, {24} with Taylor series about the still water level (z=0), since we do not know the location of the surface a priori. The nonlinear harmonics are bound to the fundamental (base) wave; they propagate with the same phase velocity.

Kinematic free surface boundary condition

$$\begin{aligned}-\frac{\partial\varphi}{\partial z} - \frac{\partial\eta}{\partial t} + \frac{\partial\varphi}{\partial x}\frac{\partial\eta}{\partial x} &= \\ &\left[-\frac{\partial\varphi}{\partial z} - \frac{\partial\eta}{\partial t} + \frac{\partial\varphi}{\partial x}\frac{\partial\eta}{\partial x}\right]_{z=0} + \sum_{n=1}^{n}\frac{z^n}{n!}\frac{\partial^n}{\partial z^n}\left[-\frac{\partial\varphi}{\partial z} + \frac{\partial\varphi}{\partial x}\frac{\partial\eta}{\partial x}\right]_{z=0}\end{aligned} \qquad \{A5\}$$

Dynamic free surface boundary condition

$$\begin{aligned}&\frac{\partial\varphi}{\partial t} + \frac{1}{2}\left((\frac{\partial\varphi}{\partial x})^2 + (\frac{\partial\varphi}{\partial z})^2\right) + g\eta = \\ &\left[\frac{\partial\varphi}{\partial t} + \frac{1}{2}\left((\frac{\partial\varphi}{\partial x})^2 + (\frac{\partial\varphi}{\partial z})^2\right) + g\eta\right]_{z=0} + \sum_{n=1}^{n}\frac{z^n}{n!}\frac{\partial^n}{\partial z^n}\left[\frac{\partial\varphi}{\partial t} + \frac{1}{2}\left((\frac{\partial\varphi}{\partial x})^2 + (\frac{\partial\varphi}{\partial z})^2\right)\right]_{z=0}\end{aligned} \qquad \{A6\}$$

Replacing the linear surface boundary conditions {23}, {24} by the expanded versions {A5}, {A6} result in an expanded velocity potential {A7} and a dispersion relation {A8} consisting of a series of decreasing contributions, with each higher order term being a correction. Recall that φ is already dependent on a {25}, so $\varphi_{(1)}$ is dependent on a (linear theory), $\varphi_{(2)}$ on a^2 (second order theory), etc.

$$\varphi = \varphi_{(1)} + ak\varphi_{(2)} + a^2k^2\varphi_{(3)}...a^{n-1}k^{n-1}\varphi_{(n)} \qquad \{A7\}$$

$$\omega^2 = gk(C_{(1)} + a^2k^2C_{(3)} + a^4k^4C_{(5)}...a^{n-1}k^{n-1}C_{(n(odd))}) \qquad \{A8\}$$

Constants are indicated with $C_{(n)}$.Non-linear waves are characterized by longer and shallower troughs and peaked crests.

One can continue with adding higher order terms as long as the solution remains stable; the Ursell number is an indication for this. Figures exist stating which theory is recommended for a given Ursell number [7].

$$Ur = \frac{L^2H}{h^3} \qquad \{A9\}$$

2nd order Stokes Theory

Elaboration of the expanded kinematic free surface boundary condition {A5} and the dynamic free surface boundary condition {A6} yields the surface elevation {A10} and velocity potential {A11}.

$$\eta = a\cos(kx-\omega t) + ka^2\frac{\cosh(kh)}{4\sinh^3(kh)}(2+\cosh(2kh))\cos(2(kx-\omega t)) \qquad \{A10\}$$

$$\varphi = a\frac{\omega}{k}\frac{\cosh(k(h+z))}{\cosh(kh)}\sin(kx-\omega t) + \frac{3}{8}a^2\omega\frac{\cosh(2k(h+z))}{\sinh^4(kh)}\sin(2(kx-\omega t)) \qquad \{A11\}$$

The dispersion relation of Stokes 2 theory is equal to the linear dispersion relation (31)

5th order Stokes Theory

Fenton expressed this in the following way (1981), with *c* being the linear phase speed and A_{ij}, dimensionless constants, and *a* the pseudo linear amplitude.

$$\eta = \sum_{i=1}^{5}(ak)_i\sum_{j=1}^{i}B_{ij}\cos(j(kx-\omega t)) \qquad \{A12\}$$

$$\varphi = \frac{\sqrt{g}}{\sqrt{k}}\sum_{i=1}^{5}(ak)_i\sum_{j=1}^{i}A_{ij}\cosh(jk(h+z))\sin(j(kx-\omega t)) - \frac{1}{2}(c-\frac{\omega}{k})^2t \qquad \{A13\}$$

The coefficients A_{ij} and B_{ij} that are used for infinite depth are given in Table A1.

Table A1: Coefficient Stokes 5 theory.

A_{11}	A_{22}	A_{31}	A_{33}	A_{42}	A_{44}	A_{51}	A_{53}	A_{55}
1	0	-1/2	0	1/2	0	-37/24	1/12	0

B_{11}	B_{22}	B_{31}	B_{33}	B_{42}	B_{44}	B_{51}	B_{53}	B_{55}
1	1/2	-3/8	3/8	1/3	1/3	-422/384	297/384	125/384

The fifth order dispersion relation is:

$$\omega^2 = gk(1+\frac{1}{2}a^2k^2+\frac{5}{4}a^4k^4) \qquad \{A14\}$$

The elaboration of the velocity potential will not be presented in this thesis.

Sharma and Dean 2nd order.

Sharma and Dean developed a wave theory for which the surface elevation is given:

$$\eta = \eta^{(1)} + \eta^{(2)} + \eta^{(3)} = \eta^{(1)} + \tfrac{1}{4}\sum_{i=1}^{N}\sum_{j=1}^{N} a_i a_j \left[K^- \cos(\psi_i - \psi_j) + K^+ \cos(\psi_i + \psi_j)\right] \quad \{A15\}$$

The velocity potential is

$$\varphi = \sum_{n}^{N} \frac{a_n g}{\omega_n} \frac{\cosh(k(h+z))}{\cosh(kh)} \sin(\psi_n) + \tfrac{1}{4}\sum_{i=1}^{N}\ \sum_{j=1}^{N} A\ \left[B \cdot C \cdot \sin(\psi_i - \psi_j) + D \cdot E \cdot \sin(\psi_i + \psi_i)\right] \quad \{A16\}$$

In which

$$K^+ = \left[D_{ij}^+ - (\vec{k}_i \cdot \vec{k}_j - R_i R_j)\right](R_i R_j)^{-1/2} + (R_i + R_j)$$

$$K^- = \left[D_{ij}^- - (\vec{k}_i \cdot \vec{k}_j + R_i R_j)\right](R_i R_j)^{-1/2} + (R_i + R_j)$$

$$D_{ij}^+ = \frac{2(\sqrt{R_i} + \sqrt{R_i})^2(\vec{k}_i \cdot \vec{k}_j - R_i R_j) + (\sqrt{R_i} + \sqrt{R_j})\ \left\{\sqrt{R_i}(\vec{k}_j^2 - R_j^2) - \sqrt{R_j}(\vec{k}_i^2 - R_i^2)\right\}}{(\sqrt{R_i} + \sqrt{R_j})^2 - \kappa_{ij}^+ \tanh \kappa_{ij}^+ d}$$

$$D_{ij}^- = \frac{(\sqrt{R_i} - \sqrt{R_j})\ \left\{\sqrt{R_j}(\vec{k}_i^2 - R_i^2) - \sqrt{R_i}(\vec{k}_j^2 - R_j^2)\right\} + 2(\sqrt{R_i} - \sqrt{R_i})^2(\vec{k}_i \cdot \vec{k}_j + R_i R_j)}{(\sqrt{R_i} - \sqrt{R_j})^2 - \kappa_{ij}^- \tanh \kappa_{ij}^- d}$$

$$A = \frac{a_i \omega_i}{k_i} \frac{a_j \omega_j}{k_j}$$

$$B = \frac{\cosh \kappa_{ij}^- (z' + d)}{\cosh \kappa_{ij}^- d} \quad \{A17\}$$

$$C = \frac{D_{ij}^-}{(\omega_i - \omega_j)}$$

$$D = \frac{\cosh \kappa_{ij}^+ (z' + d)}{\cosh \kappa_{ij}^+ d}$$

$$E = \frac{D_{ij}^+}{(\omega_i + \omega_j)}$$

$$\kappa_{ij}^+ = \left|\vec{k}_i + \vec{k}_j\right|$$

$$\kappa_{ij}^- = \left|\vec{k}_i - \vec{k}_j\right|$$

$$R_i = \left|\vec{k}_i\right| \tanh\left(\left|\vec{k}_i\right| d\right) = \frac{\omega_i^2}{g}$$

$$\psi_i = \vec{k}_i x - \omega_i t + \varphi_i$$

With *z'* being the Wheeler stretched vertical coordinate, k the directional wave number, K_{ij} interaction kernels, N the number of spectral components.

The benefit of Sharma and Dean 2nd order is that directionality is included and wave irregularity is explicitly observed. The irregularity makes Sharma and Dean 2nd order suitable for Newwave simulation while Stokes 2 will be used to model regular waves.

Kinematics

Linear wave theory is only valid up to the still water level. Therefore, the velocities above this level need to be estimated. This is done by stretching the water velocities at the still water level up to the actual water level, or by expressing the actual water level in terms of the still water level. For linear wave theory the horizontal velocities are valid up to the still water level, $-d<z<0$ these are. The horizontal velocities are considered:

$$u(z,t) = \frac{agh}{\omega}\frac{\cosh(k(h+z))}{\cosh(kh)}\cos(\omega t - kx) \qquad \{A18\}$$

Several stretching methods exist, each method has a distinctive velocity profile, extreme velocities and net volume transport; the relevant methods are presented in this section. The extreme velocities are relevant with regard to wave impact on structures. Wheeler stretching is often used for this purpose. The depth and period averaged volume transport is relevant for the flux of mass into the Comflow domain. The net volume transport with linear extrapolation is the so called Stokes drift. For Stokes waves currently Comflow uses Wheeler stretching.

Stretching is also used for another purpose. The velocities in the surface cells of Comflow are estimated by stretching of the velocities of the underlying cells. Linear extrapolation was used, Heemskerk [12] implemented quadratic extrapolation gaining a marginal increase in accuracy of propagating waves.

Linear extrapolation
Linear stretching assumes linear extrapolation of the velocities form the mean water level up to the surface elevation if this is above the mean water level. The velocities above the mean water level are thus given by:

$$u(z,t) = z\left(\frac{\partial u(z,t)}{\partial z}\right)_{t,z=0} \qquad \{A19\}$$

The expression for the mean volume transport per unit width (m^2/s) for sinusoidal waves can be split in a part underneath the mean water level and a contribution above the mean water level:

$$\bar{q} = \frac{1}{T}\int_{t=0}^{T}\int_{z=-d}^{0} u(z,t)\,dz\,dt + \frac{1}{T}\int_{t=0}^{T}\int_{z=0}^{\eta} z\left(\frac{\partial u(z,t)}{\partial z}\right)_{t,z=0} dz\,dt \qquad \{A20\}$$

The contribution to the period averaged volume transport below the mean water level is zero, as the first integral pair in the expression above is zero. The second integral pair reduces for short waves ($\tanh(kh)\approx 1$) to:

$$\bar{q} = \frac{a^2 gk}{2\omega} \qquad \{A21\}$$

In Comflow the velocities in the fluid cells are extrapolated linearly to determine the velocities in the surface cells, using the fluid (F) and surface (S) cells. In this thesis constant extrapolation is used. Quadratic extrapolation is another option to determine the surface velocities.

Quadratic extrapolation
Heemskerk developed a method to extrapolate the velocities in Comflow's fluid cells up to the free surface numerically by fitting three data points $u_n(x,z_n)$in a 2nd order function which is also existing above z=0 (m) [12]. This method was implemented in Comflow and resulted in slightly more accurate free surface velocities.

Splines
Van Reeuwijk [23] introduces the spline to interpolate a pressure profile. A spline is a piecewise continuous polynomial and is defined as:

$$u^{(j)}(z) = a_0^{(j)} + a_1^{(j)}(z - z_j) + a_2^{(j)}(z - z_j)^2 + ...a_p^{(j)}(z - z_j)^p \qquad \{A22\}$$

The index j refers to the data point. The order of the spline is one less the value of p, p being a positive integer. This could be extended to n^{th} degree extrapolation of the velocity profile.

The benefit of the spline interpolation method lies in the limited number of data to reproduce a velocity profile. Comflow's inflow boundary needs the surface elevation, and the velocities in all the inflow boundary cells below and at the surface. Vijfvinkel is able to produce these values. However, if a fine grid is used in Comflow, this implies a very large number of velocities. With the use of the spline polynomial the size of the datafiles that contain the velocity profile could be reduced impressively. The spline can be applied to construct a velocity field while only a limited data is available. This will increase the speed of the computer program.

Wheeler Stretching
Wheeler Stretching is a common stretching method in offshore engineering to determine a velocity profile for a wave (crest) hitting a structure. It stretches the prediction of the kinematics at the mean sea level to the water surface. For linear, regular waves, Comflow uses Wheeler stretching. The implication is explained below. The Wheeler stretched vertical coordinate z_W is defined as:

$$z_W = \frac{d}{(d+\eta)} z + d\left(\frac{d}{(d+\eta)} - 1\right) \qquad \{A23\}$$

In which *d* is the water depth, *z* the vertical coordinate and η the surface elevation.

Since the Wheeler stretched coordinate is dependent on the surface elevation the velocity profile underneath the mean water level are not equal for troughs and crests. This implies a contribution to net volume transport underneath the surface. The period and depth averaged volume transport per unit width is now not split in two:

$$\overline{q} = \frac{1}{T} \int_{t=0}^{T} \int_{z=-d}^{z=\eta} u(z_W(\eta), t)\, dz dt \qquad \{A24\}$$

The double integral can be reduced to a single integral in terms of the actual coordinate *z*.

$$\overline{q} = \frac{gak}{2\pi \cosh(kh)} \int_0^T \sinh\left(\frac{kh}{h+\eta}(1-\cos(\omega t - kx))\right)\cos(\omega t - kx) - \sinh\left(\frac{kh}{h+\eta}(h-d)\right)\cos(\omega t - kx)\, dt \qquad \{A25\}$$

This time integral cannot be solved analytically. Figure 1 illustrates the characteristics of a Wheeler stretched velocity profile. A volume transport takes place over the entire depth whereas linear extrapolation only causes a transport above the still water level.

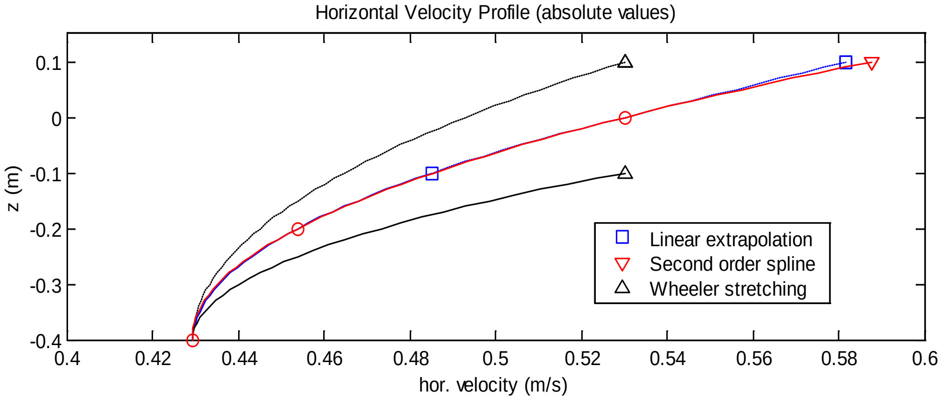

Figure 1: The horizontal velocity profiles according to different methods. For a linear wave with amplitude 0,1 (m) and period 2.02 (s) in water with depth 0.4 (m). The dotted lines represent the crests, the solid lines the troughs. The spline polynomial is of the second order and applies to potential theory, the three data points of which the spline is constructed are indicated with circles. The values at the crest and trough are emphasized with the symbol indicated in the legend.

APPENDIX B: Beji Battjes experiment

Time series of the simulation in Comflow

$\Delta x/L = 1/100$ (-) $\Delta t/T=1/500$ (-)

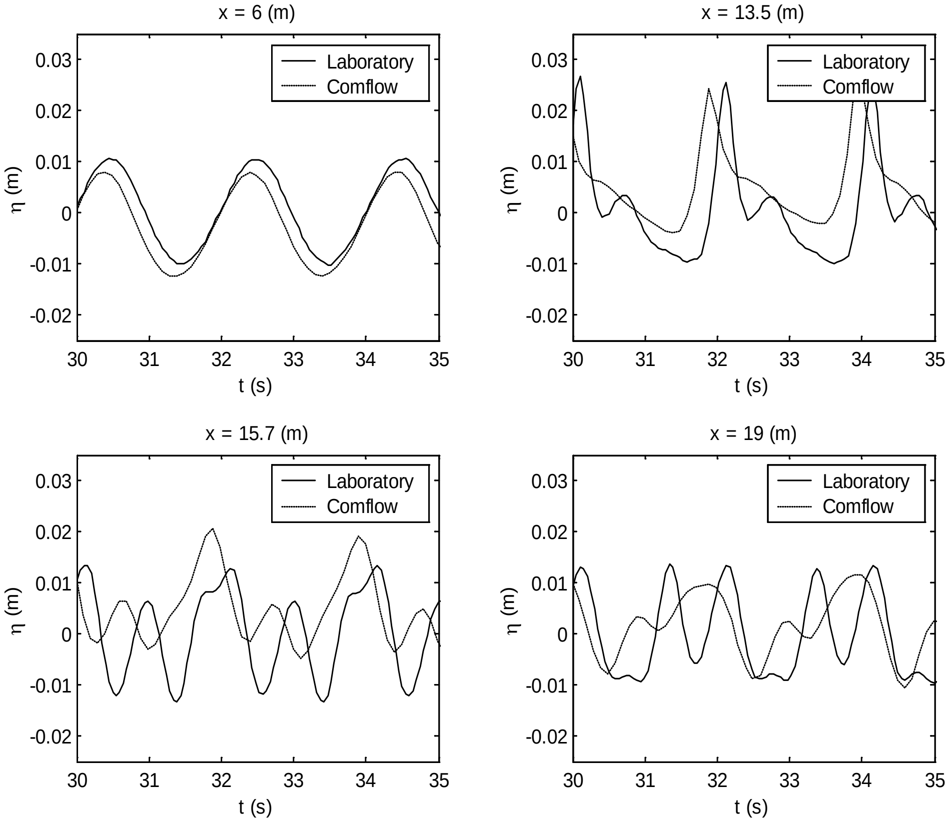

$\Delta x/L = 1/100$ (-) $\Delta t/T=1/1000$ (-)

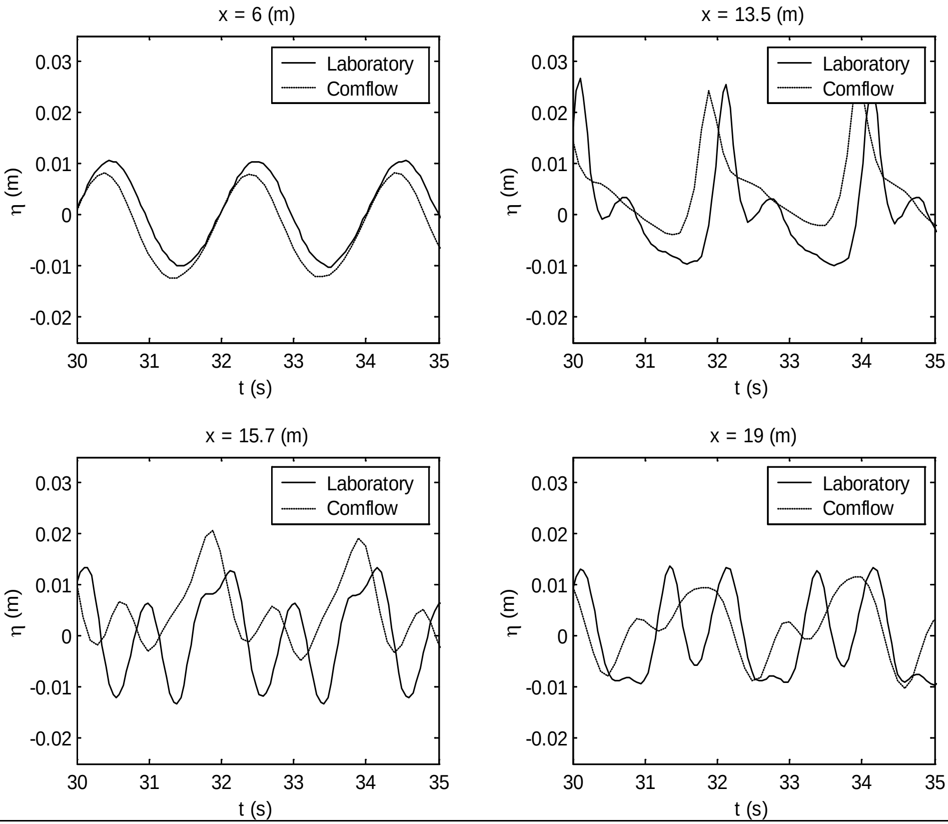

$\Delta x/L = 1/250$ (-) $\Delta t/T = 1/500$ (-)

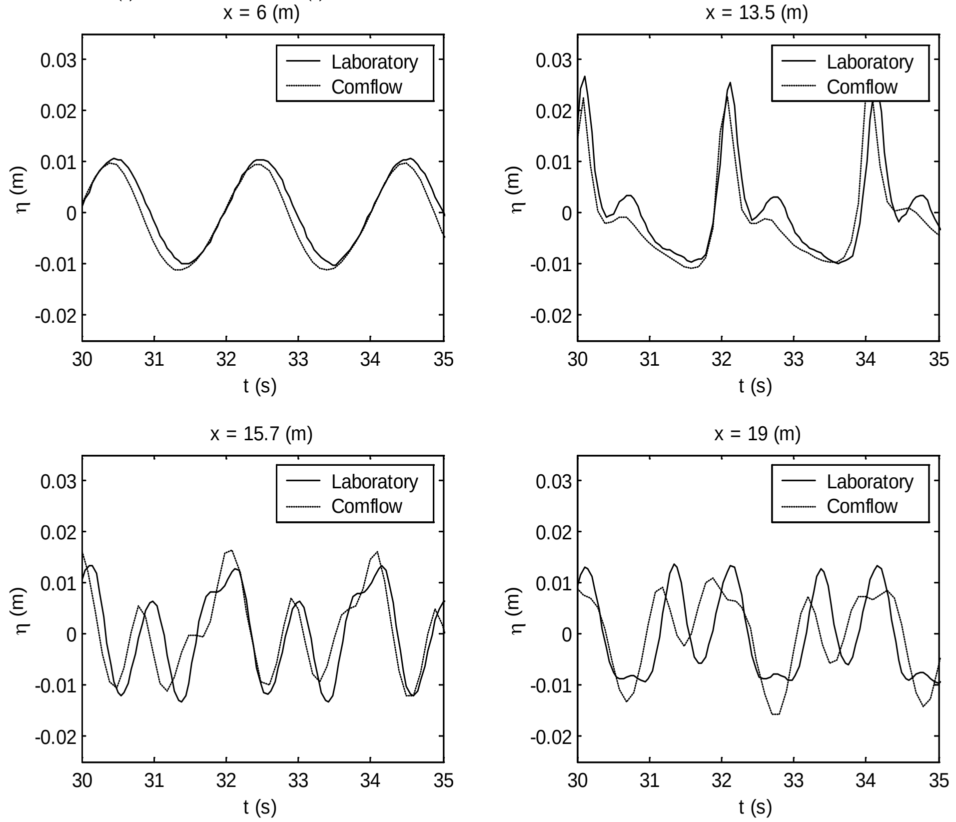

$\Delta x/L = 1/250$ (-) $\Delta t/T = 1/1000$ (-)

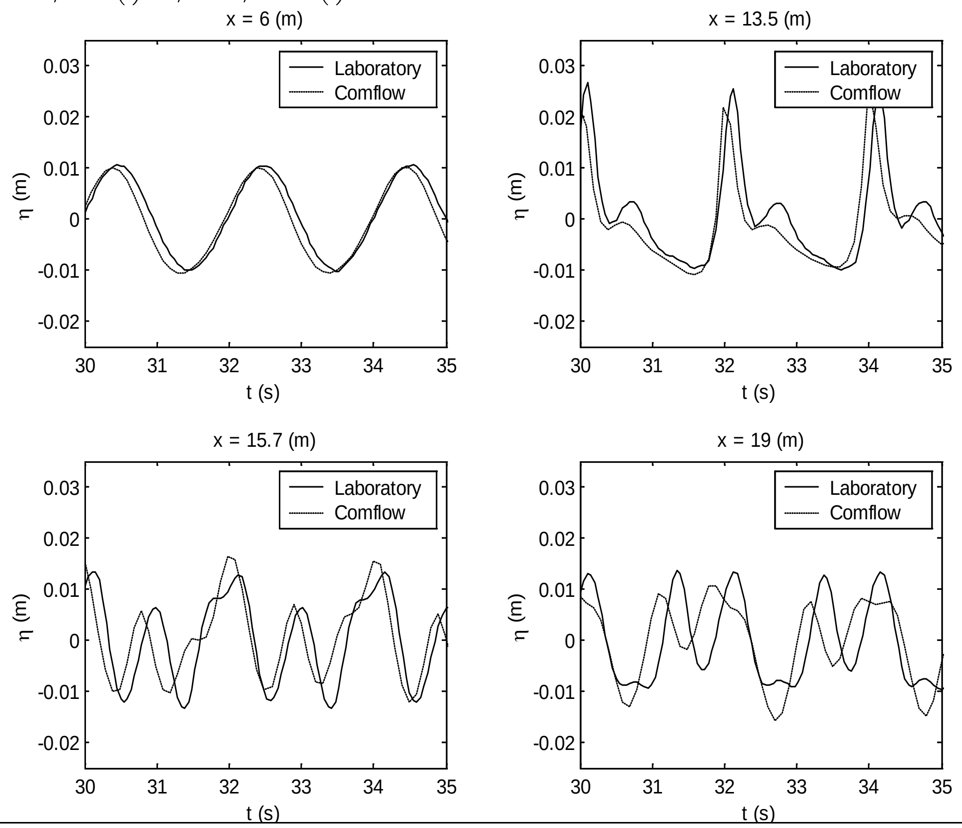

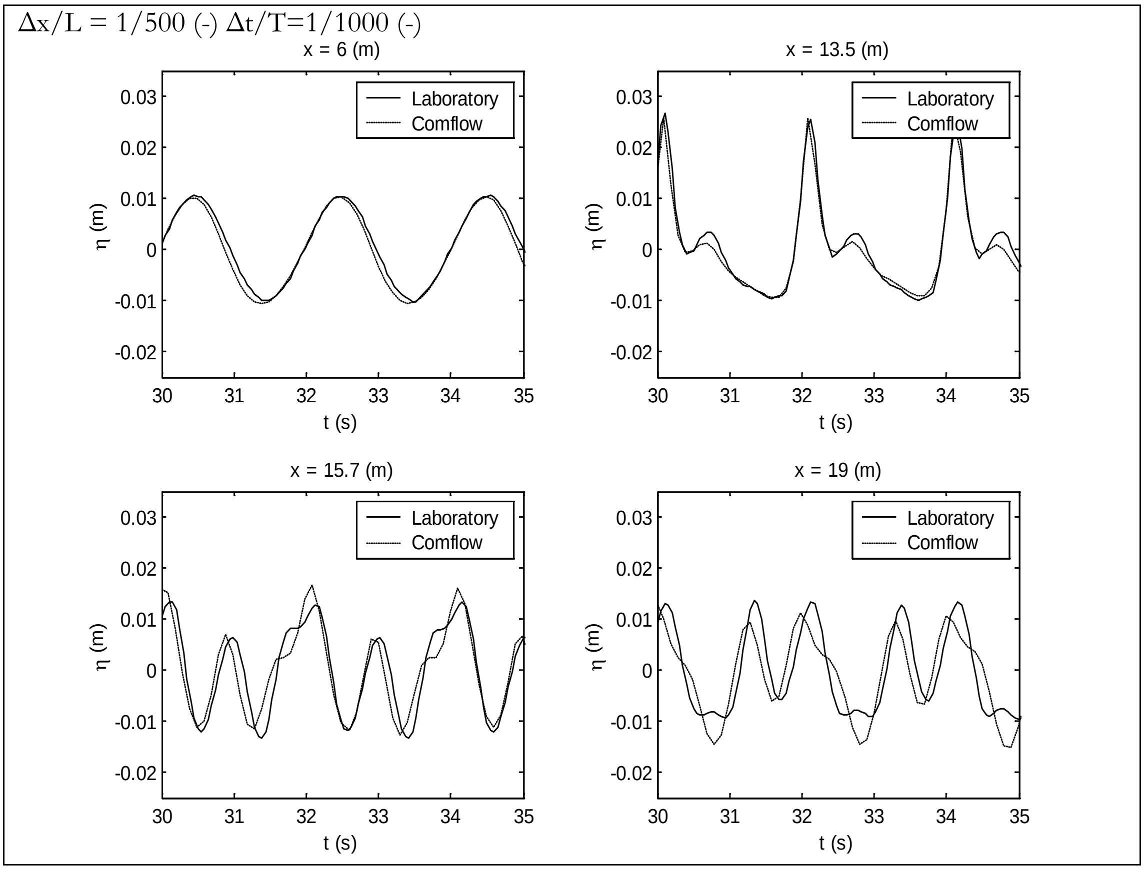

Δx/L = 1/500 (-) Δt/T=1/1000 (-)
x = 6 (m)
x = 13.5 (m)
x = 15.7 (m)
x = 19 (m)
Laboratory
Comflow
η (m)
t (s)

Amplitude spectra, $\Delta x/L = 1/500$ (-), $\Delta t/T = 1/1000$ (-)

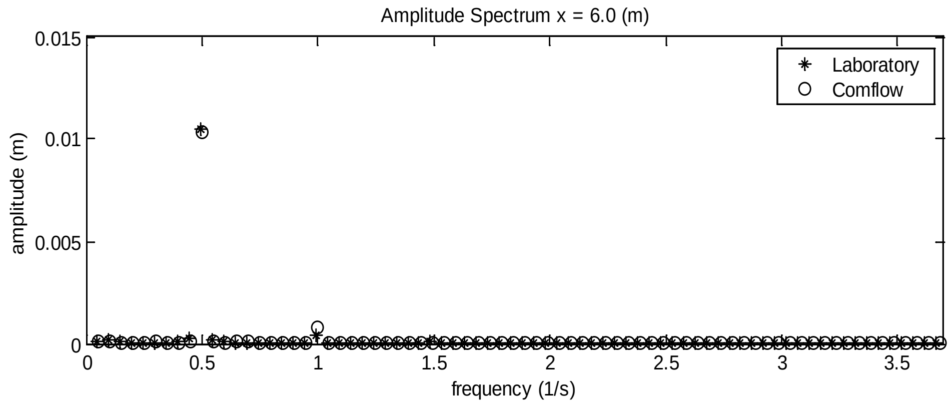

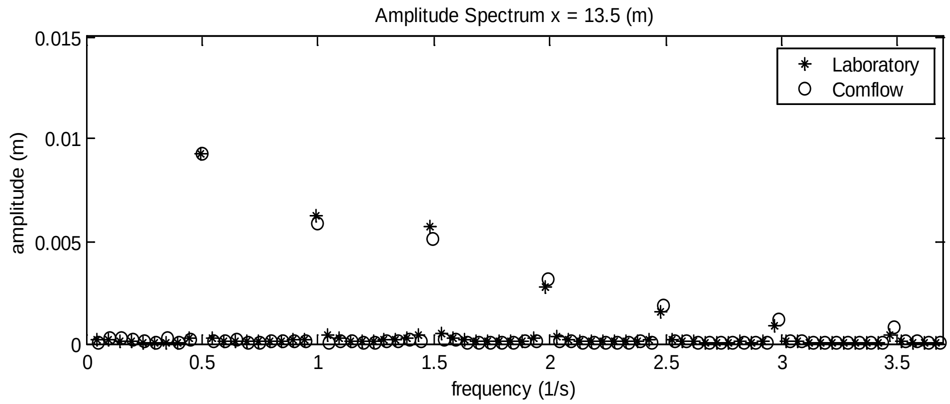

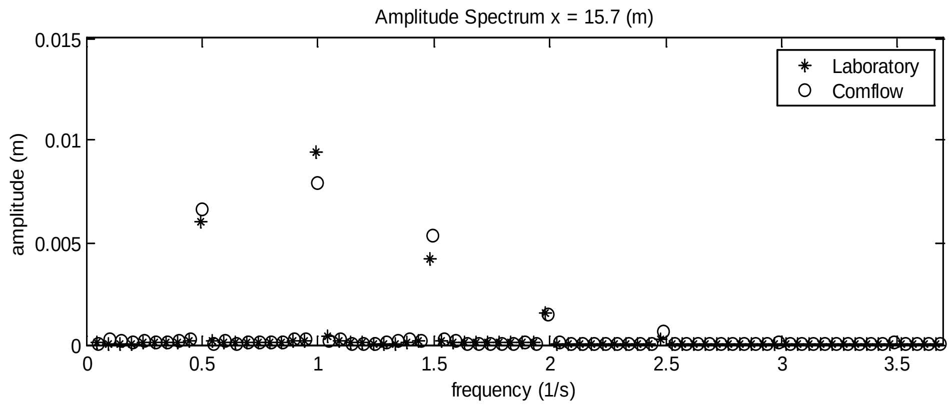

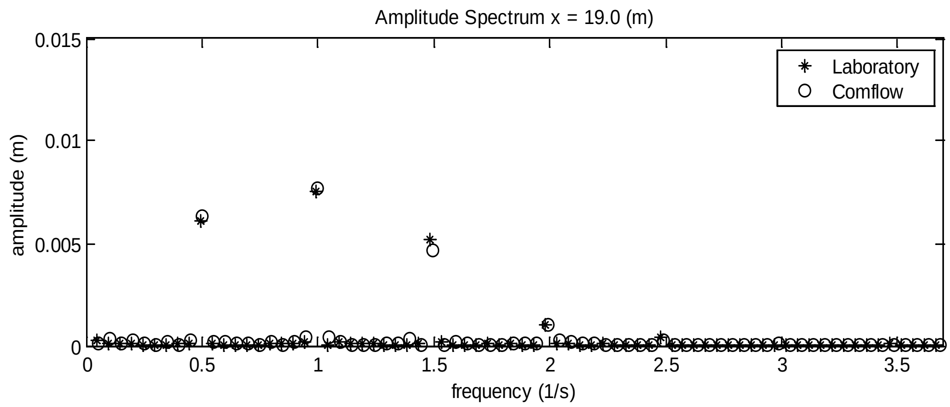

Phase spectra, $\Delta x/L = 1/500$ (-), $\Delta t/T = 1/1000$ (-)

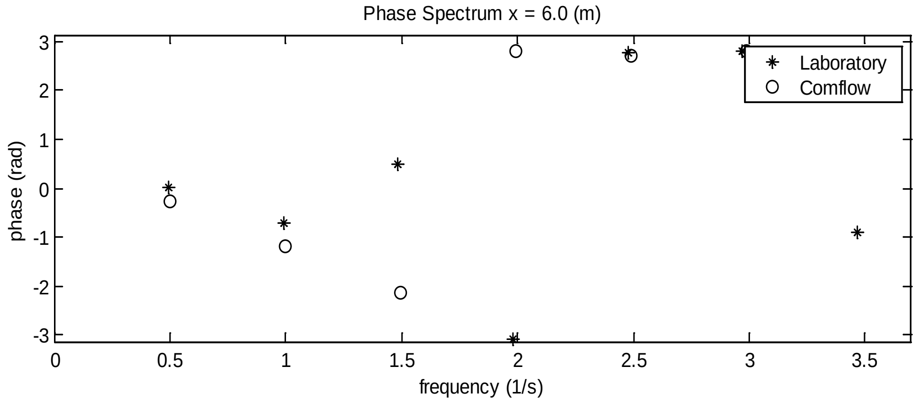

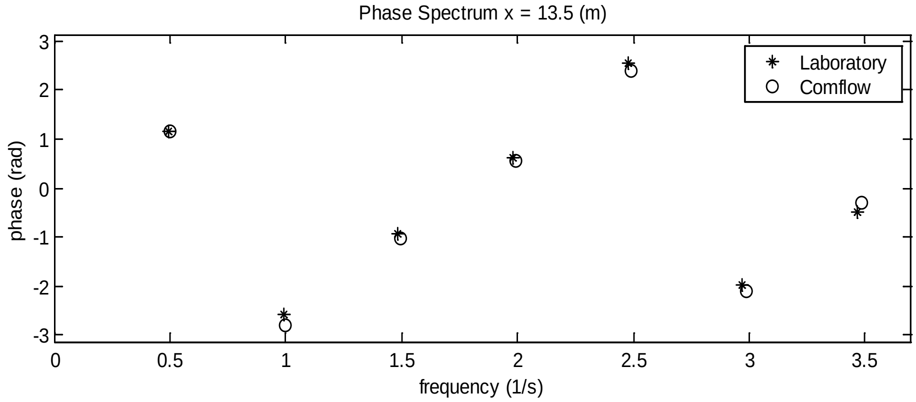

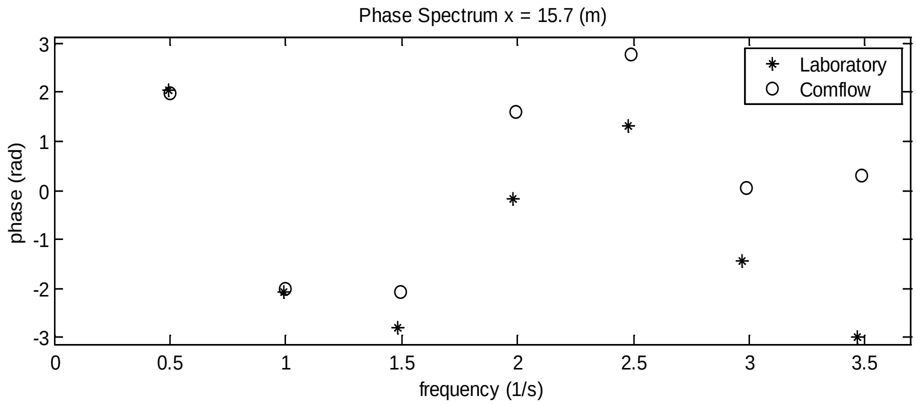

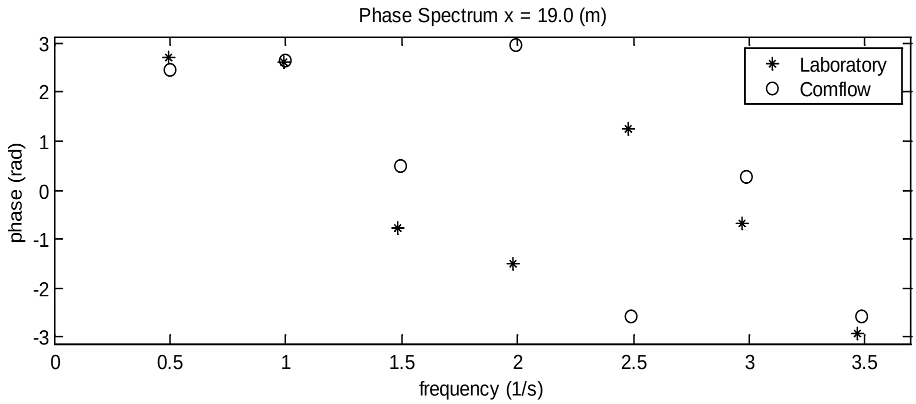

APPENDIX C: Sloshing Tank

Grid and time step reduction

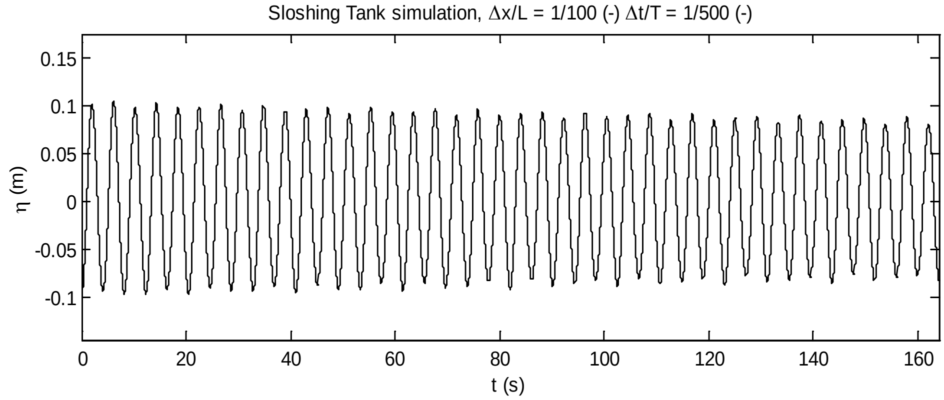

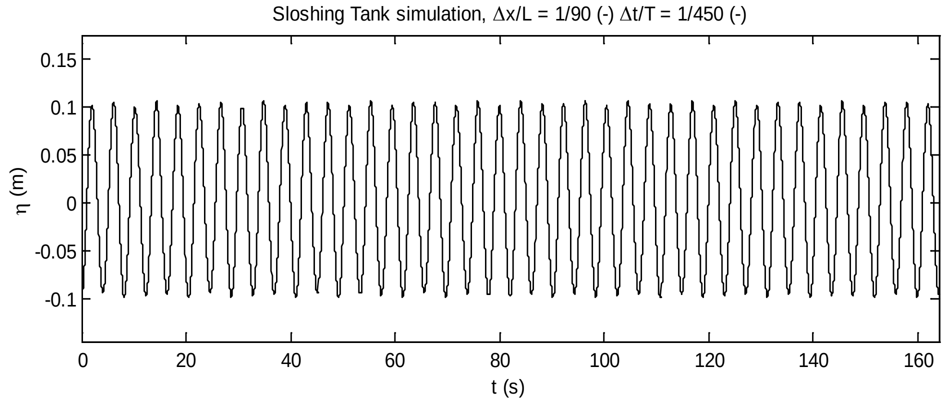

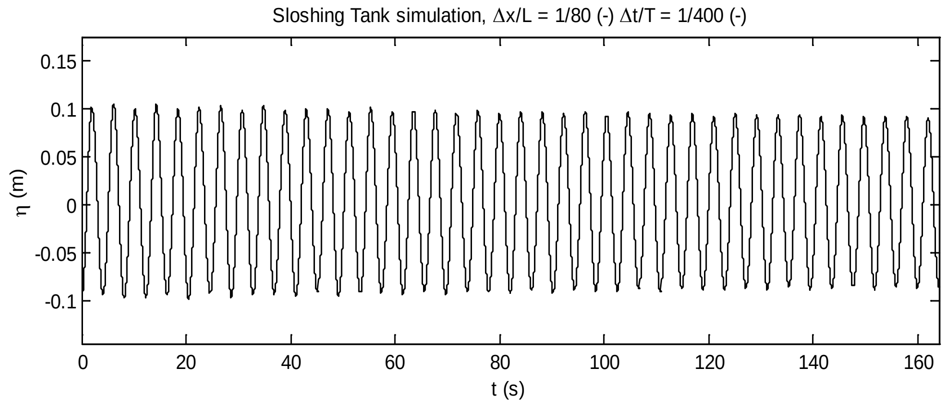

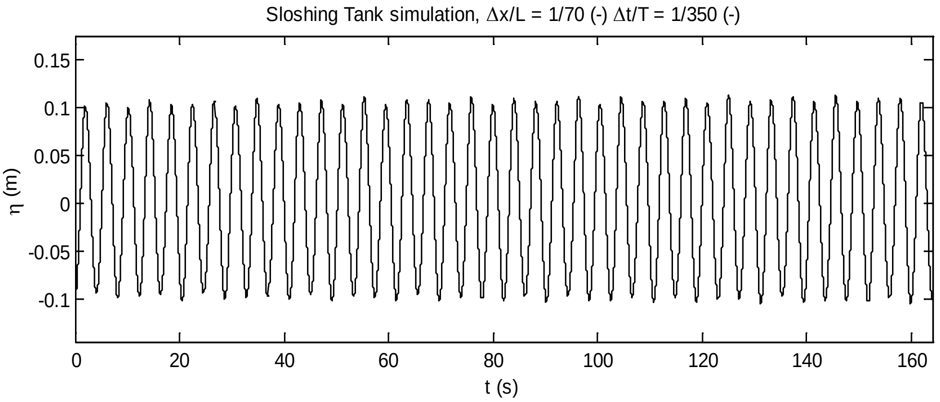
Sloshing Tank simulation, Δx/L = 1/70 (-) Δt/T = 1/350 (-)
η (m)
0.15
0.1
0.05
0
-0.05
-0.1
0
20
40
60
80
100
120
140
160
t (s)

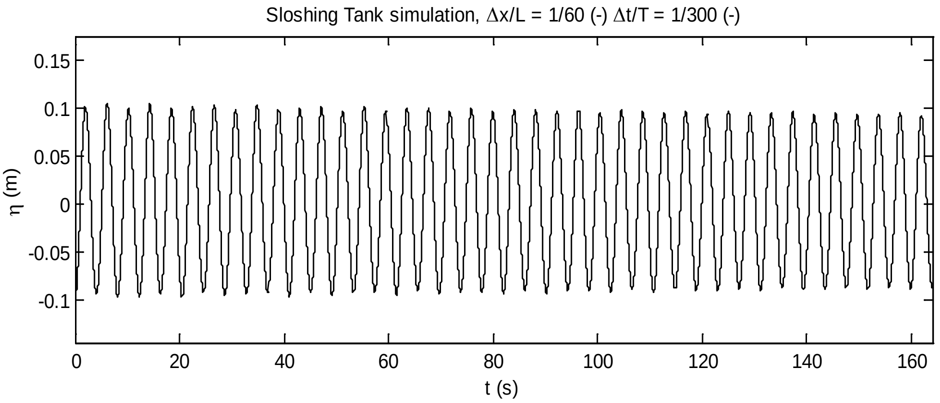
Sloshing Tank simulation, Δx/L = 1/60 (-) Δt/T = 1/300 (-)
η (m)
0.15
0.1
0.05
0
-0.05
-0.1
0
20
40
60
80
100
120
140
160
t (s)

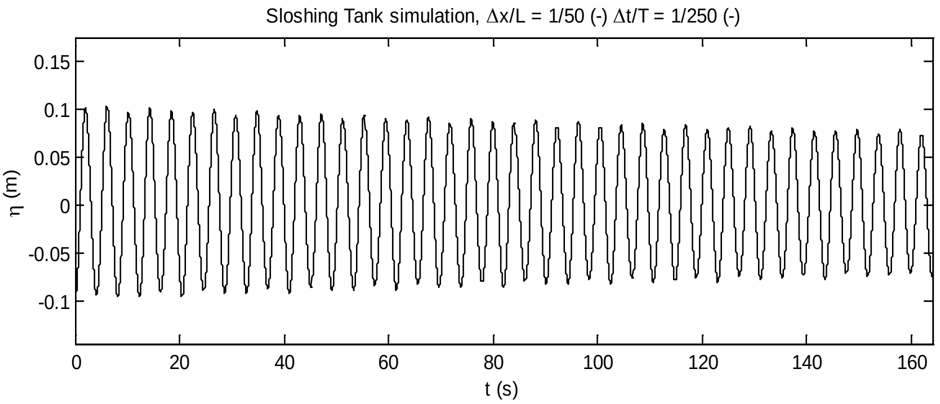
Sloshing Tank simulation, Δx/L = 1/50 (-) Δt/T = 1/250 (-)
η (m)
0.15
0.1
0.05
0
-0.05
-0.1
0
20
40
60
80
100
120
140
160
t (s)

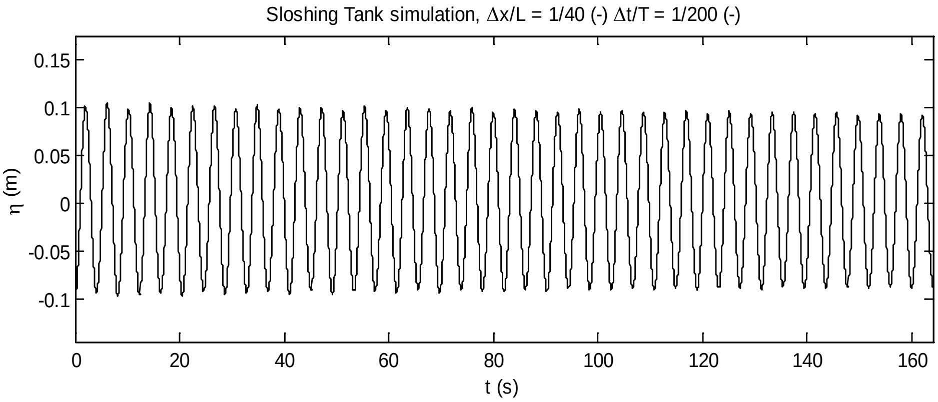
Sloshing Tank simulation, Δx/L = 1/40 (-) Δt/T = 1/200 (-)
η (m)
t (s)
0.15
0.1
0.05
0
-0.05
-0.1
0
20
40
60
80
100
120
140
160

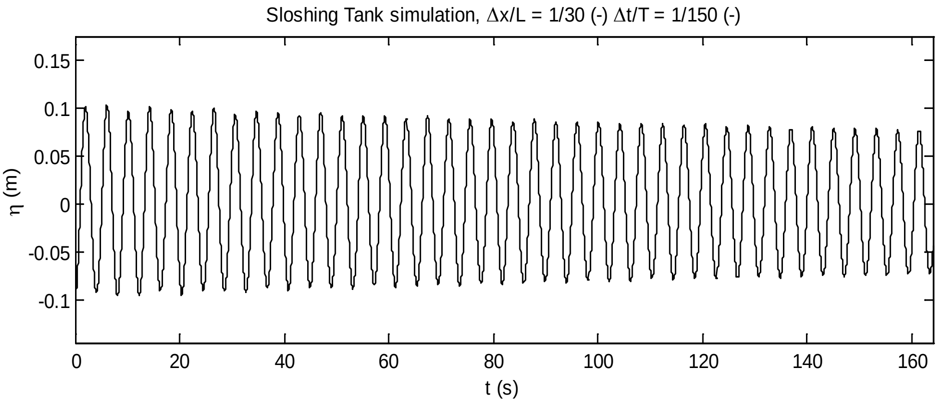
Sloshing Tank simulation, Δx/L = 1/30 (-) Δt/T = 1/150 (-)
η (m)
t (s)
0.15
0.1
0.05
0
-0.05
-0.1
0
20
40
60
80
100
120
140
160

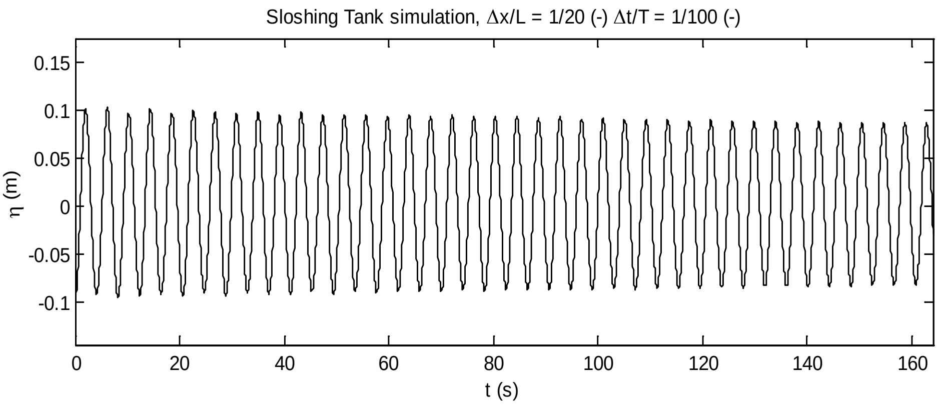
Sloshing Tank simulation, Δx/L = 1/20 (-) Δt/T = 1/100 (-)
η (m)
t (s)
0.15
0.1
0.05
0
-0.05
-0.1
0
20
40
60
80
100
120
140
160

Reduction number of cell layers

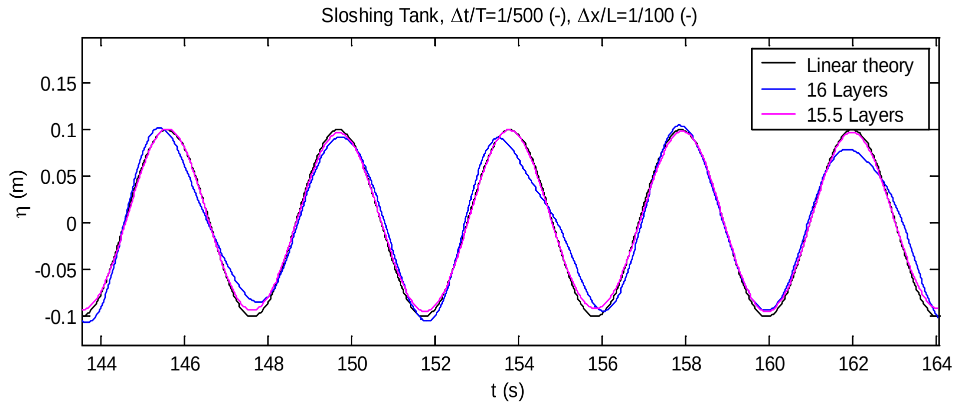

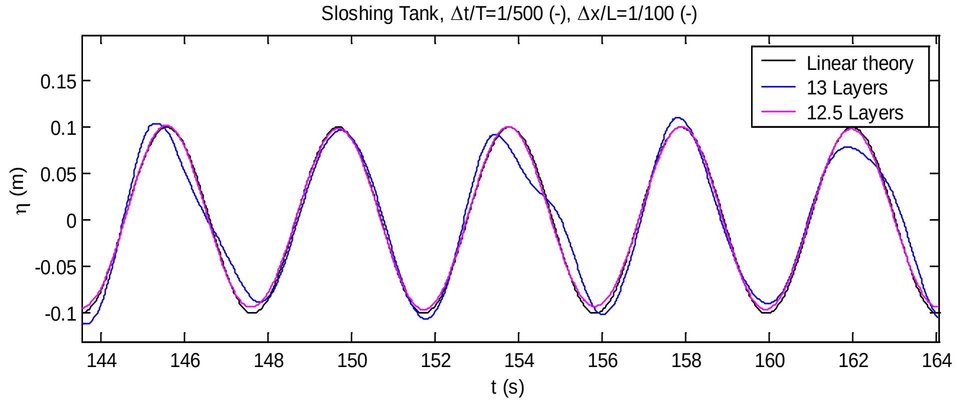

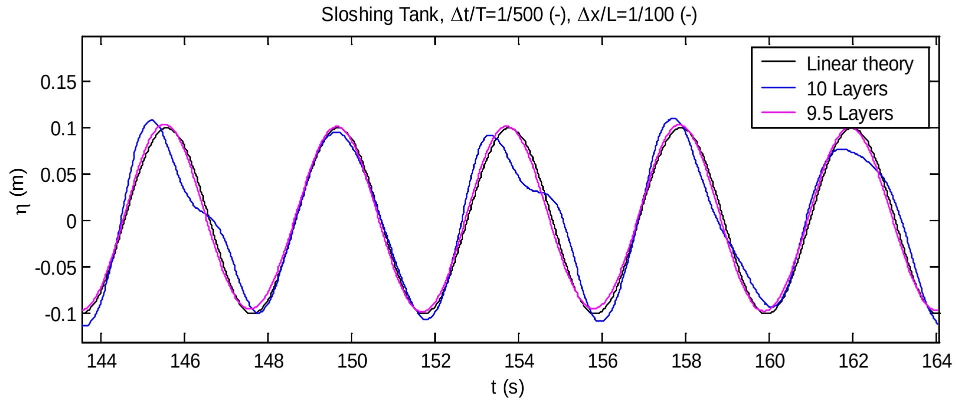

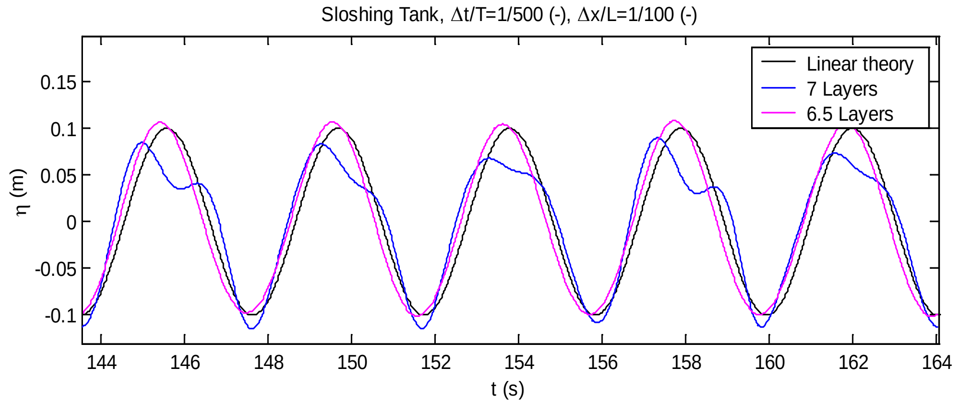

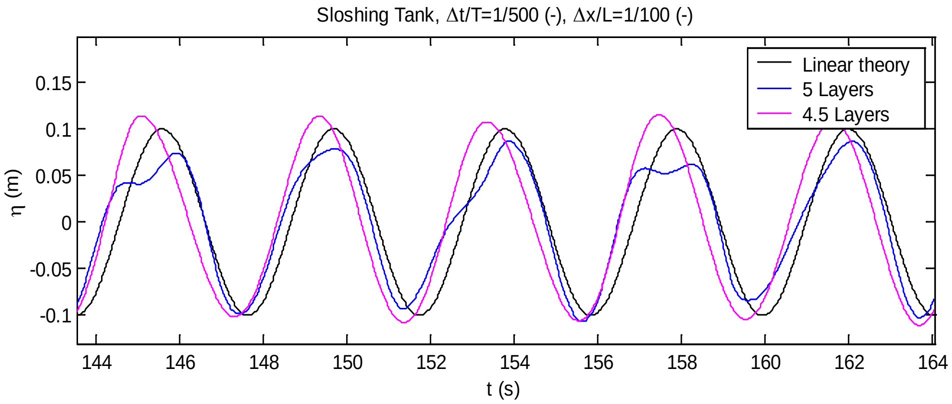
Sloshing Tank, Δt/T=1/500 (-), Δx/L=1/100 (-)
Linear theory
5 Layers
4.5 Layers
η (m)
t (s)

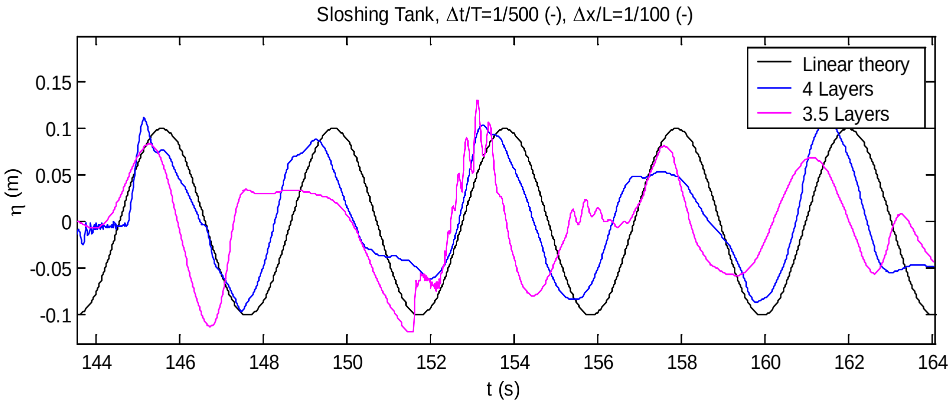
Sloshing Tank, Δt/T=1/500 (-), Δx/L=1/100 (-)
Linear theory
4 Layers
3.5 Layers
η (m)
t (s)

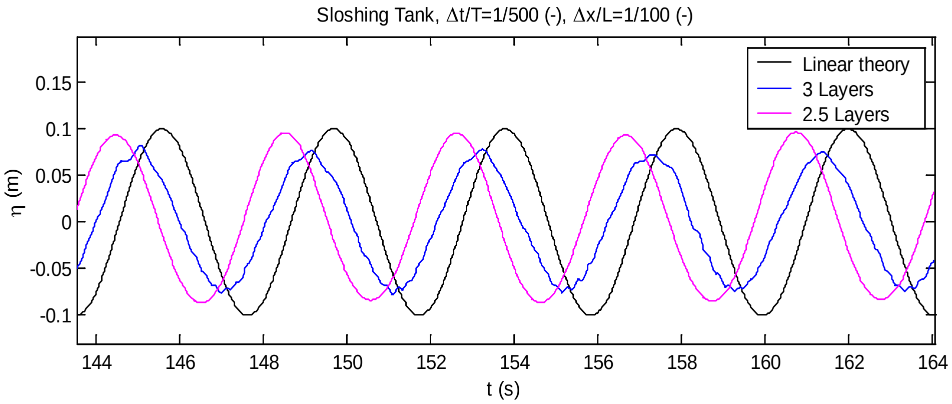
Sloshing Tank, Δt/T=1/500 (-), Δx/L=1/100 (-)
Linear theory
3 Layers
2.5 Layers
η (m)
t (s)

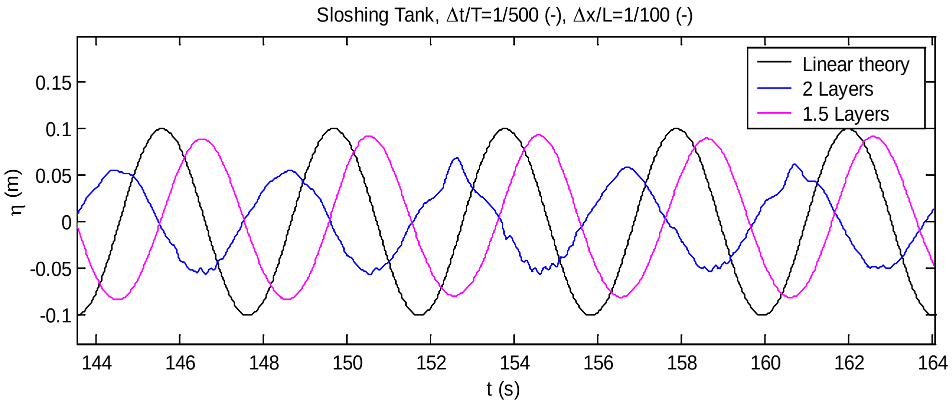
Sloshing Tank, Δt/T=1/500 (-), Δx/L=1/100 (-)
Linear theory
2 Layers
1.5 Layers
η (m)
t (s)

Formation of cusps

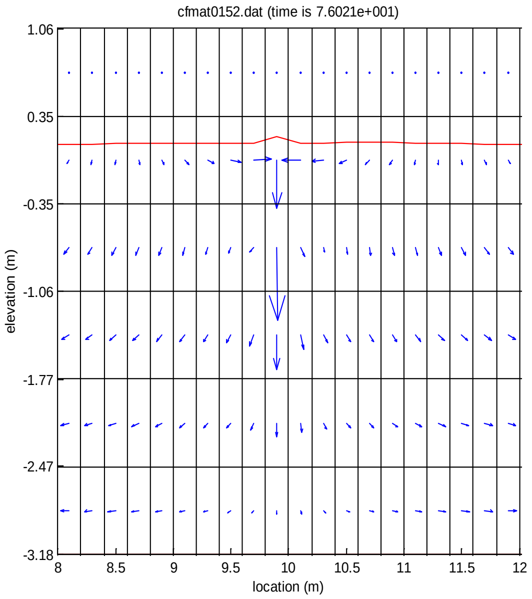

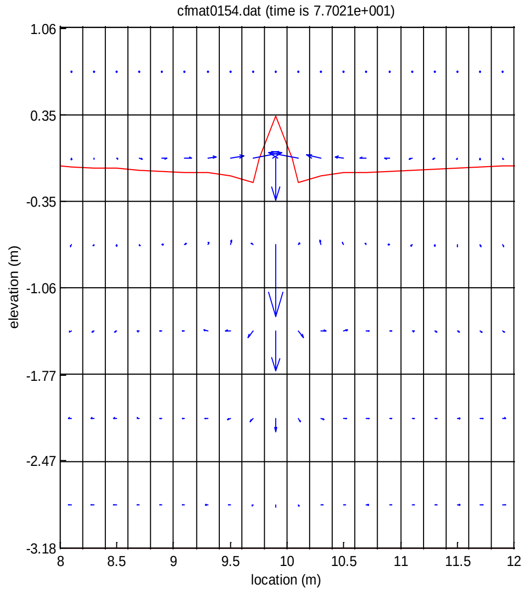

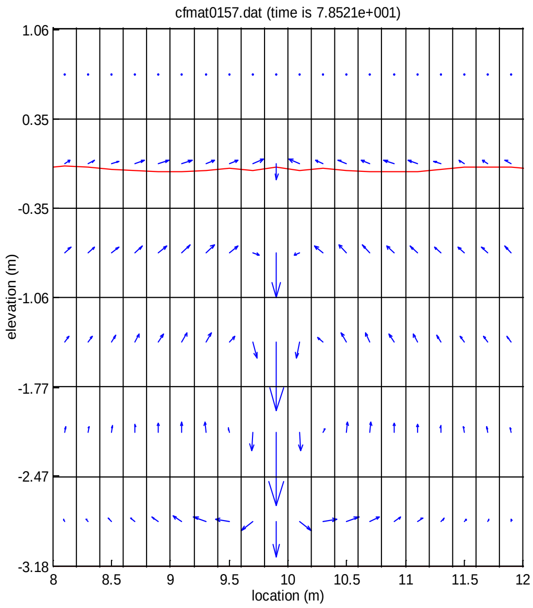

Local focusing of high frequency error waves causes a cusp. Several waves of small length converge at the location of this focus. A large cusp arises quickly and disappears quickly.

APPENDIX D: Steep Waves

Steep waves experiment in Comflow

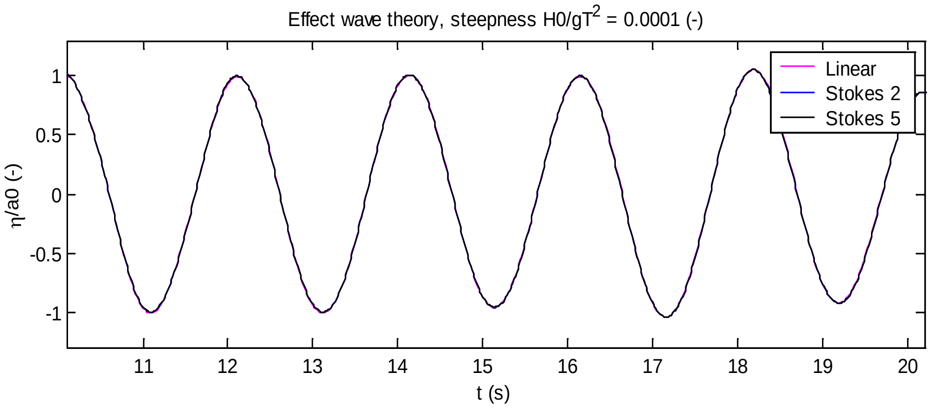

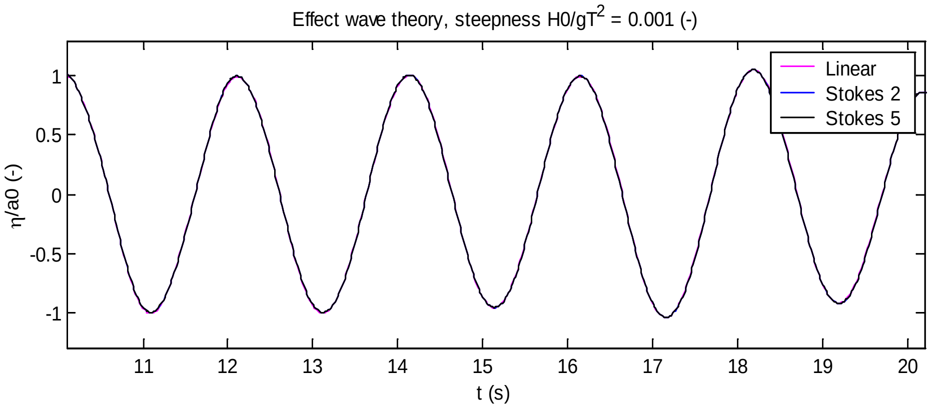

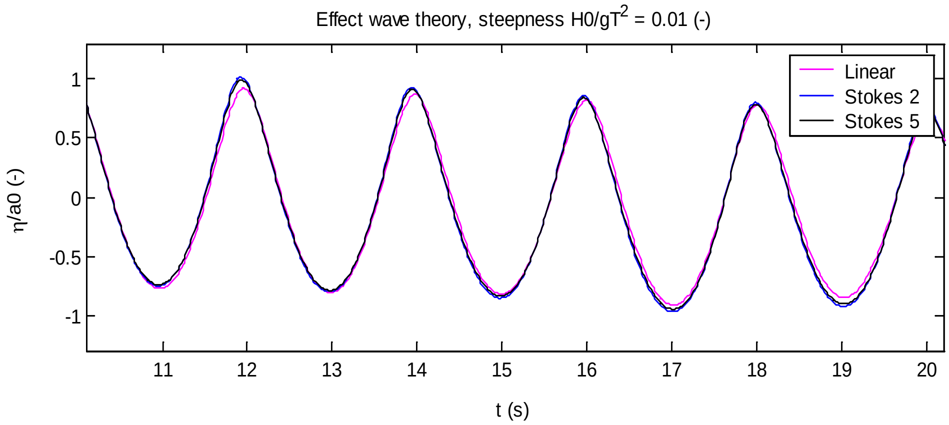

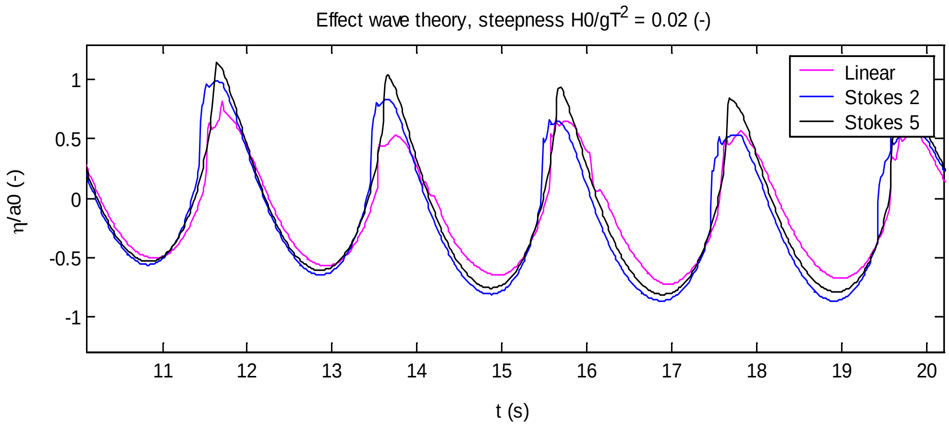

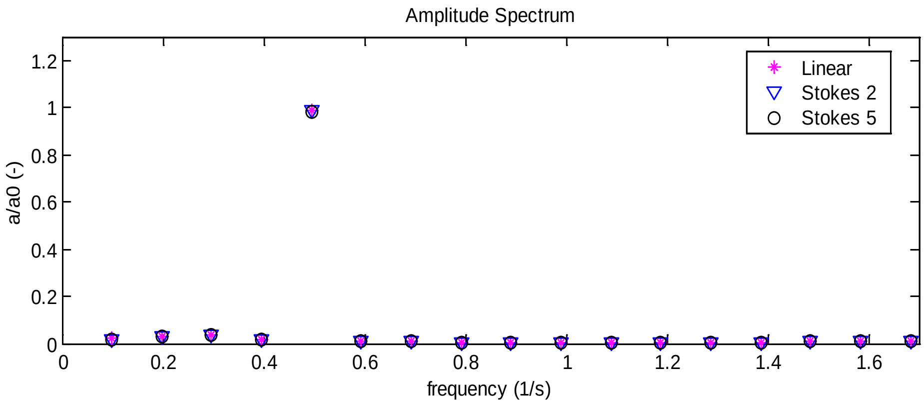

Amplitude Spectrum
Linear
Stokes 2
Stokes 5
a/a0 (-)
frequency (1/s)

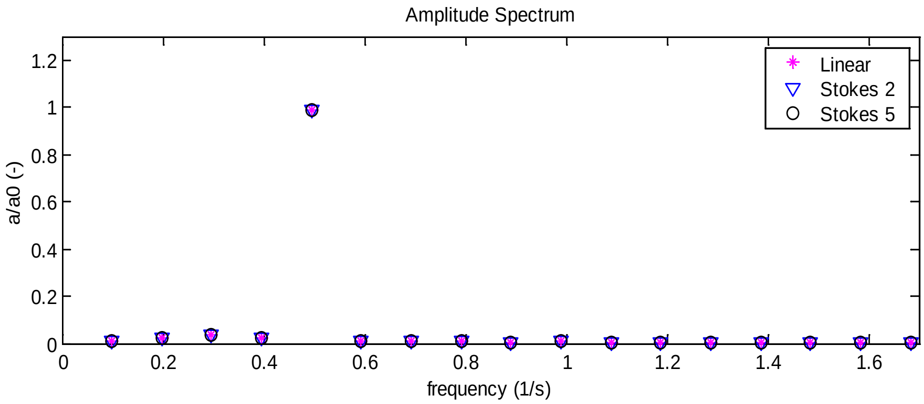

Amplitude Spectrum
Linear
Stokes 2
Stokes 5
a/a0 (-)
frequency (1/s)

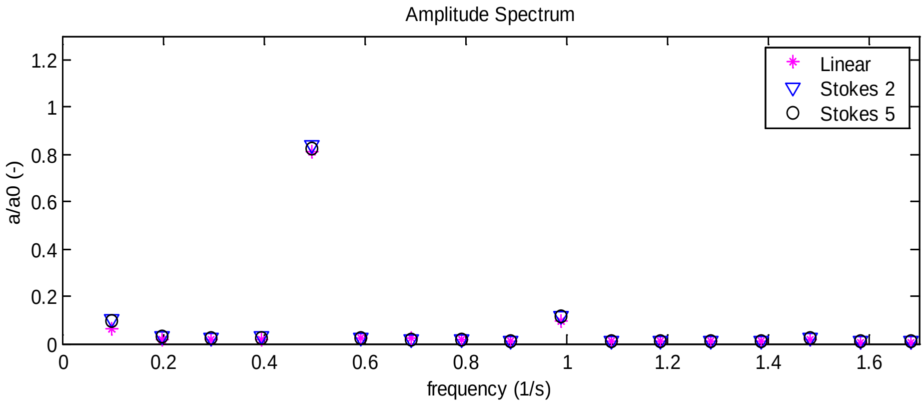

Amplitude Spectrum
Linear
Stokes 2
Stokes 5
a/a0 (-)
frequency (1/s)

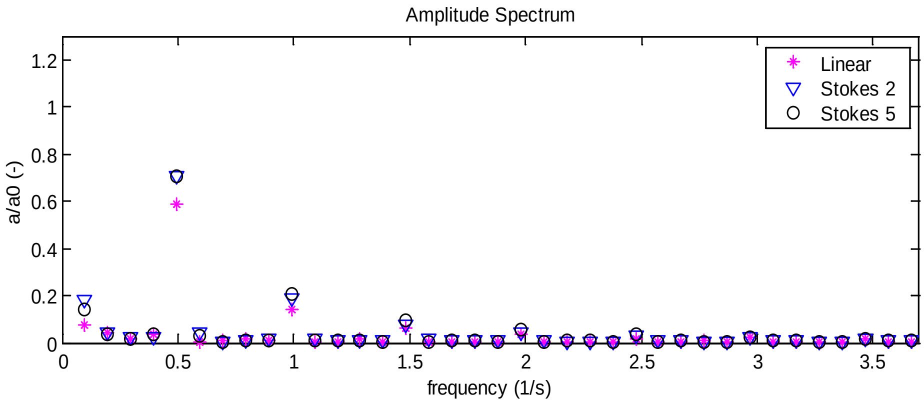

Amplitude Spectrum
Linear
Stokes 2
Stokes 5
a/a0 (-)
frequency (1/s)

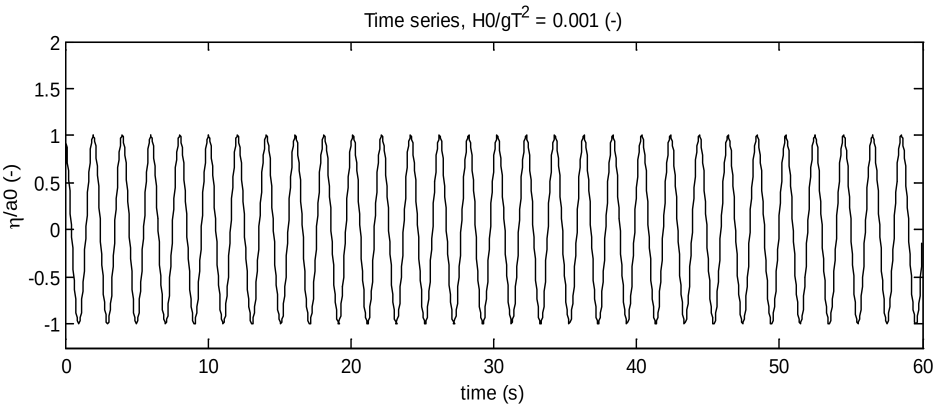
Time series, H0/gT2 = 0.001 (-)
η/a0 (-)
time (s)

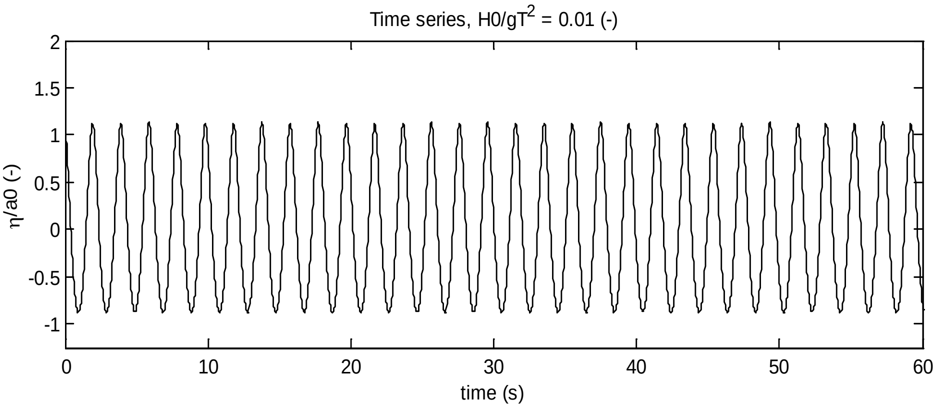
Time series, H0/gT2 = 0.01 (-)
η/a0 (-)
time (s)

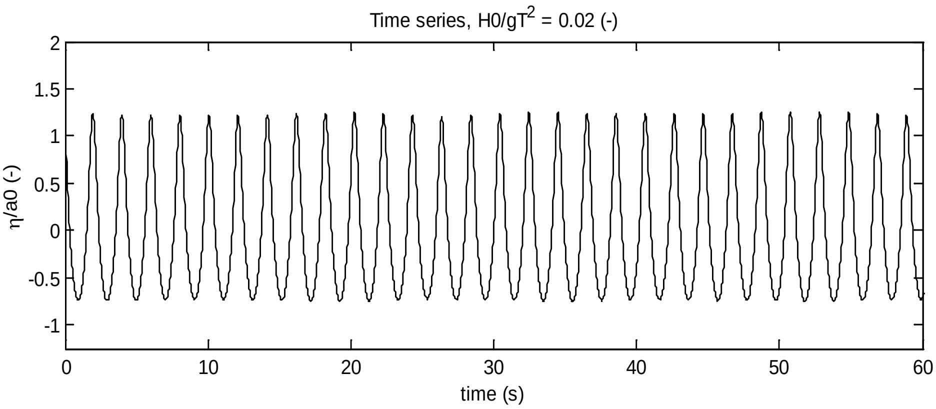
Time series, H0/gT2 = 0.02 (-)
η/a0 (-)
time (s)

APPENDIX E: Nonlinear Newwaves

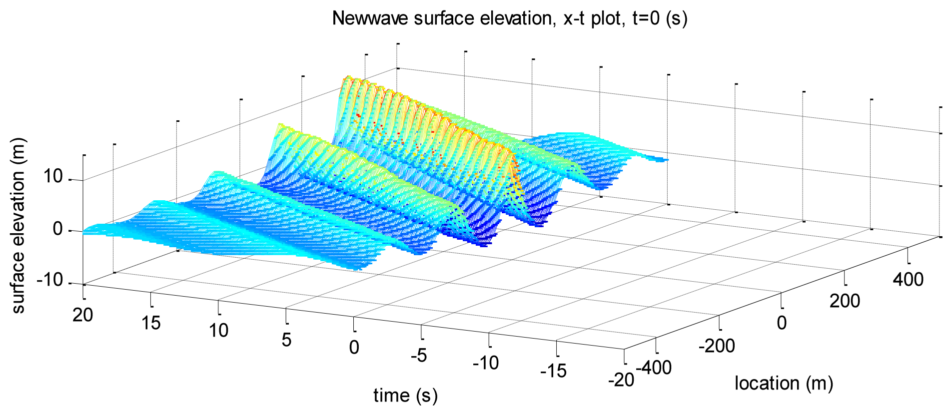

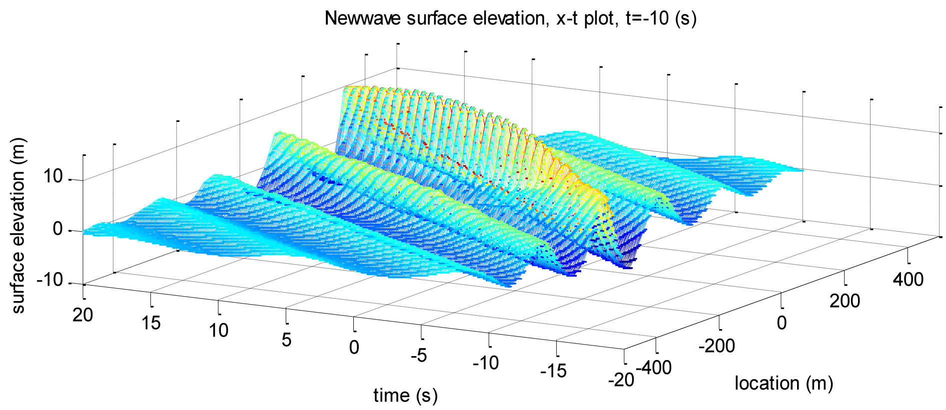

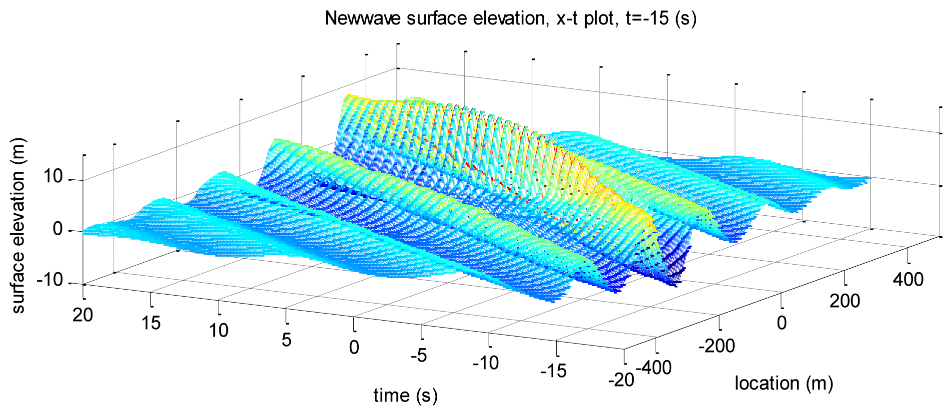

Newwave surface elevation, x-t plot, t=-20 (s)

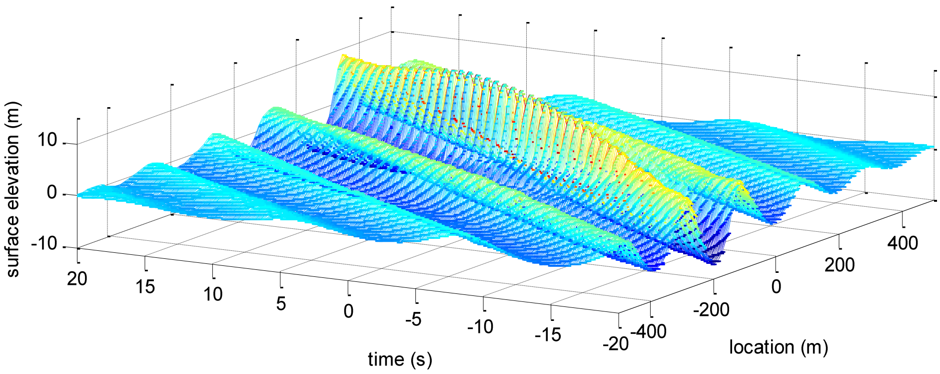

Newwave surface elevation, x-t plot, t=-25 (s)

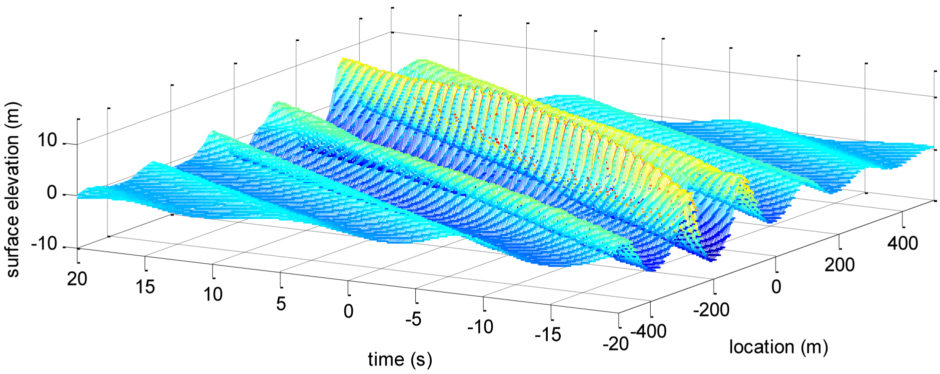

Newwave surface elevation, x-t plot, t=-50 (s)

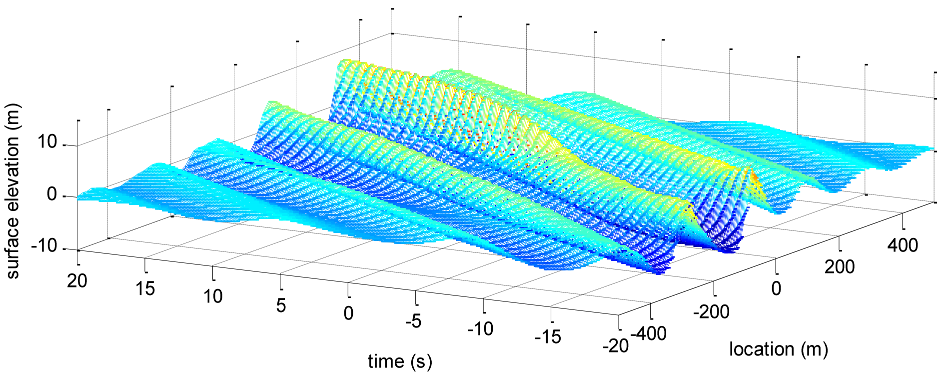

Newwave surface elevation, x-t plot, t=-75 (s)

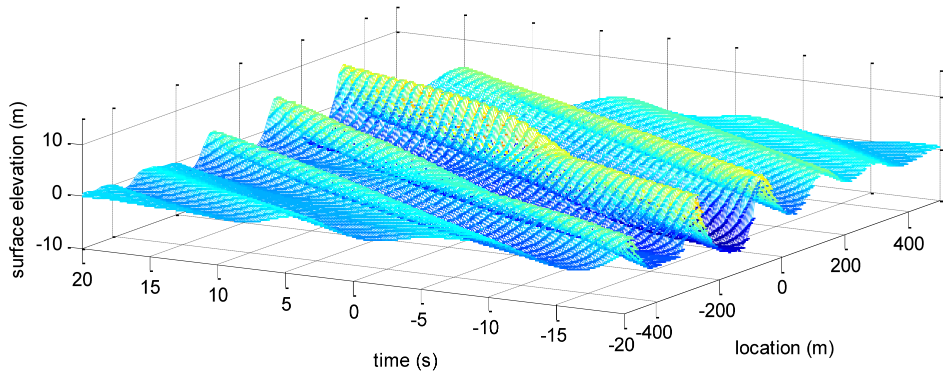

Newwave surface elevation, x-t plot, t=-130 (s)

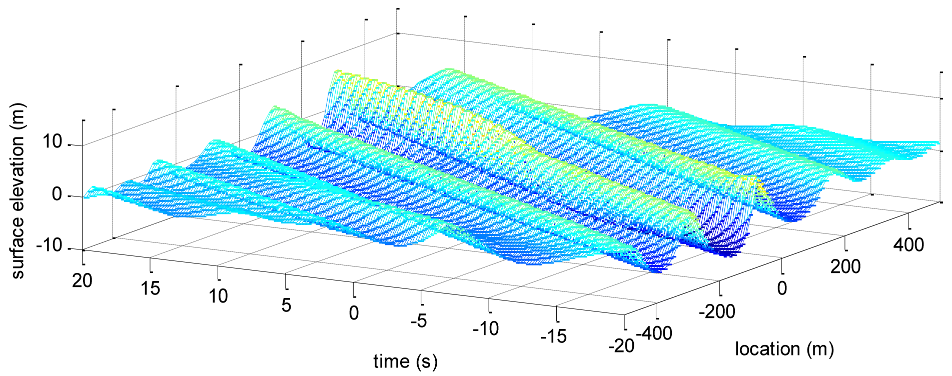

Linear Newwave surface elevation, x-t plot

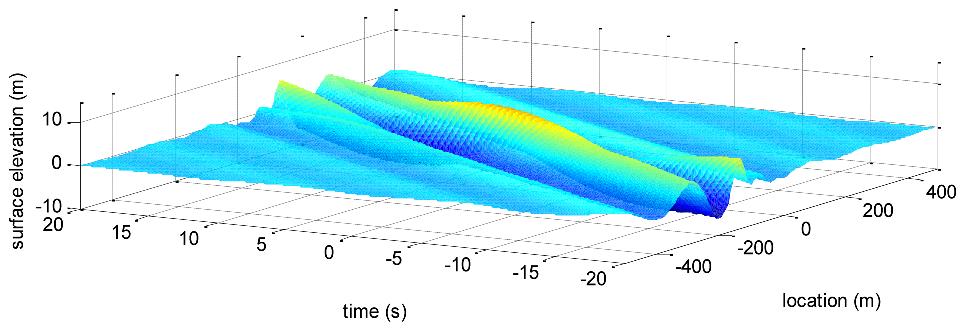

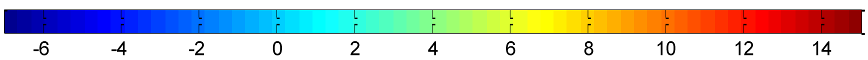

APPENDIX F: Coupling of Vijfvinkel to Comflow

Input for Vijfinkel's velocity profile code: $\eta(x,t)$ and $\varphi^S(x,t)$

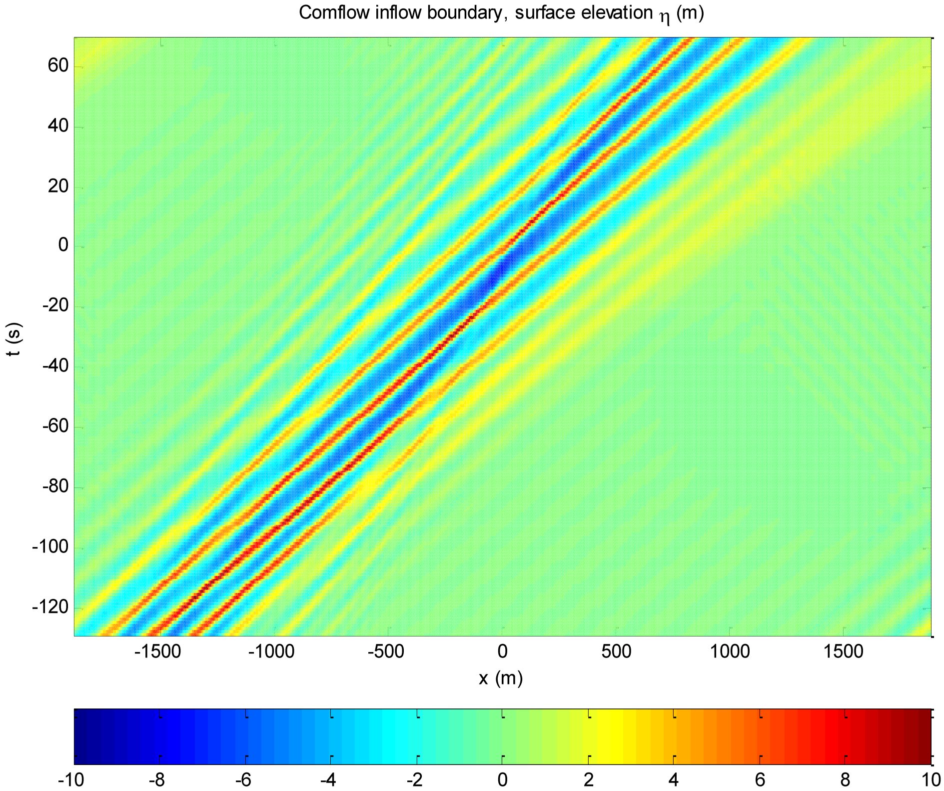

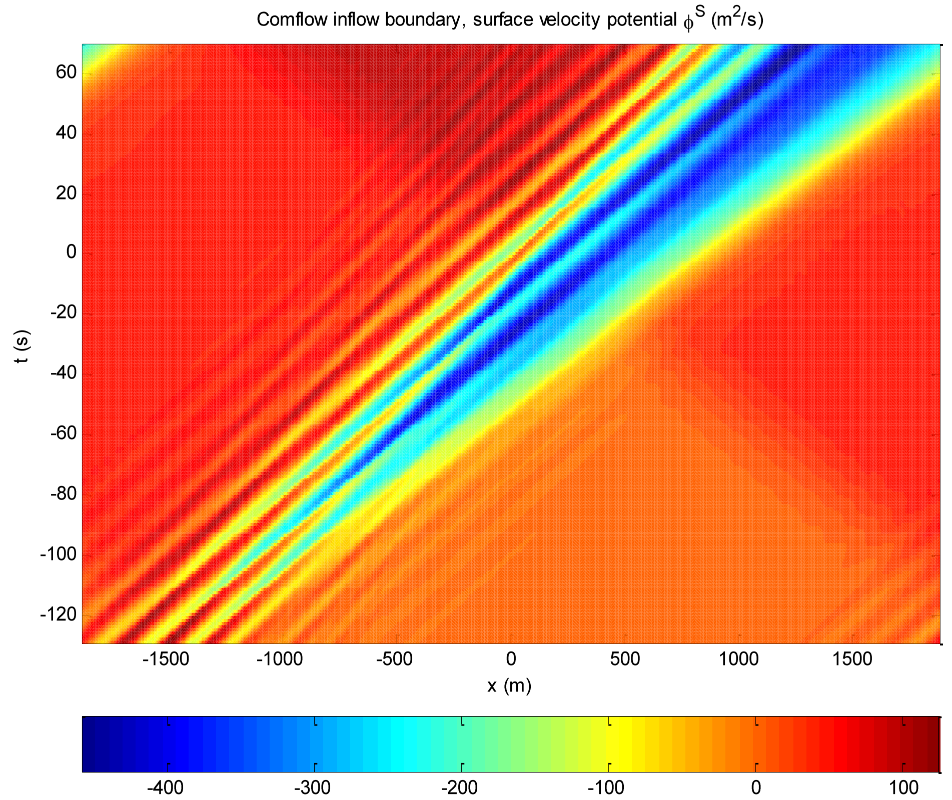
Comflow inflow boundary, surface velocity potential ϕ^S (m^2/s)
t (s)
x (m)
60
40
20
0
-20
-40
-60
-80
-100
-120
-1500
-1000
-500
0
500
1000
1500
-400
-300
-200
-100
0
100

Output velocity profile code: u(z,t) and w(z,t)